π Effective Field Theory:

Building the Bridge Between Lattice Quantum Chromodynamics and Nuclear Physics

Candidate

Lorenzo Contessi

Supervisors

Francesco Pederiva
Alessandro Lovato

Abstract

We analyze ground state properties of few-nucleons systems and ^{16}O using EFT($\not\pi$) (Pionless Effective Field Theory) at Leading Order (LO). This is the first time the theory is extended to many-body nuclear systems. The free constants of the interaction are fitted using both experimental data and Lattice Quantum Chromo Dynamics (LQCD) results. The nuclear many-body Schrödinger equation is solved by means of the Auxiliary Field Diffusion Monte Carlo method. A linear optimization procedure has been used to recover the correct structure of the ground state wavefunction. EFT($\not\pi$) as revealed to be an appropriate theory to describe light nuclei both in nature, and in the case where heavier quarks are used in order to make LQCD calculation feasible. Our results are in good agreement with experiments and LQCD predictions. In our LO calculation, ^{16}O appears to be unstable against breakup into four ^{4}He for the quark masses considered.

Introduction

Nuclear physics is an extremely fascinating and complex field. During the years, countless models and calculation methods predicted nuclear reactions and structures with increasing precision. At the present state of art, closed-form calculations are no longer sufficient to investigate the intriguing complexity of strongly interacting few- and many-body systems. The use of numerical computation permitted to approach problems never studied before. Nonetheless, the algorithms need to be constantly refined and developed to follow the improvements of technology and the requests of increasing precision, while decreasing the costs and control the approximations made. This increasing ability in solving the Schrödinger equation leads to the development of more complex theories with a sophisticated operator structures, many parameters to be fitted and better predictions for bound states or scattering problems.

The work done in the past fifty years on nuclear potentials lead to a deeper knowledge of the interaction itself. However, an interaction able to predict bound- and scattering-states together and able to provide error estimations for the theory is still far from been known. This, as well as the connection of nuclear potential with the underlying theory which is Quantum Chromo Dynamics (QCD), are some of the many points that still have to be inspected and understood about nuclei.

In this thesis, we investigated the connection between low-energy Nuclear Physics and QCD. The only known way to perform calculations in nonperturbative QCD is LQCD, which has been shown to be a successful technique in predicting hadronic observables. In the past few years improvements to this method allowed to directly compute some few-nucleon-systems like d, nn, ^{3}H, ^{3}He and, ^{4}He. However, in in current calculations, it is necessary to use unphysically large values of the quark masses. In fact, the physical values give pion mass that are too light to be constraint in a box of dimension such to make the computation feasible today. To overcome this problem the calculations were performed with heavy pions ($m_\pi \sim$ (300, 500, 800) MeV) which

are easier to be accommodated in a smaller box. Nonetheless, the large cost of the calculation makes it difficult to have a number of samples sufficient to test the convergence of the data, in particular for larger systems. Moreover, the absence of reference data or benchmark values for such high m_π makes the data interpretation complicated. The usage of Contact Effective Field Theory (EFT)s combined with few body methods can provide a systematic procedure to check those results.

The EFT method is developed for systems of particles whose scattering-length is large compared to their size. It consists of an expansions of the interaction suggesting a hierarchy of the operatorial structure, depending on the relevant Degrees of Freedom (DoF) and energy scales of the problem. In particular, the renormalized contact EFT, also know in nuclear Physics as pionless effective field theory (EFT($\not\pi$)), has been used to bridge the gap between LQCD and low-energy nuclear physics. This is motivated by the large mass of pions, too heavy to play a dynamical role in the few-nucleon Lagrangian. In the case of physical pion mass the long-range contribution of pions can not be considered trivially irrelevant. However, we demonstrate that at LO a contact interaction is enough to describe few-body systems also with lighter pions.

In order to solve the Shröedinger in few- and many-body systems we used the Quantum Monte Carlo (QMC) method. QMC is an ab initio method able to calculate observables in relatively heavy nuclei with systematically improvable precision. Three variants of the method have been used during this work, the Variational Monte Carlo (VMC), Diffusion Monte Carlo (DMC) and Released Path Diffusion Monte Carlo (RPDMC).

The goal of this work is to benchmark and to extend lattice calculations to light-nuclei and heavier systems. To achieve it, we calculate observables of α-particles and ^{16}O nuclei. We also prove the convergence in the cut-off of the EFT($\not\pi$) at LO, for ^{4}He, using both experimental and LQCD data as input for gauging the parameters. This shows the completeness of the theory at LO and its suitability.

After this successful benchmark, we extend the calculations to ^{16}O. This is the first attempt to extend LQCD results in nuclei whose central density is closer to saturation. In our study, we could not find evidence of binding in ^{16}O neither starting from experimental results nor using LQCD data as input. However, the weak binding of ^{16}O in nature suggests that more orders

of the interaction are required in order to have an accurate description of the system.

The work is organized as follows:
In chapter {1} we present a brief historical introduction, as well as the motivations of the methodology and techniques used in this work; chapter {2} will briefly introduce and review the relevant properties of EFT($\not\pi$) concerning our discussion; in Chapter {3} we review LQCD data and we propose an analysis of them in terms of T-matrix momentum poles; in Chapter {4} the methodological aspect of the calculations will be discussed; in Chapter {5} the results of the method for few-body system are examined; in Chapter {6} we discuss results obtained for ^{16}O; Chapter {7} is devoted to conclusions. and finally Chapter {8} contains all the data and calculations done during this work.

Contents

Acronyms

EFT($\not\pi$) Pionless Effective Field Theory

QCD Quantum Chromo Dynamics

LQCD Lattice Quantum Chromo Dynamics

DoF Degrees of Freedom

EFT Effective Field Theory

ET Effective Theory

RG Renormalization Group

LO Leading Order

NLO Next to Leading Order

LEC Low Energy Constant

ERE Effective Range Expansion

MC Monte Carlo

QMC Quantum Monte Carlo

VMC Variational Monte Carlo

DMC Diffusion Monte Carlo

GFDMC Green Function Diffusion Monte Carlo

RPDMC Released Path Diffusion Monte Carlo

AFDMC Auxiliary Field Diffusion Monte Carlo

LM Linear Method

1. Motivations

Nuclear potentials have a long and intriguing history, not devoid of dead ends and incognita. The first attempt to theoretically describe nucleon forces using subatomic particles (pions) was done by Yukawa [1] in 1935. The Yukawa model revealed to be good in explaining NN scattering, but multi-pion exchanges were ambiguous and not well understood until the '60s when heavy mesons have been discovered [2]. New models, as the more general one-boson-exchange [3], were developed by that time and had great success. Nonetheless, the nuclear interaction was not yet completely understood. The theory needed few bosons that had to be associated with multi-mesonic resonances which existence was debated. During the time required to clear out the controversy, many other models appeared, as the Paris [4] and Bonn [5] potentials. Those potentials were very successful in describing the phenomenology, but they gave little help in better understanding the basis of nuclear interaction.

The development of QCD appeared to give a new fundamental comprehension about nuclear potentials, but physicists soon realized that QCD can not be applied perturbatively in the low energy limit. The breakthrough appeared in 1979 when Weinberg [6] proposed to write the most generic Lagrangian consistent with the symmetries of QCD using nucleons and pions as DoF. The operators were organized in orders with respect to the number of powers of a "small" quantity present in the operator coefficients according to the *dimensional analysis* procedure. However, the theory showed to be non-renormalizable order by order, i.e. compute observables still had a dependency on an unphysical scale that can not be eliminated adding more terms in their specific order. Later, physicists realized that the motivation of the non-renormalizability of Weinberg power counting comes from nontrivial contributions of iterated pions in any angular momentum channel. A later attempt to solve the problem was made using the KSW scheme [7], which reorders Weinberg power counting treating pions as perturbations. This approach is very successful up to the first orders of the interaction, but it fails

in converging in the $^3S_1$ two body channel [8]. The impossibility to solve this problem with any contact interaction ratified the needs of dropping the theory or, at least, modifying it.

At the moment nuclear physics still has to be completely understood. It is not clear yet if it is possible to write a potential through first principles and QCD symmetries as Weinberg intended. While phenomenological potentials, as AV18, are still widely used due to their ability to provide quantitative results, the chiral potential is now gaining popularity as a compromise between the two approaches. However, this potential is still quite close in nature to a phenomenological one since it is not completely renormalizable and it requires to fix the cut-off to a certain value to which the whole potential (and observables) is dependent.

In this work, we start from EFT, but without pion exchanges. We not only explore the theory in systems in which its appropriateness is still debated, but we attempt to prove the consistency of the EFT($\not\pi$) power counting in the few- and many-body systems. Moreover, we use the same procedure that should be adopted when a consistent pionfull theory will be developed.

1.1 Motivations

In this work, we will discuss Contact Effective Potentials and their usage in few- and many-body low-energy nuclear physics. Pionless (or contact) theory does not treat pions explicitly as a finite range force, including their contact interactions. This not only avoids renormalization problems of the pionfull theory, but it also makes the interaction simpler and the power counting easier to manage because of the few scales involved in the theory. In pionless theories, in contrast with chiral potentials, chiral symmetry is heavily broken, and the pion is assumed to be too heavy to play an explicit role in the interaction.

While any interaction can be reproduced with a sum of delta functions and derivatives, the number of operators needed to reproduce observables might not be finite, making the theory not-usable. If the theory is appropriate for the considered system, we expect only a finite number of operators to be relevant. All the others will be arranged in infinite groups of decreasing importance, which are called *orders of the theory* or *orders of the interaction*. Each order is expected to give perturbative contributions to the observables. This implies that the free constants appearing in the potential must be determined in an order by order sequence. The possibility to do this is ensured by the renormalizability of the Pionless theory. Each order will then be included in perturbation theory without changing the parameters already fitted for the previous ones.

The nuclear interactions are not required to be fully relativistic since the internal momenta of nucleons are rather small. This justifies the usage of a non-relativistic many-body approach. However, pion contributions, relativistic corrections, and coulomb interactions are taken into account in the contact interactions and explicitly recovered at a higher order of the interaction. [9, 10] The pionless power counting is, in fact, a complete expansion of the interaction in the spirit of the Lepage [11] contact expansion. In the following subsections are discussed the motivations of using EFT($\not\pi$) both to describe low-energy nuclear-physics at physical pion mass and as extension of LQCD calculations.

Quantity	Mass [MeV]
M_{QCD}	~ 1000
m_π	~ 140
m_ρ	~ 780
m_N	~ 940
$m_\Delta - m_N$	~ 300
m_{1pe}	~ 20
m_{nuc}	~ 10
a_{nn}	5.4112(15) fm

Particle	Be [MeV]
d	~ 2.22
^{3}H	~ 8.48
^{4}He	~ 28.3
^{5}He	~ 27.5
^{5}Li	~ 26.6
^{6}Li	~ 32.0
^{16}O	~ 127
a_{pn}	-23.7148(43) fm

Table 1.1: The relevant mass scales and binding energies considered in this work. M_{QCD} refers to the QCD scale which defines the nucleon scale m_N. The nuclear binding scale m_{nuc} refers to the typical energy per particle of large nuclei (A$\geq$12). On the right side, the binding energy of few and many body systems are displayed. a_{nn} and a_{pn} refers to the scattering length of proton-neutron and neutron-neutron systems. m_{1pe} m_π^2/m_N, which we call the one-pion exchange scale, emerges when the inverse pion Compton wavelength is combined with the QCD mass scale.

Physical Pion mass From Tab.(1.1) it can be noticed that there is a factor two between the typical binding energy of nuclear systems (10 MeV) and the one-pion-exchange scale (20 MeV). Hence, it is not clear if pions should be explicitly treated or not for the nuclear calculations. For systems with small exchanged momenta, the pionless theory appears to be an appropriate technique, but if systems with higher exchanged moments are investigated, pions might be required. In that case, the break-down scale of the theory will be at the energy of the appearance of Δ resonances, which have a difference of mass of about $\sim$ 300 MeV with respect to nucleons. This can be further iterated when increasing the energy, requiring the explicit presence of ρ and heavier mesons in the theory. The terms in the pionless approach are ordered with respect to an expansion parameter ($\iota = \frac{Q}{m_\pi}$). We can use a rough estimation of the many-body momentum using a naive extension to A-particles of the 2-body energy-momentum dependence:

$$Q \approx \sqrt{2m_n \frac{BE}{A}} \tag{1.1}$$

that it is $> 50\%$ for Oxygen and α particles, thus we expect the LO to have large errors that can be reduced only including the next orders of the interaction. However, Eq.(1.1) refers to the average momentum but does not take into account the correlations between particles. Correlations can drastically

Scale [MeV]	$m_\pi = 300$ MeV	$m_\pi = 450$ MeV	$m_\pi = 510$ MeV	$m_\pi = 805$ MeV
m_{QCD}	1050	1226(12)	1320	1600(18)
m_π	300	449.9(4.6)	510	805.9(8.9)
$m_\Delta - m_N$	-	$\sim$260	$\sim$300	$\sim$180
m_{1pe}	$\sim$90	$\sim$160	$\sim$200	$\sim$400
m_{nuc}	$\sim$10	-	$\sim$15	$\sim$25

Table 1.2: Energies scales over a range of pion masses in LQCD calculations. When present in literature, we considered the stochastic and systematic uncertainties as an global error given by their quadratic composition.

change the convergence, that can be precisely evaluated only a posteriori, comparing the contribution of each order of the interaction. Moreover, many studies were performed in few-body systems such as deuterium and tritium using EFT($\not\pi$) [10, 12–14]. Those calculations showed that the contact power counting is successful and converges at least for the first few orders in the interaction. In this thesis we want to study the contact theory convergence at LO in bigger systems like ^{4}He and ^{16}O. The alpha particle provides the ideal test for proving the predictive power of the theory, while ^{16}O gives some useful indications about the behavior of the theory when approaching saturation density.

Unphysically high pion mass In this thesis, we also develop a EFT($\not\pi$) starting from results of LQCD calculations. This was possible because of the improvements of the Lattice calculations, which are now able to perform calculations on multi-hadron systems as deuterium, double neutron, ^{3}He and ^{4}He. Many groups are now extending calculations on the lattice in many nucleon systems [NPLQCD, PACS, CalLat, HALQCD...]. In Tab.(1.2) we are only displaying calculations in which the two particle system results bound, and consequently can be used to define a nontrivial low energy nuclear physics. LQCD calculations are still computationally very expensive. Bound states are found inside finite boxes whose length is pushed to infinity using the Lüsher method [15]. This is difficult to be done when quarks are light because the interaction length is much larger than the nucleon size, making the required length of the box impossible to be reached. Existing calculations were made feasible using unnaturally heavy quarks and larger than normal pion masses (m_π). While calculations with relatively small pion-mass have been performed by

few LQCD groups, in this work, we will focus only on the results yielding pion masses $m_\pi \sim 500$ MeV and m_π 800 MeV. The reason to focus on large pion masses, besides the fact that these were the only available calculations at the time this thesis was started, is that we are confident that pions do not play an explicit role in the interaction. It is not clear if an extrapolation to the physical pion mass from LQCD result is possible yet. However, the fact that nucleons in the $^3S_1$ channel are bound at high pion masses, but not in the physical case, might indicate the presence of a phase transition which would make difficult any extrapolations.

The data available up to now, shown in Tab.(1.2), shows how m_{1pe} increases with the pion mass. However, the average binding energy per nucleon (m_{nuc}), does not grow correspondingly. This is an evidence that the range of the interaction related to the pion mass is indeed very short, and a pionfull treatment is not necessary. The working goal is to use two and three particles observables calculated by LQCD groups in order to fit a pionless theory at LO. The potential, which requires two observables in the two-body channel and one in the three-body, is then used to make a prediction for the four-body system. The prediction is then compared with the four-body data from LQCD. This procedure is not only useful as benchmark of LQCD calculations, but it is also a consistency check for pionless theory in a framework in which it is supposed to be the appropriate theory.

An interesting fact is evidenced by data in Tab.(1.2). It shows that the nucleon mass is always 800 MeV higher than the pion mass. Even if, the two masses are correlated, the motivations for this phenomena are still debated.

In order to make predictions on ^{4}He and ^{16}O nuclei, one has to solve the Schrödinger equation for many-nucleon systems. We used QMC that is able to do it, in principle, without uncontrolled approximation. It can deal with a high number of particles (~ 90) and calculate ground state energies with only a statistical error that can be reduced systematically increasing the calculation time. The different QMC techniques used in this work are described in detail in chapter {4}.

2. Effective Field Theory

The aim of Physicists is to understand and model the nature in the simplest and most understandable way. If we needed to know perfectly all the mechanics up to the smallest components of physics in order to make conclusions on macroscopic systems, science, as we know it, would not be possible. The existence of a qualitatively and sufficiently accurate description of gravity in terms of spherical planets and $\sim \frac{1}{r}$ forces allows for the development of the Newtonian theory. The possibility to divide natural phenomena in few/many self-consistent theories with different DoF is called *separation of scales*. Its existence is not supported by any mathematical theorem, but our experience in physics shows that it is a reasonable assumption.

Atomic physics is a clear example of the concept of separation of scales, electrons and nuclei are the relevant DoF if phenomena as ionization are studied. The presence of a structured nucleus is irrelevant in the absorption process of photons of few eVs. Nonetheless, if we irradiate the atomic target with sufficiently high energy, transition in the nuclear structure may appear, revealing the limits of the Born–Oppenheimer approximation. The separation of scales is defined by the difference between the typical energy scales of the described process (eVs) and the *breakdown* energy for which the theory no longer makes sense because it lacks the correct DoF (MeV). The two ways to see the same physical systems are elements of the Renormalization Group (RG) in which it is possible to make transformations of DoFs (in this case the protons and neutron become a single particle nucleus) and the interactions among them in order to describe the same low energy observables (like ionization). The two different set of DoF and interactions that can be used to describe the system, and connected by the RG transformation, are called *theory fixed points*. They are a mathematical representation of the energy scales that we use to divide Physics.

The description of the macroscopic system (the atom) using microscopic DoF (electrons and the nucleus composed of neutron and protons) is simple

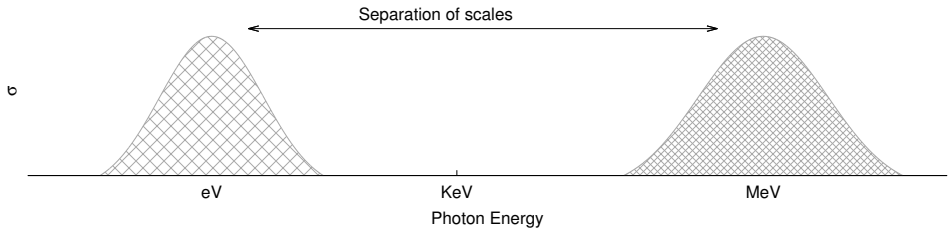

Figure 2.1: Artistic representation of a separation of scale.

in principle. However, it might be impossible to perform actual calculations, because of the large number of bodies involved and the complexity of the interaction. The microscopic description of the macroscopic physics, for instance the absorption of high energetic photons in the nucleus, is possible only if the RG transformation is reversible. Usually, this is not true and the lack of microscopic DoFs in the theory makes the description of the nucleus energy levels very complicated or even impossible.

The key to treating a scale separation is changing the system DoFs and remodeling the interaction between them. Effective Theory (ET) provides a prescription to redefine an interaction changing its the theory resolution in order to have a simpler description of the relevant system's proprieties. The new description of the problem might change the dynamic of the theory for high moments, well described only by the fundamental theory. Nonetheless, the *hard* dynamics (high moments contributions to observables) are assumed to be irrelevant because of the presence of a separation of scales.

In the Wilson [16] view of RG, if the theory contains a separation of scales one can set a breakdown cut-off Γ over which all the moments are considered hard and below which all the moments are considered soft. If there is a gap between theories it is irrelevant where to put Γ inside the gap.

The change of the degrees of freedom and the choice of Γ are equivalent to set to zero all the theory components above that threshold. In fact, the resolution of the theory is too small to be described as independent particles nor their excitation or the nucleus internal structure can be correctly described. The renormalization group flow is recovered integrating out the momenta in the gap (left inside the soft region), up to a second arbitrary cut-off $\Lambda < \Gamma$, making the interaction between the soft DoF dependent from the choice of Λ. This shows how important it is to set Γ close to the hard threshold in order to have more freedom in the choice of Λ. Nonetheless, if the gap is

sufficiently large/empty the observables are not sensible to changes in Λ if it remains inside the gap area. Since the construction of the theory integrates out all the hard components of the interaction there is no point to increase $\Lambda > \Gamma$ since operators would not change further, but it is in principle possible since $\Lambda \to \infty$ is not a theory singularity anymore.

The fact that any fixed point of the theory can be described by DoF interacting by local interactions has never been proven. However, it is the case of all known physical systems. This means that the interaction between DoF can be expanded in terms of Dirac functions δ, as described by Lepage [11]. When a δ function is used, the interaction will add a divergence in the theory. This reflects the fact that a local interaction would take into account infinite moments. A standard way to deal with this problem is the *regularization/renormalization* procedure: the δ is smeared, used to calculate observables and then pushed again to a local interaction in a second moment. The procedure is convergent because of the introduction of Γ in the redefinition of the DoFs. This procedure will be seen in detail in the next section.

The *regularization/renormalization* procedure has the same meaning as the integration over the Wilson soft cut-off Λ. The RG flow in the Lepage idea of renormalization can be seen changing the smeared δ cut-off inside the theory gap or beyond. While the most intuitive way of imposing a cut-off in momentum space is to use a sharp function, it is usually more convenient to use a smooth function.

If it is possible to flow a hard theory to a soft one and it is possible to define the breaking cut-off Γ the observables will become Λ-independent when the latter is sufficiently large, and the theory is called *renormalizable*. If all the operators of the new theory show such behavior, the theory is *completely renormalizable*. A theory is called *renormalizable order by order*, if its operators can be divided into groups for which their cumulative contribution does not depend on Λ (but any single contribution might). If the theory can not give cut-off independent observables even summing operators, the theory is not renormalizable and lacks predictive power. We do not know how to treat non-renormalizable theories in order to make prediction.

The role of EFT is to find a convenient operator expansion to describe the soft interaction. In order to have the simplest description of the problem, the new operatorial expansion should be arranged in such a way that the operators most contributing to the Lagrangian are as few as possible. It will

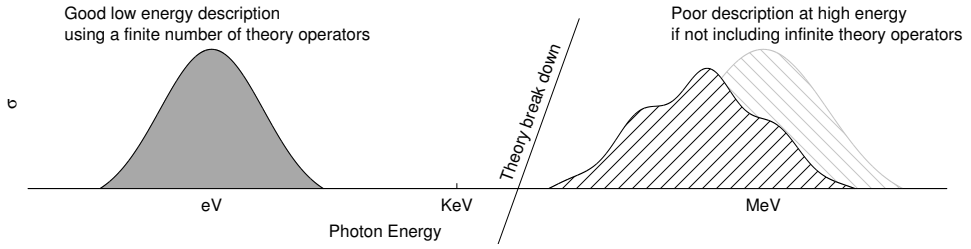

Figure 2.2: Qualitative description of a separation of scales (like atomic photo-absorption). The low-energy observables will be described with good precision, but the theory can not resolve the most energetic dynamics. The break down of the theory can occur at different energy for different observables.

be possible to recover the complete picture of the problem including all the infinite terms of the expansion. The possibility of integrating out the majority of the operators in the full Lagrangian in the soft momentum region makes the study of any problem easier with respect to the complete one. In fact, this allows to arrange operators in *orders* of decreasing importance for each of them. This is impossible to do if there is no separation of scales or the DoF are not appropriate to describe the problem. Operators whose contribution to any observable drops when flowing from the fundamental to the low energy theory are called *irrelevant*. Operators that contribute more and more are called *relevant*. All the others are called to be *marginal*.

The position of any operator inside the hierarchy is defined by its contribution to observables but also from its behavior under renormalization procedure, that can be used in order to cancel residual Λ dependencies order by order. The ordering in presence of this kind of theory will be discussed in more detail later, in the framework of the $\not\pi$ theory. The common procedure consists of initially arranging the potentials in orders with respect to increasing powers of a small parameter which helps to have a naive idea of the interaction, then adjust it in order to renormalize the theory. We expect each order contribution to observables to be suppressed with respect to the previous ones by a factor $\left(\frac{m}{M}\right)^n$, where M is *some* scale of the fundamental theory (e.g. the nucleon breaking energy for atomic photon-scattering) and m is a relevant scale of the low energy theory (e.g. the ionization energy) not know a priori. As long as there is a separation of scales in the system such that $M \gg m$ only few operators need to be included in the description, according to the empirical statement that the soft theory should have smaller complexity with respect the underlying one.

While many fields in physics display an evident separation of scales, in others, like nuclear physics, its existence is still not clear and debated. In this case, the presence of meson exchange makes the whole picture much more complicated and does not allow for a clear, or natural, definition of m and M. To give a hierarchy to the operators of such theory both the naive power counting and renormalization arguments should be used.

A classical reading on ET about the usage of point-like particles and contact (δ) expansions in the limit of small energy can be found in the work of P. Lepage in Ref.[11]. For a more formal description of the problem Wilson's work [16] gives a clearer description of RG in the case of scale separation. The construction of Polchinski [17] (and the Effective Average Action for infrared cut-offs [18]) describes the problem using smooth cut-off functions as Lepage examples do, but in a Wilson-like approach.

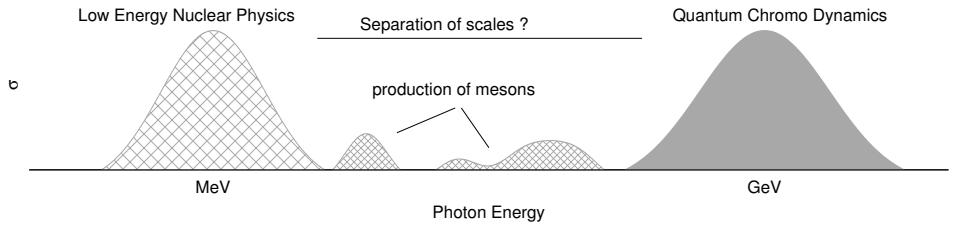

Figure 2.3: In nuclear/hadronic physics, the meson production at energies between the typical scale of nuclear bound and nucleon mass makes the scales separation less obvious.

2.1 Renormalization

In this section, the Lepage theory of potential renormalization will be shown. We will define a cut-off Λ in order to use a divergent theory to predict observables. The procedure is the same we will follow when EFT($\not\pi$) nuclear potential will be introduced later in this chapter. In fact, nuclear potentials can be re-expanded in terms of contact interactions and derivatives of the same kind as the one described in this section.

3D simple contact interaction

The simplest example of regularization and of the necessity of introducing a regularization procedure is the 3D-δ potential in quantum mechanics. In the whole section, we will assume units such that: $\frac{\hbar^2}{2m} = 1$.

The Schrödinger equation with contact interactions reads:

$$\left(-\nabla^2 - \lambda\delta\left(\vec{x}\right)\right)\psi\left(\vec{x}\right) = E\psi\left(\vec{x}\right) \tag{2.1}$$

which, in momentum space, can be rewritten as:

$$\left(\hat{k}^2 - E\right)\psi\left(\vec{k}\right) = \lambda\int\frac{d^3q}{\left(2\pi\right)^3}\psi\left(\vec{q}\right). \tag{2.2}$$

Applying $\left(\hat{k}^2 - E\right)$ to the wave function and dividing for the eigenvalues, then integrating both sides with respect to k one finds:

$$\begin{aligned}\frac{1}{\lambda}\cancel{\int\psi\left(\vec{k}\right)d^3\vec{k}} &= \cancel{\int\psi\left(\vec{q}\right)d^3\vec{q}}\int\frac{d^3k}{\left(2\pi\right)^3}\frac{1}{\left(\left|k\right|^2 - E\right)}\\ \frac{1}{\lambda} &= \int\frac{d^3k}{\left(2\pi\right)^3}\frac{1}{\left(\left|k\right|^2 - E\right)} = \int_0^{+\infty}\frac{dk}{\left(2\pi\right)^3}\frac{k^2}{\left(\left|k\right|^2 - E\right)}.\end{aligned} \tag{2.3}$$

In this integral we find the first appearances of divergences in the theory. In fact, the integral can be trivially generalized to any dimension D, but it converges only if $D < 2$.

To overcome the problem one needs to *regularize* and then *renormalize* the theory. The *regularization* consists in truncating the integrals in order to

make observables finite. A new parameter Λ, corresponding to the maximum value of the momentum up which we want to perform integration is introduced in the theory. The most natural regularization procedure consists in truncating integrals using a sharp function. Alternatively, a smearing function that suppresses high moments can be used. Dimensional regularization is the third option to make integrals finite. It consists in changing the integral dimension to make expectation values finite, then restoring it in a second moment.

When the cut-off is introduced, the observables become dependent on it. However, the cut-off is not a physical quantity, so we need to *renormalize* the theory introducing a cut-off dependence in the interaction strength too.

$$\frac{1}{\lambda_\Lambda} = \int_0^\Lambda \frac{dk}{(2\pi)^3} \frac{k^2}{\left(|k|^2 - E\right)}. \tag{2.4}$$

If the energy were the only relevant observable in the problem, this procedure would have no predictive power since the coupling will require an observable to be fitted and the observable will be completely defined by the interaction. However, once λ_Λ is determined in this manner, it can be used to calculate any other observable in the problem. In fact, observable estimations will be finite and cut-off independent when the cut-off is high enough.

To prove the predictive power of this exercise, consider the scattering of two particles with a delta potential. The Lippmann-Schwinger [19] equation for the T-matrix between two states $|\vec{p}\rangle$ and $|\vec{p'}\rangle$:

$$\langle\vec{p'}|T|\vec{p}\rangle = \langle\vec{p'}|V|\vec{p}\rangle + \langle\vec{p'}|V\frac{1}{p^2 - H_0 + i\eta}|\vec{p}\rangle\,, \tag{2.5}$$

where p^2 is the particle energy and H_0 is the free Hamiltonian. With the insertion of the unitary relation:

$$\mathbb{1} = \int d^3\vec{q}\,|\vec{q}\rangle\,\langle\vec{q}|, \tag{2.6}$$

remarking that

$$H_0\,|\vec{q}\rangle = |\vec{q}|^2\,|\vec{q}\rangle \tag{2.7}$$

and using

$$\langle\vec{q_1}|V|\vec{q_2}\rangle = -\frac{\lambda}{(2\pi)^2} \tag{2.8}$$

where q_1 and q_2 are momentum eigenstates, it can be written:

$$\langle \vec{p'}|T|\vec{p}\rangle = -\frac{\lambda}{(2\pi)^3}\left[1 + \int d^3\vec{q}\frac{1}{p^2 - q^2 + i\eta}\langle \vec{q}|T|\vec{p}\rangle\right] \tag{2.9}$$

Notice that $\langle \vec{p'}|T|\vec{p}\rangle$ does not depend from $\langle \vec{p'}|$. Hence we can substitute $\langle \vec{q}|T|\vec{p}\rangle$ in Eq.(2.9) with $\langle \vec{p'}|T|\vec{p}\rangle$ obtaining:

$$\langle \vec{p'}|T|\vec{p}\rangle = \frac{1}{(2\pi)^3\left[I - \frac{1}{\lambda}\right]}, \tag{2.10}$$

where

$$I = \int \frac{d^3\vec{q}}{(2\pi)^3}\frac{1}{p^2 - q^2 + i\eta} \tag{2.11}$$

which is not convergent. The relation between the matrix element and the cross section is:

$$\sigma = \frac{8\pi^{11/2}}{\Gamma(3/2)}\left|\langle \vec{p'}|T|\vec{p}\rangle\right|^2, \tag{2.12}$$

where $\langle \vec{p'}|T|\vec{p}\rangle$ is finite and cut-off dependent. The energy of the system is used to fix λ_Λ for each cut-off. The method of renormalization and regularization gives a prediction of σ which is finite. The further step is to demonstrate that observables are cut-off independent when the cut-off is high.

Eq.(2.4) for large Λ can be computed as:

$$\frac{1}{\lambda_\Lambda} = \frac{\Lambda - \sqrt{|E|}\,Arctan\left(\frac{\Lambda}{\sqrt{|E|}}\right)}{2\pi^2} \approx \frac{1}{2\pi^2}\left(\Lambda - \sqrt{|E|}\frac{\pi}{2}\right) \tag{2.13}$$

Which leads to:

$$E = \left(\frac{2\Lambda}{\pi} - \frac{4\pi}{\lambda_\Lambda}\right)^2. \tag{2.14}$$

The two previous equations show the dependence of the parameter λ_Λ with respect to the cut-off Λ assuming the binding energy of the system is the fixed observable in the theory. It can be noticed that the energy in Eq.(2.14) can not be held finite for $\Lambda \to +\infty$ if λ_Λ is finite too. This kind of behavior is common in contact theory and will be found also in the case of $\not\pi$ theory.

Eq.(2.11) can be refined if $\Lambda \to +\infty$:

$$I_\Lambda = \int_0^\Lambda \frac{d^3\vec{q}}{(2\pi)^3}\frac{1}{p^2 - q^2 + i\eta} \approx \frac{1}{2\pi^2}\left(\Lambda + ip\frac{\pi}{2}\right). \tag{2.15}$$

Inserting Eq.(2.14) and Eq.(2.15) in Eq.(2.10) then using Eq.(2.12) the cross-section can be finally computed:

$$\begin{aligned}\sigma = \frac{8\pi^{11/2}}{\Gamma(3/2)}\frac{1}{\left|(2\pi)^2\left[I_\Lambda - \frac{1}{\lambda_\Lambda}\right]\right|^2} = \\ \frac{8\pi^{11/2}}{\Gamma(3/2)}\frac{1}{\left|\frac{1}{\pi^2}\left[\left(\Lambda + ip\frac{\pi}{2}\right) - \left(\Lambda - \sqrt{|E|}\frac{\pi}{2}\right)\right]\right|^2} = \\ \frac{4\pi}{E - p^2}\end{aligned} \tag{2.16}$$

which is cut-off independent.

This example illustrates how divergences appear even with apparently simple potentials of standard quantum mechanics. It is, in this case, the consequence of the extreme singularity of the interaction. The process of regularization and renormalization changes the Hamiltonian and introduces a cut-off dependence in the couplings. However, since the cut-off is not a physical quantity, observables should not depend on it. In Eq.(2.10) we have the cancellation of all the divergences, this is true for any other observable in the problem. It should be noticed that the cancellation comes only with the limit of $\Lambda \to +\infty$ when we can approximate $Arctan\left(\Lambda/\sqrt{|E|}\right)$ with $\pi/2$. A residual dependence is expected if the condition $\Lambda \gg |E|$ is not satisfied.

Cut-off regularization is only one of the methods which can be used in order to regularize/renormalize potentials. Other methods, as dimensional regularization might be used instead. For more details about regularization of deltas in three and other dimensions, as well as different regularization method, look at Ref.[20].

2.2 Contact effective field theory

The construction of an Effective Field Theory consists of the (re)expansion of an underlying fundamental theory on a new set of operators. These operators obey to the same relevant symmetries as the original interaction and act on the relevant low-energy DoF. The resulting terms are then reordered in such a way that they can be treated within perturbation theory according to a suitable small parameter.

For many nucleon-systems, we want to **consider processes in which exchanged momentum between particles is much smaller than the pion exchange mass-scale.** This allows to neglect the long range part of the pion interaction since they are too heavy to be created as off-shell particles.

To construct the effective interaction, it is sufficient to take into account all the possible field diagrams which share the relevant symmetries with the underlying theory. The fundamental, fully relativistic, theory which in principle allows the description of nuclei from the first principle is QCD. Low-energy processes in nuclear physics involve momenta small enough to justify the use of a non-relativistic approach. Consequently, the nucleon number is conserved and the nuclear dynamics can be described within a non-relativistic many-body theory, while the nuclear potential needs to include only parity and time-reversal conserving operators, and satisfy invariance under small Lorentz boosts. All relativistic correction will be sub-leading, and appear at next to next to leading order ($\mathrm{N^2LO}$), together with the Coulomb force [21, 22].

The general Lagrangian of a $\not\pi$-EFT is written as [9]:

$$\begin{aligned}\mathcal{L}^{2b} &= N^\dagger\left(i\partial_0 + \tfrac{\vec{\nabla}^2}{2m_N} + \tfrac{\vec{\nabla}^2}{8m_N^3} + ...\right)N + C_0 N^\dagger N N^\dagger N + \\ &+\frac{C_2}{8}\Big[N^\dagger\left(\overleftarrow{\nabla} - \overrightarrow{\nabla}\right)N N^\dagger\left(\overleftarrow{\nabla} - \overrightarrow{\nabla}\right)N - \\ &-N^\dagger N N^\dagger\left(\overleftarrow{\nabla} - \overrightarrow{\nabla}\right)^2 N\Big] + ...\,,\end{aligned} \tag{2.17}$$

Hence the nucleon field is redefined in such a way that the term $N^\dagger m_N N$ is canceled. This field transformation is intuitive since nucleons are slow particles and their dynamics will not have any role in the scattering matrix. The following description will take into account one coupling channel of the inter-

action, while the extension to all the channel is trivial and will be considered later.

Dimensional analysis and naive power counting

The dimensional analysis gives a naive idea about the magnitude of each coefficient in the expansion (2.17). However, this analysis should be taken only as an indication since correlations in the system and renormalization process might change the order of operators drastically. Since in Natural systems [9] there are only two mass scales, m_π and m_N, which we suppose much larger than the exchanged moments, the counting of mass powers is straightforward. In the following, we will consider the example of nuclear systems neglecting spin and isospin dependencies. The extension of the theory is trivially achieved repeating the same expansion and projecting it in each spin-isospin channel allowed by the system.

The action of the system is a dimensionless quantity, hence the Lagrangian should have dimension $\mathfrak{D}(\mathcal{L}) = l^{-4}$ which, in units of $\hbar = c = 1$, is m^4. Considering that the Lagrangian is a dimensional quantity, any coupling constant in the theory will have a dimension that has to be justified by the presence of mass scales. For example, if a coupling C has dimension $\mathfrak{D}(C) \approx \frac{1}{M^3}$ one should expect that M^3 is a combination of m_π and m_N.

The fermionic field has dimension $\frac{3}{2}$ since:

$$\mathfrak{D}(\mathcal{L}) = \mathfrak{D}\left(N^\dagger \left(\frac{\vec{\nabla}^2}{2m_N}\right) N\right) = 4, \tag{2.18}$$

where $\mathfrak{D}(X)$ indicates the dimensionality of X. $\mathfrak{D}\left(\frac{\vec{\nabla}^2}{2m_N}\right) = 1$, and then $\mathfrak{D}(N) = 3/2$. It is possible to calculate the dimensionality of all the coupling constants in Eq.(2.17) in the same way:

$$\mathfrak{D}(C_0) = \frac{1}{M^2} \tag{2.19}$$

$$\mathfrak{D}(C_2) = \frac{1}{M^4}. \tag{2.20}$$

One performs the complete calculation of the mass dependence of any diagram using the general relation

$$\mathfrak{D}\left(C_{n,D}\right) = \frac{(4\pi)^{N-2}}{M^{D-4}}, \tag{2.21}$$

where N is the number of fermionic fields attached to the operator and D is the dimension of the relative operator. Each Low Energy Constant (LEC) is expected to behave according to the mass scale power defined by the operatorial structure, with a fine-tuning $\Delta_{n,D}$ coming from the very particular correlations of the system.

$$C_{n,D} = \Delta_{n,D}\frac{(4\pi)^{N-2}}{M^{D-4}}, \tag{2.22}$$

Nonetheless, we expect $C_{n,D}$ to be of the same magnitude as its mass dependence. Hence $\Delta_{n,D} \sim 1$, this is called *naturalness* condition. Naturalness is not strictly required by the power counting since the contribution of a specific operator depend on the correlation of the system too. However, it is desirable and expected if the system does not present not-trivial correlations.

It becomes clear that, in the case of contact interaction, the more derivative powers are present in a given Lagrangian term, the more it will be demoted in the power counting.

Coefficient	**Operator**	**# of N fields**	**Mass Power**	**Naive Order**
kinetic $(\frac{1}{2m_N})$	$\approx \nabla^2$	2	M^{-1}	LO
C_0	$\mathbb{1}$	4	M^{-2}	NLO
C_2	$\approx \nabla^2$	4	M^{-4}	$\mathrm{N^2LO}$
D_0	$\mathbb{1}$	6	M^{-5}	$\mathrm{N^3LO}$
C_4	$\approx \nabla^4$	4	M^{-6}	$\mathrm{N^4LO}$

The simplest EFT is a theory that does not predict any bound states nor shallow resonances in the T-matrix. Such theory is just a free theory with perturbations. The nucleons propagate free subjected to a small contact potential, which is perturbative with respect to the free propagator.

As described in section {2.1}, in order to calculate the Low Energy Constants (C_0, C_2, ...) one has to choose a few observables to be fitted. At this point, any two-body observable, such as the scattering length at zero energy a_0, will be sufficient to fit the NLO constant C_0. When the next order is included, a new constant appears in the two-body interaction, e.g. it can be

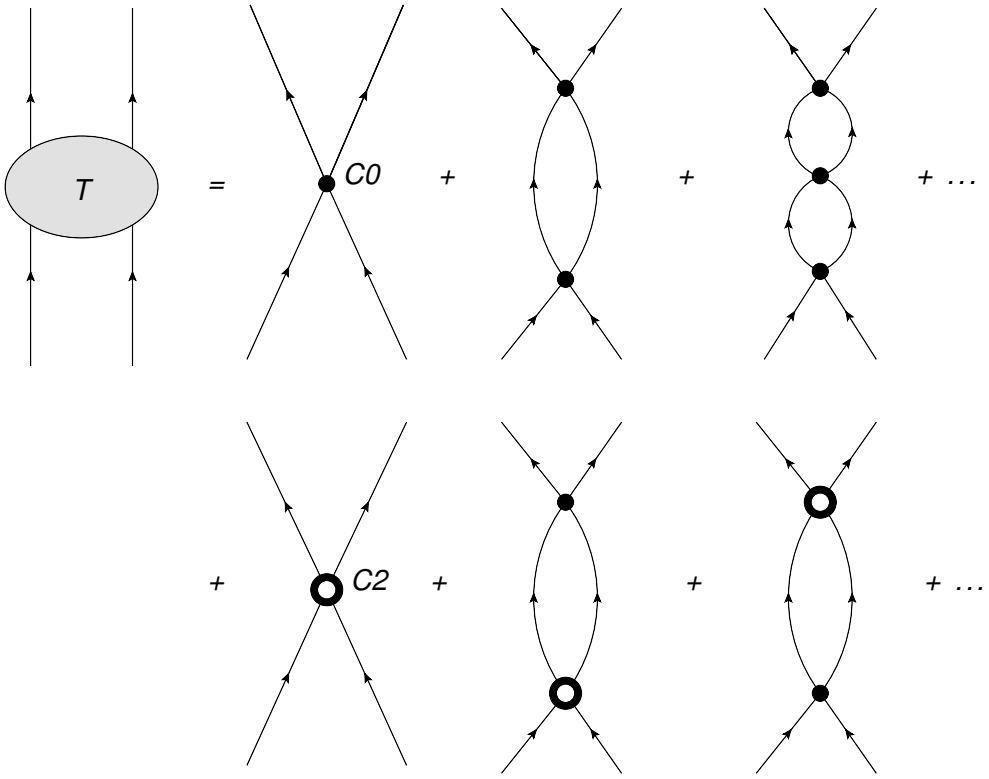

Figure 2.4: T-matrix diagrammatic expansion. The relative importance of each contribution is driven by the mass power of vertexes. The bold vertex represents C_0, which contribute to the amplitude as $1/M^2$ and the empty circles are $C_2 \approx 1/M^4$ vertexes.

fitted with the system effective range r_0. Any new diagram has to be included according to perturbation theory and it will modify the value of the first fixed observable (a_0). To recover the correct scattering length after the new inclusion, we need to add a *counterterm* with the same structure of the therm used to fit the observable, but at the higher order. For example, when fitting C_2 and the relative counter term C_0^*, C_0 should NOT be modified. Although, C_2 and C_0^* should be fitted together in order to reproduce the observables (a_0 and r_0). In the same way, the inclusion of more orders of the interaction will not modify the other already fitted parameters.

It should be noticed that there are two kinds of possible expansions, one in the power of the mass-scale in the vertexes $\left(\frac{Q}{M}\right)^n$ and one in the number of loops of the diagram. The T-matrix will be calculated including the diagrams as shown in Fig.(2.4) up to a given order:

$$
\begin{aligned}
T(p) = &-iC_0\left(\Lambda\right) + \\
&- iC_0^2 \int \frac{d^4l}{\left(2\pi\right)^3} \left[\frac{1}{l^{[0]} + p^{[0]} - \frac{\left(\vec{l}+\vec{p}\right)^2}{2m_N} + i\epsilon}\right] \left[\frac{1}{-l^{[0]} + p^{[0]} - \frac{\left(\vec{l}+\vec{p}\right)^2}{2m_N} + i\epsilon}\right] + \\
&- iC_0C_2 \int \frac{d^4l}{\left(2\pi\right)^3} l^2 \left[\frac{1}{l^{[0]} + p^{[0]} - \frac{\left(\vec{l}+\vec{p}\right)^2}{2m_N} + i\epsilon}\right] \left[\frac{1}{-l^{[0]} + p^{[0]} - \frac{\left(\vec{l}+\vec{p}\right)^2}{2m_N} + i\epsilon}\right] + \\
&\cdots ,
\end{aligned}
\tag{2.23}
$$

where the integrals are performed in 4-momentums and p is the momentum of the incoming particles in the center of mass frame. Loops can be simplified using the residual theorem to integrate out $l^{[0]}$ and changing the integration variable $\vec{l} + \vec{p} \to \vec{l}$:

$$
\begin{aligned}
&T^{(n)}_{1loop}(p) = \\
&- i\alpha \int \frac{d^4l}{\left(2\pi\right)^3} l^{2n} \left[\frac{1}{l^{[0]} + p^{[0]} - \frac{\left(\vec{l}+\vec{p}\right)^2}{2m_N} + i\epsilon}\right] \left[\frac{1}{-l^{[0]} + p^{[0]} - \frac{\left(\vec{l}+\vec{p}\right)^2}{2m_N} + i\epsilon}\right] = \\
&\qquad\qquad - i\alpha \int \frac{d^3\vec{l}}{\left(2\pi\right)^3} \frac{\vec{l}^{2n}}{\vec{l}^2 - 2m_N p^{[0]} - i\epsilon}
\end{aligned}
\tag{2.24}
$$

Where α represents the product of the LEC attached to any loop. On the top of the power counting, one has to renormalize the theory as described in sec.{2.1}. After the regularization, the integral becomes:

$$
T^{\Lambda,n}_{1loop}(p) \sim \Theta_{2n+1}\Lambda^{2n+1}, \tag{2.25}
$$

where n indicates the momentum power in the loop vertex. Θ is a function depending on the regularization scheme. It can be calculated that in the particular case of dimensional regularization with minimal subtraction $\Theta = 0$.

We do not require the theory to be renormalizable term by term, but the cut-off dependency should disappear when all the contribution of a given order are included, meaning, in this case, that the theory is renormalizable is order by order. This has important consequences in the power counting scheme since we expect any divergent term of a given order to have the same behavior in the cut-off when this is large. If a term of an order of the theory is missing,

the cut-off dependency of the others will not be compensated. In this case, the appearance of divergencies at large Λ is an effect of the missing term, at it does not mean that the theory itself is not renormalizable. Looking at the large cut-off behavior we have a powerful tool to understand if the theory is complete. However, the process of promoting or demoting a term for renormalization reasons is not an artifact of renormalization process, but it is rather due to nontrivial correlations between particles and it should not depend on the regularization scheme.

2.3 Short range forces in presence of poles

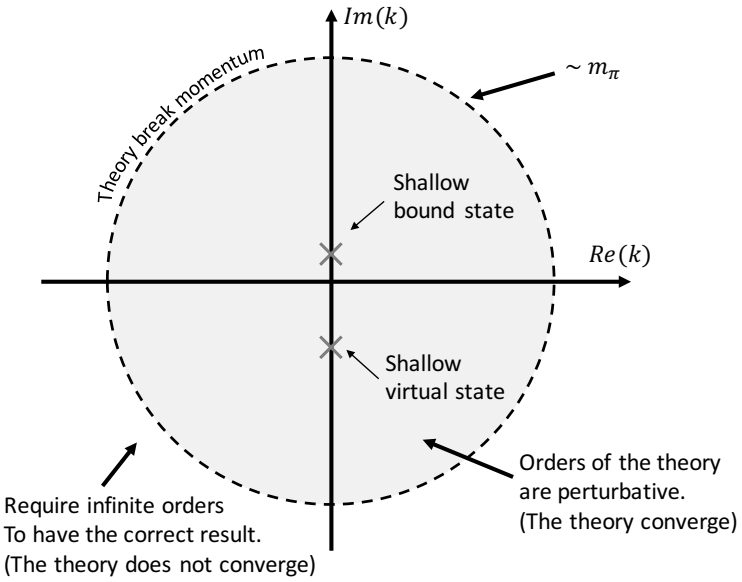

Figure 2.5: The LO of the two-body scattering matrix has to be calculated including all the loops in order to recover the correct pole in the complex momentum plane.

The case of a bound system (or a system with a shallow virtual state) is much different from the already discussed case. In nature, the two-nucleon system shows a bound state (deuterium) with an energy of about BE(d)= 2.22 MeV, which corresponds to a binding momentum $k_{pole} = \sqrt{M_N B}$ that is reflected in a pole of the T-matrix. Moreover, this system has a second shallow pole in the ${}^3S_1$ channel. It is related to a virtual state and it affects the scattering length making it much larger than the typical dimension of the nucleon. The perturbative theory described above is not able to recreate such poles of the T-matrix inside its range of convergence. In other words, this means that it is not possible to recreate the poles with a contact EFT without summing infinite diagrams.

In order to describe a system with poles in the T-matrix, we have to

promote two-body interactions, in the channels in which we have poles, to the LO. The poles in the two-body system are in S-wave. Therefore we need to treat the corresponding operators in a nonperturbative way as shown in Fig.(2.6).

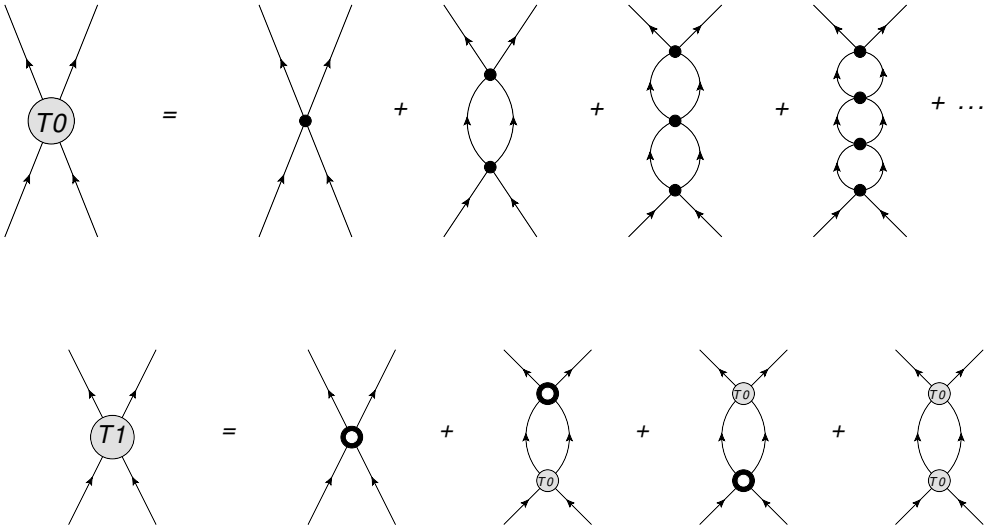

Figure 2.6: In the atop panel the LO contribution to the T-matrix and in the bottom one the NLO one calculated in perturbation theory. Notice how the LO is treated not perturbatively. Empty circles are the NLO vertex, C_2, associated to momentum square operator.

The sum of infinite diagrams is not a trivial task. However, it can be performed analytically taking the loop contribution from Eq.(2.24) and recalling that vertex contribution at LO is C_0. Defining the transfer momentum as $\vec{k}$:

$$\begin{aligned} T^{(0)} = & \\ & C_0^\Lambda + C_0^\Lambda T_{1loop}^\Lambda\left(\vec{k}\right) C_0^\Lambda + C_0^\Lambda T_{1loop}^\Lambda\left(\vec{k}\right) C_0^\Lambda T_{1loop}^\Lambda\left(\vec{k}\right) C_0^\Lambda + ... \\ & = C_0^\Lambda \sum_{i=0}^{\infty} C_0^\Lambda T_{1loop}^\Lambda\left(\vec{k}\right) \\ & = \frac{C_0^\Lambda}{1 - C_0^\Lambda T_{1loop}^\Lambda\left(\vec{k}\right)} \end{aligned} \tag{2.26}$$

The integral (2.24) can be performed choosing a regularization. In the following example, it has been done with a sharp cut-off regularization.

$$T_{1loop}^{(0),\Lambda}\left(\vec{k}\right) = -\frac{m_N}{4\pi}\left(ik + \Theta_1\Lambda + o\left(\frac{k^2}{\Lambda}\right)\right) \tag{2.27}$$

From Eq.(2.26) and Eq.(2.27) one can calculate the LO contribution to the T-matrix:

$$\begin{aligned} T^{(0)} &= \frac{4\pi}{m_N} \frac{1}{\frac{4\pi}{m_N C_0} + ik + \Theta_1 \Lambda + o\left(\frac{k^2}{\Lambda}\right)} \\ &= \frac{4\pi}{m_N} \frac{1}{\bar{C_0^\Lambda} + ik + o\left(\frac{k^2}{\Lambda}\right)} \end{aligned} \tag{2.28}$$

Where the Λ cut-off dependency has been absorbed in the effective coupling $\bar{C_0^\Lambda}$:

$$\bar{C_0^\Lambda} = \frac{4\pi}{m_N C_0} + \Theta_1 \Lambda. \tag{2.29}$$

From Eq.(2.28) it is possible to find the corrections of the LO observable. Recalling the relation: $\frac{1}{1+x} \overset{x\leq 1}{=} \sum_{n=0}^{\infty} x^n$:

$$T^{(0),\Lambda} = \frac{4\pi}{m_N} \frac{1}{\bar{C_0^\Lambda} + ik} \left(1 + O\left(\frac{k^2}{\Lambda}\right) + ...\right) \tag{2.30}$$

where, for any finite cut-off Λ, the leading order is still affect by a correction of order $\frac{1}{\Lambda}$. Eq.(2.30) highlights how the power counting expansion will fail if the typical exchanged momentum is higher than the used cut-off.

The contributions of sub-leading order diagrams are much easier to be evaluated than the LO since they are treated perturbatively as in the case of the weakly interacting theory. New diagrams should be added to Eq.(2.28) with the purpose of canceling residual cut-off divergences up to the corresponding $T^{(n)}_{1loop}(p)$ power introduced in Eq.(2.24). It is then clear that any sub-leading loop should not be iterated more than once in order not to bring more Λ contributions than those needed in order to perform renormalization. In other words, not only it is worthless to treat sub-leading orders non-perturbatively, but it can also be inconsistent with the renormalization scheme.

Contact theory and Effective Range Expansion

The expansion of the potential in terms of contact interactions can be described both in terms of a Dirac's δ in coordinate space or in terms of power of the center of mass momentum $|\vec{k}|$ in momentum space. It leads to a T-matrix expansion (Eq.(2.28)) very similar to the Effective Range Expansion (ERE) known from elementary scattering theory:

$$T(k) = \frac{2\pi}{m_N} \frac{1}{\left|\vec{k}\right| cot\left(\delta_0\right) - ik} \tag{2.31}$$

with

$$\left|\vec{k}\right| cot\left(\delta_0\right) = -\frac{1}{a_0} + \frac{1}{2} r_0 \left|\vec{k}\right|^2 + r_1 \left|\vec{k}\right|^4 + \cdots \tag{2.32}$$

where δ_0 is the phase-shift, a_0 is the scattering length at zero energy, r_0 is the effective range and depends, as r_1, on the length of the interaction. In all the systems we will discuss, the N-N scattering length is unexpectedly larger than the typical nucleon radius both in the ${}^1S_0$ and ${}^3S_1$ channels. Hence, it is convenient to rewrite the above expansion around the momentum corresponding to the binding energy of deuterium, which is a relevant scale of the theory:

$$\begin{array}{lccccc} \left|\vec{k}\right| cot\left(\delta_0\right) = & -\gamma_t & +\frac{1}{2}\rho_d \left(\left|\vec{k}\right|^2 + \gamma_t^2\right) & +\omega_2 \left(\left|\vec{k}\right|^2 + \gamma_t^2\right)^2 & +... \\ & \mathcal{O}\left(Q\right) & \mathcal{O}\left(Q^2\right) & \mathcal{O}\left(Q^4\right) & \end{array} \tag{2.33}$$

where γ_t, ρ_d and ω_2 are expansion parameters [1]. The same hierarchy in terms of exchanged momentum can be done as in EFTs. In fact, the similarity between Eq.(2.31) using Eq.(2.32) and Eq.(2.28) is impressive and one can identify the low energy scattering parameters with EFT quantities at a given order like in:

$$\frac{1}{a_0} = \frac{4\pi}{m_N C_0} + \frac{2}{\pi}\Lambda. \tag{2.34}$$

This can also be compared with the example worked out in sec.{2.1} where we fixed the scattering amplitude. Calculating the behavior of the LEC fitting the scattering length we obtain:

[1] From [23]: $\gamma_t^1 = 4.318946$ fm, $\rho_d = 1.764$ fm and $\omega_2 = 0.389$ fm$^-3$

$$C_0(\Lambda) = \frac{4\pi}{m_N} \frac{1}{\frac{1}{a_0} - \Theta_\Lambda \Lambda}. \tag{2.35}$$

It is interesting to notice that using a sharp cut-off regularization, at LO there are no terms proportional to $|k|^2$ in the denominator. This reflects the fact that the contact theory is equivalent to an expansion around small momenta and the scattering length a_0 is correctly predicted at leading order while the effective range r_0 is associated to the NLO of the theory. The picture changes if the number of shallow poles of the T-matrix is multiple. In this case, more operators need to be promoted at LO. Nonetheless, this is not the case as $1/a_0 \gg r_0/2 \simeq a_0/m_\pi$, so the effective range is sub-leading with respect the scattering length.

Unnaturaly large scattering length

In two-body nuclear T-matrix we can notice the presence of a shallow momentum pole. His presence it is the consequence of the large scattering length compared with the typical nucleon size. In fact, in those systems $\aleph := a_0^{-1} \sim Q$ (Typical exchanged momentum of the system) [12], meaning that the inverse of the scattering length enters as a new mass scale in the power counting and the theory might require a rearrangement in the hierarchy of the operators. The mechanism fo rwich this happens is similar to the one that determine the need of a vertex promotion at LO when momentum poles are present in the convergence radius of the theory discussed in sec.{2.3}. However, the peculiar shallow character of this pole has deeper consequences in the power counting which results perturbed beyond the LO promotion.

The description of the system is unchanged when $Q \ll \aleph$, but the power-counting should be made in terms of $\left(\frac{Q}{\aleph}\right)^n$ instead of $\left(\frac{Q}{m_\pi}\right)^n$. The picture changes if $Q \sim \aleph$ because each loop in the expansion become equally important. However, we can sum them as we did in Eq.(2.26) at LO in a new contact interaction, whose magnitude is now $\aleph$ dependent. This is the case of the operator $C_2 k^2 \vec{p}' \cdot \vec{p}$ where $C_2^\Lambda \sim C_0^\Lambda \frac{(4\pi)^2}{M^2 c}$ in the natural case. After the Wilson sum of Eq.(2.26), a new mass dependence $\aleph$ is added in the T-matrix amplitude in the S-wave (obtained using $Q \sim \aleph$):

$$T^{(2),(\Lambda)} \propto \frac{\left(1+O\left(\frac{\aleph}{\Lambda}\right)^3\right)}{\bar{C_0^\Lambda} - 2C_2^{(\Lambda)}k^2 + 4\left(C_2^{2(\Lambda)} - C_4^{(\Lambda)}\right)k^4 + \frac{im_N k}{4\pi}\left(1+\frac{k^2}{2m^2}\right)} \tag{2.36}$$

which is not much different from the natural one that can be extracted further expanding Eq.(2.30):

$$T^{(2),(\Lambda)} \propto \frac{\left(1+o\left(\frac{k}{\Lambda}\right)^4\right)}{\bar{C_0^\Lambda} - 2C_2^{\Lambda}k^2 + \frac{im_N k}{4\pi}\left(1+\frac{k^2}{2m^2}\right)}. \tag{2.37}$$

Notice that the relative order of operators has changed. The k^4 terms are promoted at $o\left(\frac{\aleph}{\Lambda}\right)^3$ because of the introduction of $\aleph$. The promotion appears only in the channel where the shallow poles exist (S-wave). Eq.(2.36) shows how the shape parameter appears at the same order as the first P-wave contribution in this kind of theories. Normally $C_2^\Lambda \sim C_0^\Lambda \frac{(4\pi)^2}{M^2 c}$ and M is a mass-scale of the theory identified as m_π. However, the presence of $\aleph$ makes it $C_2^\Lambda \sim C_0^\Lambda (4\pi)^2 \left(\frac{1}{m_\pi^2 c} + \frac{1}{m_\pi \aleph c}\right)$ which is of order $\frac{1}{m_\pi}$ as long as $\aleph$ is small. The theory is then correctly described up to N2LO when promoting the P-wave channel operators. The same procedure can be lead to the promotion and/or demotion of other sub-leading order operators, such as relativistic corrections.

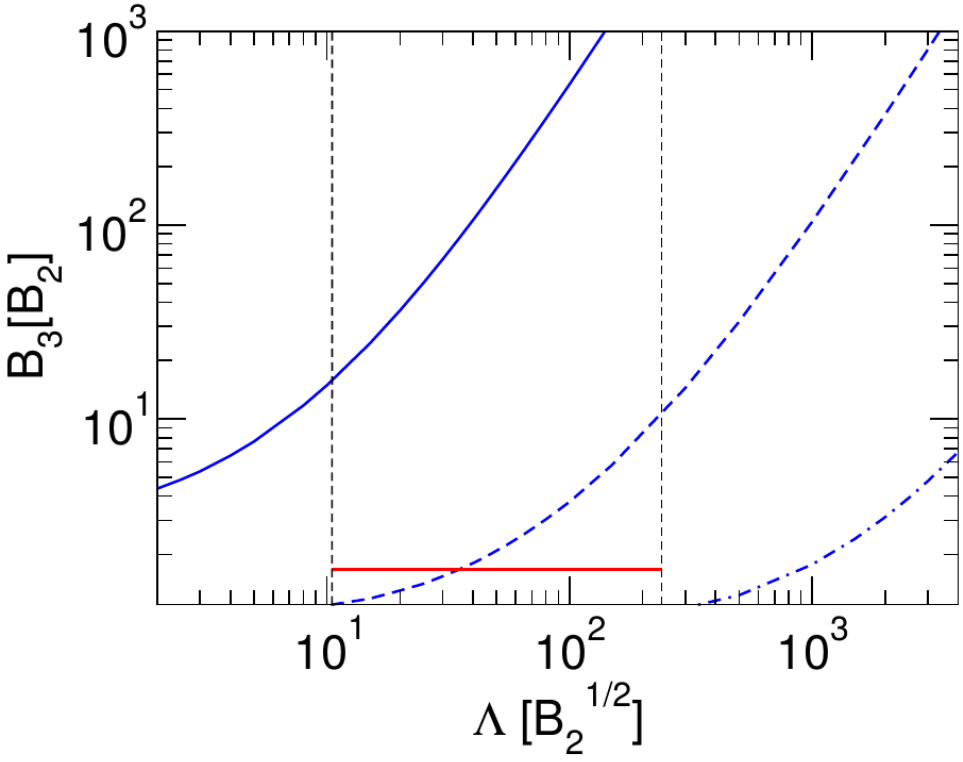

Figure 2.7: From Ref.[24]: The shallowest three-body binding energies indicated by the solid, dashed, and dash-dotted lines as a function of the momentum cut-off Λ. The vertical dashed line indicates the cut-off range in which the three-body system has exactly two bound states. The horizontal solid line shows the energy at which the shallowest three-body state is fixed.

Short range forces in three-body systems

The three-body system in the presence of an attractive interaction is an example of how the naive power counting unexpectedly fails already at LO. In fact, all the observables which concern more than two-body can no longer be properly renormalized. As it can be seen in Fig.(2.7), by increasing the cut-off the three-body binding energy calculated using only two-body interactions becomes increasingly bound without showing any sign of convergence. To cure the divergence one needs to add a three-body term that compensates the Λ dependence making observables renormalizable. Nonetheless the inclusion of a three-body operator of contact type it is sufficient not only for the three-body system, whose binding energy is now fixed by the new LEC, but also for the four-body system that shows observables independent from the cut-off as

well, as can be seen in Fig.(2.8).

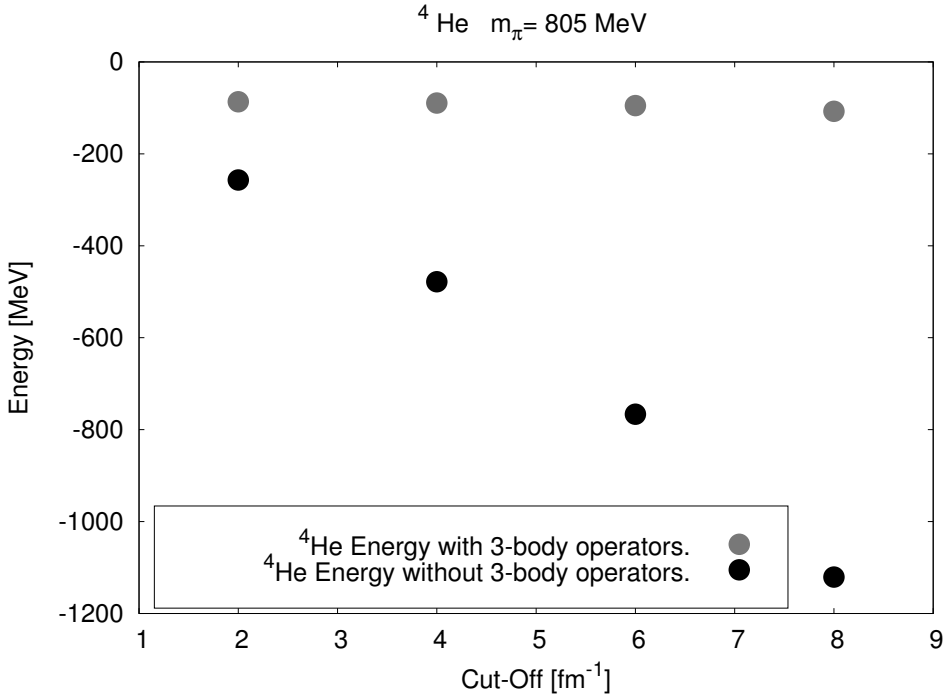

Figure 2.8: Four body binding energy in pion-less theory. The black points are the energy using the two-body Hamiltonian fitted on deuterium and dineutron. The gray points represent the Helium energy using the same two-body Hamiltonian with the addittion of a three-body piece fitted on ^3He.

This effect is unexpected since naive power counting predicts three-body LEC to behave as $D \propto \frac{1}{M^5}$. However, the dynamic of the three-body system enhance its contribution to be of the same order as the two-body interaction at LO. This effect has been widely studied in the three-boson case, where it is possible to show that the addiction of a three-body interaction can change the scattering length of the attractive two-body force, leaving two-body observables unchanged. This is known as *Thomas* collapse found in 1935 [25]. This is an effect similar to the *Efimov* effect found in 1970 [26]. The three-body energy diverges in the presence of a zero range interaction. According to the Efimov effect, when an attractive potential becomes close to a two-body contact interaction, the bound states energy of the three-body system diverges, while more and more virtual states turn into real bound states. In our case, it makes the number of bound states with the same symmetry infinite in the

limit of infinite cut-off. At the same time, as many states become real, the deeper ones will become very bound and eventually they will exit from the radius of convergence of the theory.

When the new LEC is fitted in order to renormalize the theory, one needs to chose which state, among the many created by increasing the cut-off, will be fixed by the new counterterm. If it is chosen the three-body LEC to fix the shallower bound-state, in order to maintain the correct number of excited states in the three-nucleon system, an infinite number of artificial states will appear at deeper energies. Nonetheless, those states are all outside the convergence radius of the theory and become an artifact of the renormalization process without physical meaning. This procedure makes the three-body LEC change sign when a new state becomes bound. The renormalization procedure has then a periodic behaviour (*limiting cycle*) whose analytic form has been calculated in ref. [24, 27, 28] to be

$$D = \lambda_3 \Lambda^4 = c \frac{sin\left(s_0\, ln\left(\Lambda/L_3\right) - arctan\left(1/s_0\right)\right)}{sin\left(s_0\, ln\left(\Lambda/L_3\right) + arctan\left(1/s_0\right)\right)}, \tag{2.38}$$

where c, L_3 and s_0 are theory dependent parameters.[2] .

[2] $s_0 \approx 1.0064$ and Λ/L_3 is a dimensionful parameter that determines the asymptotic phase of the off-shell amplitude [29]

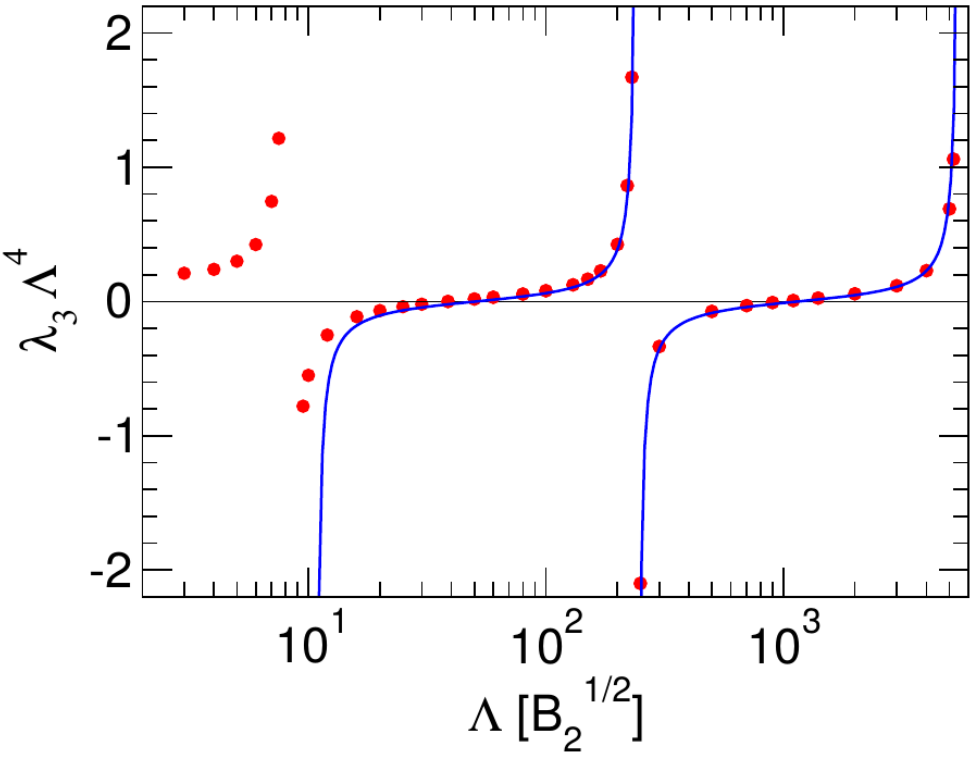

Figure 2.9: From Ref.[24]: The three-body coupling constant λ_3 as a function of the cut-off parameter Λ. Noticed that the "Limit Cycle" of the coupling changes sign when a new bound state appears, according with Eq.(2.38).

2.4 Pion-less Effective Field Theory

According to the dimensional analysis of Sec.{2.2} and the considerations about shallow poles described in Sec.{2.3}, at LO the two nucleon Lagrangian reads

$$\mathcal{L}_{LO}^{2b,c} = N^\dagger \left(i\partial_0 + \frac{\vec{\nabla}^2}{2m_N} \right) N + C_0^c N^\dagger N N^\dagger N \,, \tag{2.39}$$

where the index c refers to the spin or isospin singlet and triplet channels ($^3S_1$ and $^1S_0$). In the nuclear case, the two-body T-matrix has two shallow poles, one associated with the deuterium boundstate and one with the large scattering length of the $n-n$ system. Hence, two operators in the Lagrangian at LO should be included and treated non-perturbatively. Their vertexes

are the two LO constants C_0^s and C_0^t[3] (associated with the ${}^3S_1$ and the ${}^1S_0$ states respectively). The interaction has to be regularized and renormalized in such a way that the Lagrangian can be transformed into an Hamiltonian containing only local interaction, suitable to be used within coordinate defined many-body methods. This is achieved by using an ultraviolet cut-off Λ in momentum space and introducing the regulator function f_Λ. In momentum space, a customary choice is:

$$f_\Lambda(q) = \frac{1}{\Lambda\sqrt{\pi}} e^{-q^2/\Lambda^2}. \tag{2.40}$$

By using the former regulator, the two-body Hamiltonian in coordinate space reads [30]

$$H_{2b}^{LO} = \sum_i -\frac{\vec{\nabla}_i^2}{2m_N} + \sum_{i<j} \left(C_0^{\mathbb{1}} + C_0^{\sigma\sigma}\, \vec{\sigma_i}\cdot\vec{\sigma_j}\right) e^{-r_{ij}^2\Lambda^2/4}. \tag{2.41}$$

The specific choice of the operator corresponding to the low energy constants (LECs) $C_0^{\mathbb{1}}$ and $C_0^{\sigma\sigma}$, namely $\mathbb{1}$ and $\vec{\sigma_i}\cdot\vec{\sigma_j}$ can be replaced by any other equivalent form under a Fierz transformation in SU(2) and calculated from C_0^s and C_0^t.

Since the two-body interaction is attractive in both channels, a three-body interaction should be introduced in the Hamiltonian:

$$\mathcal{L}_{LO}^{3b,c} = D_0^c N^\dagger N N^\dagger N N^\dagger N. \tag{2.42}$$

As for the two-body case, there is some freedom in choosing the operator to be included in the Hamiltonian formulation of the three-body force. For simplicity we use a central potential derived by renormalizing the theory with the same f_Λ used in the two-body sector

$$H_{3b}^{LO} = \sum_{i<j<k} D_0 \sum_{cyc} e^{-\left(r_{ik}^2 + r_{ij}^2\right)\Lambda^2/4}, \tag{2.43}$$

where $\sum_{cyc}$ are cyclic permutation between particles i,j and k.

The expansions present in the theory introduce the need of several extrapolations that have to be kept under control. The EFT($\not\pi$) expansion introduces a residual error of the order of the inverse of the mass-scale that has to be corrected order by order. Regularization and renormalization introduce another

[3] note that C_0^s and C_0^t are often called C_1 and C_2 in papers where only interaction at LO is used.

source of error of order $1/\Lambda$. At LO the regularized theory is then expected to be affected by a systematic error of order $\mathcal{O}\left(1/m_\pi, 1/\aleph, 1/\Lambda\right)$. However, the cut-off dependence can be estimated by extrapolating results to sufficiently large cut-offs. Power counting errors are more difficult to assess and calculations at sub-leading order are required for their estimation. In order to have an estimate of the magnitude, one could use a generalization of the two-body momentum formula for a many-body system starting from the binding energy B_A of the A-body system

$$Q_A = \sqrt{2m_N \frac{B_A}{A}}, \tag{2.44}$$

and taking the ratio of this quantity to some relevant mass scale of the theory. For instance as seen in Sec.{1.1}, at $m_\pi \sim 800$ MeV the ^{4}He binding energy is $B_4 \sim 100$ MeV[30] and the ratio with the nucleon mass Q_A/M_N is about 0.17. At physical m_π the binding energy per particle in ^{16}O is not much different from the one of ^{4}He (about 10%). Therefore, we expect that the systematic uncertainty due to the truncation at LO should be very similar in the two cases.

The extrapolation in the cut-off requires particular attention if, as in the case of coordinate defined many-body methods, it is hard to push results for arbitrary high cut-off. However, the naturalness assumption (Eq.(2.21)) and the known behavior with the cut-off running (Eq.(2.30)) make it possible to have a controlled extrapolation of the result. LO observables suffer a cutoff systematic which is removed only in the limit $\Lambda \to \infty$. The cut-off dependence of an observable at leading order is given by

$$\mathcal{O}_\Lambda = O + \frac{\mathcal{C}_0}{\Lambda} + \frac{\mathcal{C}_1}{\Lambda^2} + \cdots \tag{2.45}$$

Where O is the observable at $\Lambda \to \infty$ while $\mathcal{C}_0$ and $\mathcal{C}_1$ are fitting parameters. The number of powers of Λ needed to perform a meaningful extrapolation is not a priori known. The standard prescription consists of truncating the expansion when adding additional powers of $1/\Lambda$ no longer influences O. A practical example will be discussed in detail in the case of ^{4}He.

Next To Leading Order

The NLO potential includes both new momentum dependent operators and counterterms with the same structure as the LO. The first one can be fitted on observables as the two-body effective range (r_0), while momentum independent counterterms are required in order to re-fit the observables used to define the theory at LO. It has to be recalled that LO and NLO should be included in perturbation theory and NLO LECs should be fitted in order to recover both the LO and NLO observables without changing the LO ones.

Defining the interaction of two nucleons in the center of mass in which $\vec{p}$ is the ingoing relative momentum, $\vec{p}'$ is the outgoing one, $\vec{q} = \vec{p}' - \vec{p}$ is the momentum transfer and $\vec{k} = \vec{p}' + \vec{p}$, the NLO potential takes the form

$$V_{NLO}(\vec{p},\vec{p}') = C_0^{(1)} + C_2^{(1)}\left(p^2 + (p')^2\right) = C_0^{(1)} + C_2^{(1)}\left(q^2 + k^2\right). \tag{2.46}$$

As in the case of LO the potential is defined in the two possible two-body channels. The regulator f_Λ is included in order to regularize/renormalize the theory:

$$V_{NLO} = f_\Lambda(\vec{q})\left[C_0^{(1)} + C_2^{(1)}\left(q^2 + k^2\right)\right]. \tag{2.47}$$

As for LO, it is possible to transform the potential into a coordinate dependent form. This can be done with a Fourier transform of the momentum matrix element

$$\begin{aligned} V_{NLO}(\vec{r},\vec{r}') &= \int \tfrac{d\vec{p}}{(2\pi)^3}\tfrac{d\vec{p}'}{(2\pi)^3}\langle\vec{r}|\vec{p}\rangle\, V_{NLO}(\vec{p},\vec{p}') f_\Lambda(\vec{p}'-\vec{p})\,\langle\vec{p}'|\vec{r}'\rangle \\ &= \tfrac{1}{8}\int \tfrac{d\vec{k}}{(2\pi)^3}\tfrac{d\vec{q}}{(2\pi)^3} e^{i(\vec{q}\cdot\vec{x}+\vec{k}\cdot\vec{y})} V_{NLO}(\vec{k},\vec{q}) f_\Lambda(|q|) \\ &= \tfrac{1}{8} V_{NLO}\left(-i\vec{\nabla}_y, -i\vec{\nabla}_x\right)\int \tfrac{d\vec{q}}{(2\pi)^3} e^{i(\vec{q}\cdot\vec{x})} f_\Lambda(|q|)\int \tfrac{d\vec{k}}{(2\pi)^3} e^{i(\vec{k}\cdot\vec{y})} \\ &= \tfrac{1}{8} V_{NLO}\left(-i\vec{\nabla}_y, -i\vec{\nabla}_x\right)\delta_\Lambda(\vec{x})\,\delta(\vec{x}) \end{aligned} \tag{2.48}$$

where

$$\vec{x} = \frac{\vec{r}-\vec{r}'}{2} \qquad \text{and} \qquad \vec{y} = \frac{\vec{r}+\vec{r}'}{2}. \tag{2.49}$$

$\delta_\Lambda(\vec{x})$ is the Fourier transform of f_Λ, i.e. a smeared δ function.

Noticed that the derivative does no longer act on the test function when a matrix element is calculated. In fact,

$$\begin{aligned}\langle\psi|V_{NLO}|\phi\rangle &= \int d\vec{r}\int d\vec{r}'\psi^*(\vec{r})V_{NLO}\left(\vec{r},\vec{r}'\right)\phi(\vec{r}') \\ &= \int d\vec{x}\int d\vec{y}\psi^*(\vec{x}+\vec{y})\left[V_{NLO}\left(-i\vec{\nabla}_r,-i\vec{\nabla}_y\right)\delta_\Lambda(x)\delta(\vec{y})\phi(\vec{x}-\vec{y})\right].\end{aligned} \tag{2.50}$$

The calculation is split in the center of mass and relative momentum pieces:

$$\begin{aligned}\langle\psi|q^2\delta_\Lambda\left(\vec{x}\right)|\phi\rangle &= -\int d\vec{x}\,\psi^*\left(\vec{x}\right)\phi\left(\vec{x}\right)\nabla_x^2\delta_\Lambda(x) \\ &= -\int d\vec{x}\,\delta(x)\left[\phi\nabla^2\psi^* + 2(\vec{\nabla}\phi)\cdot(\vec{\nabla}\psi^*) + \psi^*\nabla^2\phi\right]\end{aligned} \tag{2.51}$$

where we used the definition of $\delta(\vec{y})$ to remove the $\vec{y}$ integration.

$$\begin{aligned}\langle\psi|k^2\delta_\Lambda\left(\vec{x}\right)|\phi\rangle &= -\int d\vec{x}\int d\vec{y}\,\psi^*\left(\vec{x}+\vec{y}\right)\phi\left(\vec{x}-\vec{y}\right)\nabla_y^2\delta(\vec{y}) \\ &= -\int d\vec{x}\,\delta(x)\left[\phi\nabla^2\psi^* - 2(\vec{\nabla}\phi)\cdot(\vec{\nabla}\psi^*) + \psi^*\nabla^2\phi\right].\end{aligned} \tag{2.52}$$

Summing up with the EFT coefficients,

$$\langle\psi|V_{NLO}|\phi\rangle = \int d\vec{x}\;\;\delta_\Lambda\left(\vec{x}\right)\left[C_0^{(1)} + C_2^{(1)}\left(\psi^*\left(\vec{x}\right)\nabla_x^2\phi\left(\vec{x}\right) + \phi\left(\vec{x}\right)\nabla_x^2\psi^*\left(\vec{x}\right)\right)\right]. \tag{2.53}$$

This can be directly used in numerical diagonalization calculations. In Monte Carlo (MC) method (see Chapter{4}), only diagonal matrix elements are considered, and the relation is further simplified as

$$V_{NLO}\left(\vec{x}\right) = \int d\vec{x}\;\;\delta_\Lambda\left(\vec{x}\right)\left[C_0^{(1)} + C_2^{(1)}\,2\,\mathcal{R}e\left(\phi^*\left(\vec{x}\right)\nabla_x^2\phi\left(\vec{x}\right)\right)\right]. \tag{2.54}$$

3. LQCD calculations and T-matrix poles analysis

In this chapter we discuss the applicability of EFT($\not\pi$) to the most recent LQCD calculations in low-energy nuclear physics. EFT($\not\pi$) can describe a finite number of poles of the few-body T-matrix inside its breaking-scale, and its convergence in the effective expansion is directly related to the momentum of the poles. Hence, to understand the theory limits at high pion-mass it is necessary to study the pole structure of the results of LQCD calculations.

Finally, we conclude that EFT($\not\pi$) can be well applied to the large m_π cases studied by LQCD calculations. However, some disagreement emerges when comparing the results of LQCD calculations obtained with different procedures and by different groups. Nonetheless, the pioneering nature of calculations, as well as the significant statistical errors in the computed observables, makes it difficult to draw definitive conclusions. On the other hand, an alternative method able to benchmark the consistency of the results of LQCD calculations would be of great help to solve controversies.

3.1 LQCD calculations

The recent advances in the LQCD method, as well as the increasing computational power available, allow now, to simulate few nucleons systems. However, the calculations are not trivial, and require substantial high-performance computing resources and complex statistical analysis. One of the limiting factors is the size of the box used in the calculation, that should be made arbitrarily large in order to extract observables in the continuum limit. In fact, the calculations rely on the Lüscher formula for calculating scattering observables. Bound states are instead calculated looking at the behavior of stationary states density in the box when its width is enlarged. This procedure is unreliable with light quarks because the size needed to make finite size corrections negligible are still too expensive for present calculations. Hence, all the calculations have been performed using unphysical high quark mass: which fixed the pion mass to $m_\pi = \{300, 450, 510, 805\}$ MeV. Even if most calculations have been for the whole baryonic octet and hyper-nuclei, in this section we will focus on the nucleon sector that is of most interest for our purposes. A brief resume of the available data, for different m_π's, will follow.

Calculations at $m_\pi \sim 805$ MeV have been performed by the NPLQCD [31, 32], PACS-CS [33] and CalLat[34] groups. PACS-CS calculated the results with two distinct methods, only one of which has been analyzed in this chapter. Boundstates have been extracted from the behavior of stationary states in the in all the cases except for CalLat calculations, where deuterium and di-neutron binding energies are calculated from the scattering length a_0 and the effective range r_0 in a similar way as we are going to do later in this section.

$m_\pi \sim 510$ MeV data have been analyzed by PACS-CS [35] up to the four-body sector. Moreover, the same m_π has been analyzed by HAL QCD[36] collaboration with a different method. Their analysis consists in the estimation of the interaction between hadrons as function of their relative distance. Basically, an empirical potential is calculated from the energy of the system in different configurations. This can be done if nucleons are sufficiently distant and can be identified as independent particles. The obtained potential has only two-body components, that can be divided into channels and used to make estimations of many-body observables. This approach predicts the absence of any bound state of two nucleons and the only presence of virtual

states.

Calculations for $m_\pi \sim 450$ MeV have been performed by NPLQCD [37], while the lowest m_π investigated is ~ 300 MeV, done by PACS-CS [38, 39].

A summary of available binding energies, scattering lengths and effective ranges can be found in Tab.(3.1). For sake of simplicity, the LQCD errors shown in the tables have been contracted, symmetrizing and composing them quadratically, i.e.

$$1.00\,\binom{+0.02}{-0.05}\,\binom{+0.12}{-0.16} \leftarrow 1.00\left(\sqrt{0.05^2+0.16^2}\right). \tag{3.1}$$

where in the first bracket represents the asymmetric stochastic error and the second one the asymmetric systematic error of the LQCD calculation In the case in which the error of observables were not directly accessible it has been calculated with standard error propagation.

In Tab.(3.1) it can be noticed that a pattern is visible in the results for two body systems: the bindings strength and scattering lengths increase with the pion mass. Errors in the scattering lengths are especially large, this is the reflection of the fact that $1/a_0$ is close to zero and shallow poles are present in the systems T-matrix. This would imply that the appropriate nuclear theory to treat this data is EFT($\not\pi$) with shallow poles. However, the relative strength between central values of a_0 and r_0 requires some precautions. At $m_\pi \sim 800$ many calculations are available, but only two calculations out of three are compatible in few sigmas, PACS-CS predict a much lower binding with respect to NPLQCD and CalLat. This might be due to the different Lattice methods used. In fact, the earlier PACS-CS data have been calculated using the quenched approximation[1], while the more recent NPLQCD calculations are performed fully dynamical. However, more investigations might be required in order to clarify this discrepancy. CalLat group finds a second, very shallow, bound state in the ${}^3S_1$ channel. It is most probably related to the kind of analysis used to extract the states, conceptually different from the one used by NPLQCD and PACS-CS. Nonetheless, it might indicate the missing of a shallow bound state in NPLQCD and PACS-CS $m_\pi \sim 800$ MeV data.

[1]The quenched approximation consists in neglecting the fermionic loops in the calculation.

Last, it should be noticed that in the case of NPLQCD calculation ($m_\pi \sim 800$ MeV, in the $^3S_1$ channel), $a_0 \sim 2r_0$: limit in which the T-matrix presents a double pole.

$^3S_1$ channel					
Collaboration	m_π [MeV]	$a_0\,[m_\pi^{-1}]$	$r_0\,[m_\pi^{-1}]$	B_{np} [MeV]	B^*_{np} [MeV]
CALLAT[34][40]	800	9.18(40)	3.78(17)	30(3)	3.3(1.2)
NPLQCD[31][32]	800	7.45(91)	3.71(47)	19(5)	-
PACS-CS[33]	800	-	-	9.1(1.3)	-
PACS-CS[35]	500	-	-	11.5(6.1)	-
NPLQCD[37]	450	-25(123)	7.8(4.1)	14(3)	-
PACS-CS[38]	300	-	-	14.5(2.5)	-
Nature[41]	140	3.85	1.24	2.22	-
$^1S_0$ channel					
Collaboration	m_π [MeV]	$a_0\,[m_\pi^{-1}]$	$r_0\,[m_\pi^{-1}]$	B_{np} [MeV]	
CALLAT[34][40]	800	10(1)	3.3(2)	21.8(5.8)	
NPLQCD[31][32]	800	9.5(1.4)	4.6(4)	16(4)	
PACS-CS[33]	800	-	-	5.5(1.5)	
PACS-CS[35]	500	-	-	7.4(1.4)	
NPLQCD[37]	450	47(165)	6.7(2.2)	12.5(4.9)	
PACS-CS[38]	300	-	-	8.5(1.8)	
Nature[41]	140	-16.85	1.95	-	

Table 3.1: Proton - neutron LQCD results in $^1S_0$ and $^3S_1$ channels.

Multi nucleon systems			
Collaboration	m_π [MeV]	$B_{^3\mathrm{He}}$ [MeV]	$B_{^4\mathrm{He}}$ [MeV]
NPLQCD[32]	800	53.9(10.7)	107.0(24.2)
PACS-CS[42]	800	18.2(4.5)	27.7(9.5)
PACS-CS[35]	500	20.3(4.5)	43.0(14.4)
PACS-CS[38]	300	21.7(13)	47(21)
Nature	140	7.7	28.3

Table 3.2: LQCD results for few nucleons systems.

3.2 T-MATRIX POLES

From Tab.(3.1) it is difficult to compare and relate scattering lengths and binding energies in a systematic way. We propose an analysis of the data in terms of T-matrix momentum poles, which can be calculated both from scattering parameters and binding energies and directly compared. Moreover, this kind of analysis is of great interest in order to understand the limits of applicability of EFT($\not\pi$) . The large value of a_0 makes evident that the zero-energy component of the T-matrix is dominant, therefore an expansion around the zero momenta is the most natural choice. (ERE):

$$T = \frac{4\pi}{m_N}\frac{1}{kcot\left(\delta\right) - ik} = \frac{4\pi}{m_N}\frac{1}{-\frac{1}{a} + \frac{1}{2}r_0k^2 + \cdots - ik} \tag{3.2}$$

$$T \approx \frac{4\pi}{m_N}\frac{1}{-\frac{1}{a} + \frac{1}{2}r_0k^2 - ik} \tag{3.3}$$

which is truncated assuming the low momentum limit. Truncated T-matrix shows two poles in the complex momentum plane:

$$-\frac{1}{a} + \frac{1}{2}r_0k^2 - ik = 0 \xrightarrow{k=i\kappa} -\frac{1}{a} - \frac{1}{2}r_0\kappa^2 + i\kappa = 0, \tag{3.4}$$

$$\kappa_\pm = \frac{1}{r_0}\left(1 \pm \sqrt{1 - \frac{2r_0}{a}}\right). \tag{3.5}$$

These represent relevant states of the system (they might be resonances, bound or virtual states). Reverting the equation, it is possible to write a_0 and r_0 in functions of the poles:

$$r_0 = \frac{2}{\kappa_+ + \kappa_-} \qquad a = \frac{\kappa_+ + \kappa_-}{\kappa_+\kappa_-}. \tag{3.6}$$

In order to make meaningful comparisons, poles are also calculated from two-body binding energies. This can be done analytically:

$$\kappa_B E = \sqrt{m_N B_d}, \tag{3.7}$$

where m_N and B_d are, respectively, the nucleon mass and the two-body system binding energy. It is possible to compare Eq.(3.7) and Eq.(3.5) poles directly. In Tab.(3.3) are shown the position of the poles for two-body systems, for the available pion masses and data.

$^3S_1$ channel				
Collaboration	m_π [MeV]	$\kappa_+[m_\pi]$	$\kappa_-[m_\pi]$	$\kappa_{BE}[m_\pi]$
CALLAT	805	0.38(3)	0.15(1)	-
NPLQCD	805	0.29(40)	0.25(35)	0.22(3)
PACS-CS	805	-	-	0.15(1)
PACS-CS	510	-	-	0.24(6)
NPLQCD	450	0.29(21)	-0.04(15)	0.30(3)
PACS-CS	300	-	-	0.41(4)
Nature	140	1.29	0.33	0.33
$^1S_0$ channel				
Collaboration	m_π [MeV]	$\kappa_+[m_\pi]$	$\kappa_-[m_\pi]$	$\kappa_{BE}[m_\pi]$
CALLAT	805	0.47(4)	0.13(2)	-
NPLQCD	805	0.25(12)	0.18(9)	0.20(2)
PACS-CS	805	-	-	0.12(2)
PACS-CS	510	-	-	0.19(2)
NPLQCD	450	0.28(13)	0.02(9)	0.28(5)
PACS-CS	300	-	-	0.31(3)
Nature	140	1.08	-0.06	-

Table 3.3: Table of poles calculated using ERE (κ_+/κ_-) and binding momentum (κ_{BE})

The same poles are shown in Fig.(3.2) and Fig.(3.3) in order to give a graphical and more intuitive visualization of their behavior with the pion mass. In the plots, the poles calculated from ERE expansion (red circles) and bound states (blue triangles) are displayed. Data of different groups but with the same pion mass have been slightly shifted in order to have a cleaner visualization.

The energy of the poles induced by bound states in units of m_π show much smaller variation. The physical deuterium shows a pole at a similar momentum than the other poles indicating a smooth transition in m_π. However, in the $^1S_0$ channel the same pole seems to disappear at the physical pion mass. This might suggest a nontrivial m_π dependence or a phase transition that has still to be understood in that channel. Three-body boundstates seem to share the same flat behavior seen in the two body case showing an invariance with respect to m_π. On the other hand, alpha particle bounds are more fluctuating

and difficult to be interpreted. Moreover, errors are still too large to outline any conclusion.

Poles calculated with the ERE in the two body system are of particular interest. In fact, it can be noticed that in the physical case we have two poles, a shallow one and one at very large momentum. As expected, in deuterium the shallow pole coincides with the pole calculated using the binding energy, while the other one is at almost $\sim 1.5\, m_\pi$, outside the range of convergence of ERE and the low momentum limit. Hence, it should be concluded that it is an unphysical pole destined to disappear with the inclusion of more ERE orders. Other interesting data are found at $m_\pi \sim 450$ MeV, where we have the appearance of a bound state, a pole at the same position and a shallower pole which do not correspond to any bound state found. The second pole in ${}^1S_0$ is consistent with a virtual state. However, if it were a bound state, it would be very close to the unitary limit. We conclude that that shallowest pole at $m_\pi \sim 450$ and ${}^1S_0$ channel should be on the negative momentum plane, otherwise LQCD precision is not enough to distinguish a weakly-bound state. The affinity of the bound state and the deeper ERE pole is impressing. This might imply that further terms of the T-matrix truncation are negligible for this m_π. However, comparing data at $m_\pi \sim 450$ with physical mass one, would expect the deepest pole not to be real and the shallower to represent a bound state. The position of the poles is also interesting because, in our experience of T-matrix poles, the shallow state is usually more robust than the deeper one. The behavior of poles at small m_π is still a puzzle, which might be solved only having access to higher orders of the ERE expansion.

$m_\pi \sim 810$ MeV is the mass where the most data are present, but they are not always compatible. Grey dots represent the binding energies calculated by CalLat group from scattering parameters. They have been calculated using the same procedure as ours, with a different truncation of the T-matrix. The red and gray results in agreement in few standard deviations, which might reflect a partial residual dependence of the data on the shape parameter. Nonetheless, the gray poles are in completely agreement with the bound found by NPLQCD, but not with PACS-CS data in the ${}^1S_0$ channel. If trusting the unquenched, and more recent calculation (NPLQCD), the consistency of gray dots imply that the shape parameter has still some relevance, but further contributions to the T-matrix poles are merely perturbative.

NPLQCD finds a double pole, which central value almost perfectly agrees

with the bound-state in both channels. The position of poles is expected since it has been used by NPLQCD in fitting the scattering length and effective ranges. However, ref.[43] states that it is not possible to describe double poles using a finite range potential, and the presence of a long range potential is hardly justifiable in a heavy pion mass context. It is also impossible that the two poles are projections of two resonances very close to the real axis, since they would not respect the Wigner bound[44] and the causality principle. We have to conclude that, in order to describe the two poles using a standard potential, the two poles should be distinct (as it is permitted by the error bands) and their degeneracy is just a coincidence. Nonetheless, one of the two poles might turn to be not real if more parameters are included in the ERE, running out from the theory convergence radius or becoming unphysical for other reasons. Should be noticed that, since the NPLQCD scattering parameters has been extracted considering the bound state pole in the fit, their ERE and bound poles errors can not be considered independent. This explains the extraordinary proximity of the poles, of much less than one standard deviation in all the cases.

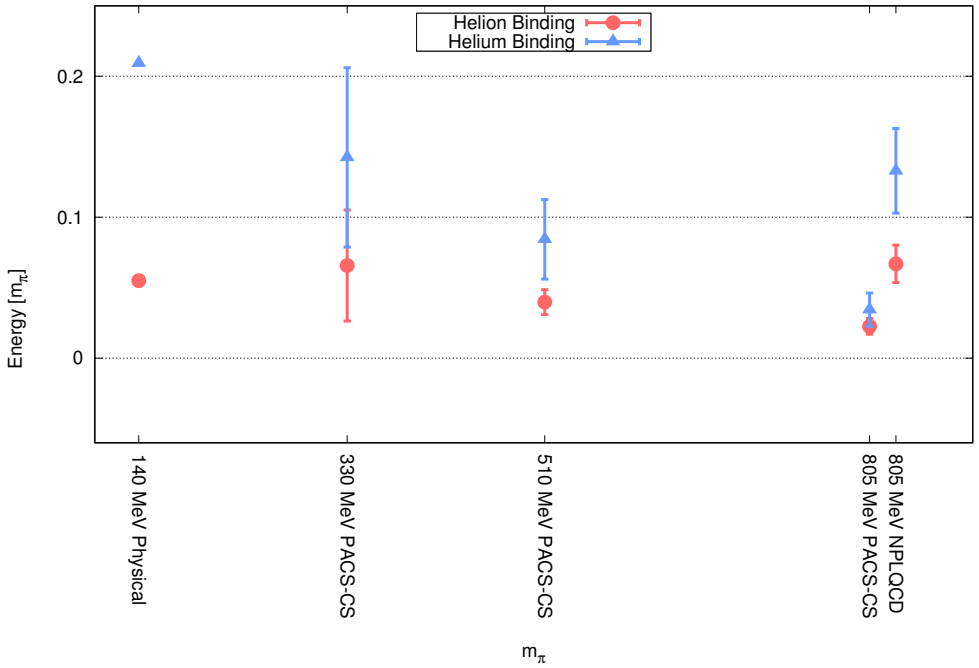

Figure 3.1: Binding energy of ^{3}He and ^{4} He. See text for full description.

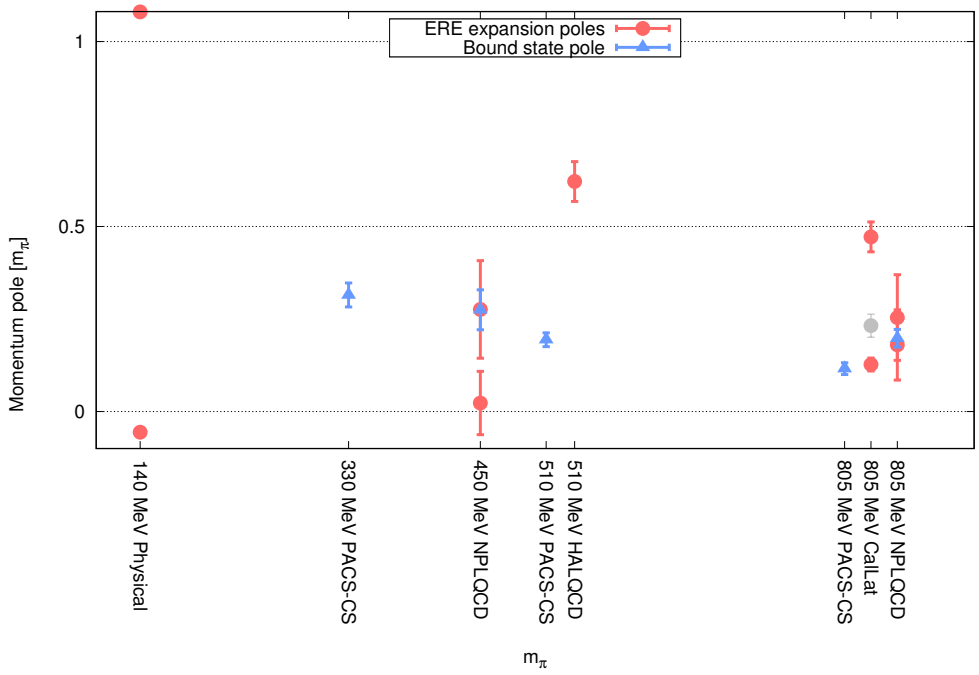

Figure 3.2: $^1S_0$ poles. See text for full description.

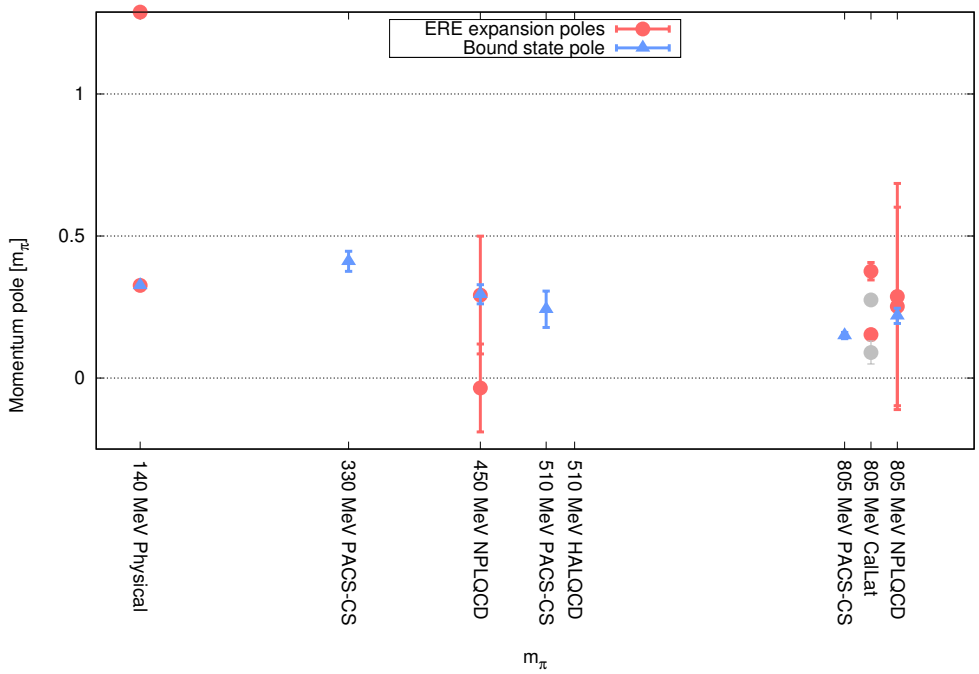

Figure 3.3: $^3S_1$ poles. See text for full description.

The last comment on the LQCD results concerns the EFT($\not\pi$) applicability on them. In fact, in sec.{2.3} we compared EFT($\not\pi$) and ERE claiming that the first is equivalent to the second in the limit of small momenta. E.g. the LO is associated to ERE truncated at a_0. Hence, ERE can be truncated to a_0 only in the low momentum limit, where

$$| \frac{1}{a} | \gg | \frac{r_0}{2} k^2 | \tag{3.8}$$

$$| \frac{1}{a} | \gg | \frac{r_0}{2} k^2 | \longrightarrow | \frac{r_0}{2} a k^2 | \ll 1. \tag{3.9}$$

The behavior of $\frac{a}{2} r_0 k_{pm}^2$ flowing with the relative value of a_0 and r_0 is shown in Fig.(3.4). It can be noticed that the two poles do not satisfy the relation (3.9) together. Hence, one concludes that the truncation at a_0 might be possible only for the shallowest pole. In other words, EFT($\not\pi$) defined as in sec.{2.4} will be not able to describe the deepest pole, introducing a new breaking scale at momentum $k_+ < m_\pi$. The possibility of describing two poles using EFT($\not\pi$) with no changing in the power counting appears to be complicated and it is still debated. Nonetheless, it would be possible promoting a new operator at LO as it has been done with the appearance in the theory of the firs shallow pole. This criticality appears especially at $m_\pi \sim 450$ MeV (not used in this work) where the error excludes the possibility that the shallowest pole refers to the bound state found, where at $m_\pi \sim 800$ MeV the error on the poles leave the possibility to have a deep pole and a relatively shallow bound state. A possibility to explain the weird behavior of shallow poles is that the shallow poles are present in the T-matrix, but they do not correspond to any real states (they are known as shallow states). It has been proved that this phenomenon are possible in quantum mechanics.[45–47] However, how to discriminate a real state from a shadow one in LQCD is still unknown and would require a deeper study of the phenomena.

Nonetheless, the success of EFT($\not\pi$) in predicting observables as well as its renormalizability at $m_\pi \sim 800$ MeV suggests that the powercounting at LO as defined in sec.{2.4} is correct in the framework of this work.

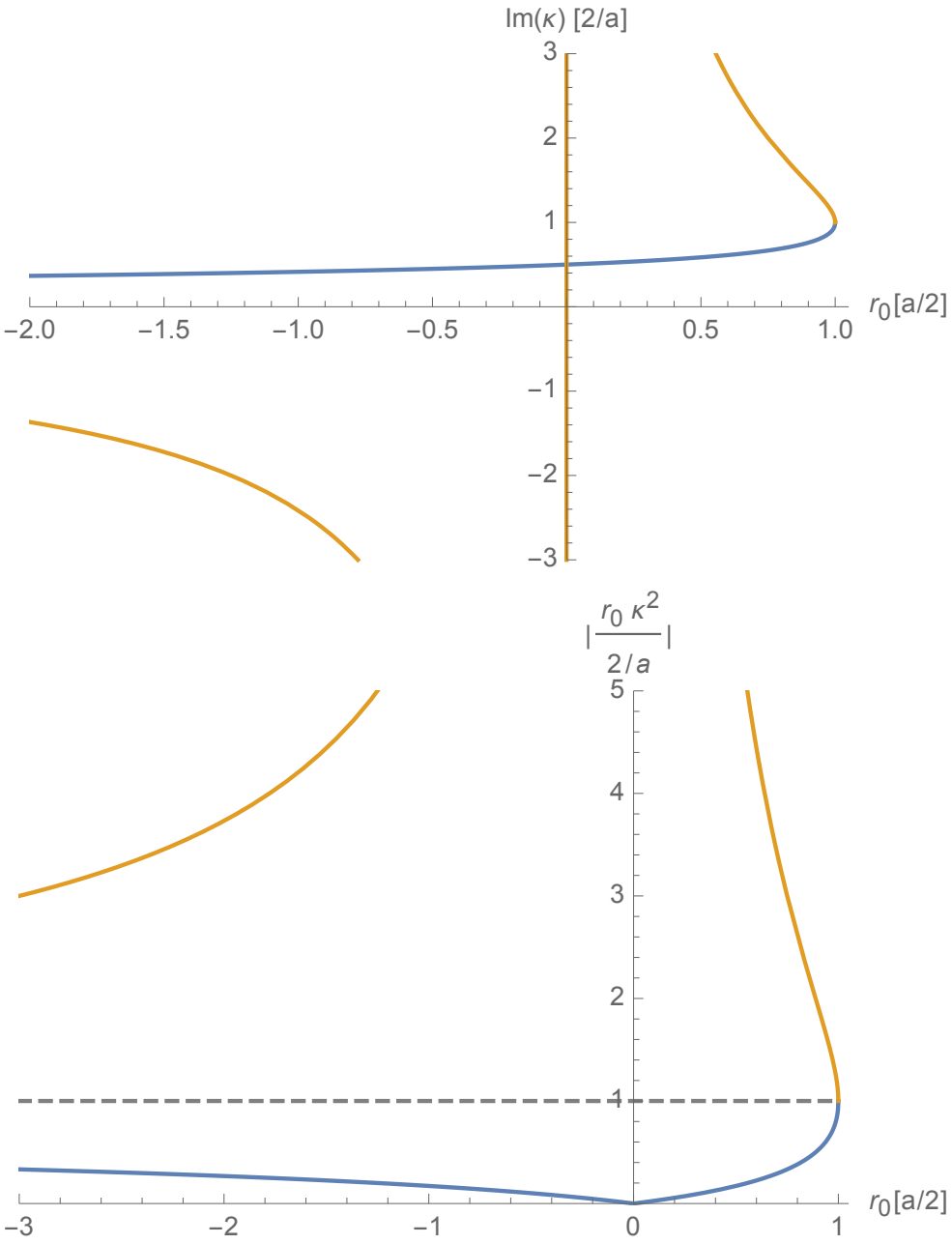

Figure 3.4: $\frac{a}{2} r_0 k^2$ evaluated on the T-matrix poles. In orange the deepest pole and in blue the shallower one. On the top panel is shown the case if $a > 0$ and $r_0 > 0$. On the bottom pannel: if $a < 0$ and $r_0 > 0$. $r_0 > a/2$ case is forbidden by Wigner bond.

4. Monte Carlo Methods

In order to understand low energy nuclear physics one has to develop and use non relativistic models, and to make predictions to be confronted with experiments. Hence, one should be able to solve the Schrödinger equation for nucleons with the modeled interaction in the systems of interest. We are mainly interested in light and medium nuclear binding energies, masses and radii, that require a method able to make predictions for multi-nucleon, heavily correlated, systems. We chose to use QMC, because it is an ab initio method that can calculate, in principle, exact observables in relatively heavy nuclei with improvable precision. Among the many QMC methods available in the literature, in this work we chose to use prevalently AFDMC, which can handle big systems of fermions [48, 49].

MC is a method to transform integrals in sums of functions evaluated on samples (usually called *walkers*) of a distribution such that the sum converges to the integral with a statistic error coming only from the impossibility to have infinite samples. The absence of truncations or uncontrolled approximations makes MC a powerful ab initio method able to perform reliable integration of complex multiparticle systems and complex interactions with high accuracy.

VMC method is capable of computing quantum mechanical observables from a known wave function. The variational principle is exploited to find the system ground state, this is done minimizing the energy with respect to the wavefunction used. The minimization procedure is done "by hand" in most of the nuclear MC codes, while in more recent calculations, including this work, an automatic minimization has been implemented, allowing to have results very close to the correct ones. The sampling procedure makes the integration very efficient allowing to calculate multi-dimensional integrals with fairly small errors. However, the accuracy of the method is limited by the needs of knowing the wavefunction that has to be parametrized making the final result dependent on what, and how many, are the parameters used.

DMC overcomes the lack of knowledge of the ground state function using

an imaginary time propagation of the initial walker configuration in order to project out its high energy components. The projected wave function can be sampled and used to compute ground-state observables of the system. In our case, the propagation is performed in the coordinate space, but diffusions in momentum or other basis are also possible, as shown by Configuration Interaction Monte Carlo [50] and other methods. Since we are using EFT potentials, which are naturally developed in momentum space, the momentum basis appears to be the most natural choice. However, EFT potentials can be easily Fourier-transformed in coordinate space. The transformation is convenient since coordinate defined methods are not limited in the maximum momentum of the interaction and can perform calculation even for high cutoff. Moreover, the ab initio nature of this methods very well marries the EFT idea of a potential from the first principles and makes QMC ideal to perform the calculations done during this work.

DMC shows some criticalities with fermionic systems where the wave function is not positive. The propagation process does not contain any information about the statistical nature of the particles being diffuse, hence the *walkers* will soon approach the bosonic state annihilating any fermionic contribution and spoiling the calculation. This is the so-called *sign problem*[51]. In order to alleviate it, one introduces the fixed-phase (or constrained-path in the case of complex Hamiltonians) procedure described later in section {4.2} and discussed in details in the references [48, 51–54]. The constrained-path approximation mitigates the sign problem and introduces a source of systematic errors which is difficult to be estimated.

RPDMC method unleash the constraints of the system letting the sampled wave function to decay to the ground state. This allows to estimate the constrained-path systematic error but reintroduces the sign problem that will increase the calculation error exponentially.

The most common limitation of Green Function Diffusion Monte Carlo (GFDMC), as well as other ab initio methods, is the difficulty to manage the amount of memory required to store the degrees of freedom of the system, which can be extremely large for a many-particle system. This kind of methods scale, if no improvements are made, as $A!$.

In the following sections, a brief overview of different kinds of MC and QMC used during this work will be given.

4.1 Variational Monte Carlo

The expectation value of quantum mechanical observables on a trial wave function Ψ can be rewritten as an integral. For example the expectation value of the Hamiltonian reads:

$$E = \frac{\langle\Psi|H|\Psi\rangle}{\langle\Psi|\Psi\rangle} = \frac{\int \Psi^* H\Psi}{\int |\Psi|^2} = \int |\Psi|^2 \frac{H\Psi}{\Psi}, \tag{4.1}$$

where $|\Psi|^2$ can be seen as a probability distribution (we are assuming $\int |\Psi|^2 = 1$). The calculation is, in general, not trivial even for simple systems. However, it can be approached using many numerical methods (as finite difference, Numerov, ...) discretizing the integration space. The limit of the above-mentioned methods is the number of dimensions of the integral that it is possible to calculate. Exploiting the central limit theorem it is possible to overcome the problem, integrating functions in a multidimensional space efficiently.

We can rewrite the integral as:

$$I = \int \mathcal{I}(x) d^a x = \int \frac{e(x)}{P(x)} P(x) d^a x = \int g(x) P(x) d^a x, \tag{4.2}$$

where $e(x)$ is the function to be integrated and $P(x)$ is a probability distribution of the variable x, strictly positive and normalized to one. Applying the central limit theorem [55] the integral can be computed as

$$I_N = \sum_{x \in P(x)}^{N} g(x) \xrightarrow{N\to\infty} I \tag{4.3}$$

where I_N is a normal distribution which has mean value I and variance $\sigma_N^2 = \frac{\int g^2(x) P(x) d^a x}{N+1} - \left(\frac{\int g(x) P(x) d^a x}{N+1}\right)^2$. Which can be systematically reduced increasing statistics ($\sigma \approx 1/\sqrt{N}$). The probability distribution of I_N for large N is

$$P\left[I_N\right] \overset{N\to\infty}{=} \frac{1}{\sqrt{2\pi\sigma_N^2}} e^{-\frac{(S_N - I)^2}{2\sigma_N^2}}. \tag{4.4}$$

$P(x) \equiv |\Psi|^2$ and $g(x) \equiv \frac{H\Psi}{\Psi}$. The probability $P(x)$ might be difficult to sampled. One of the simplest, yet wildly used, way to do it is the Metropolis

algorithm [56]. It consists of moving, with a random walk, a point (the walker) in the configuration space. Then accept/reject with a probability w defined as: [51]

$$w = \frac{|\Psi_T(new\ point)|^2}{|\Psi_T(old\ point)|^2} \tag{4.5}$$

After a sufficiently large number of moves, the walker's path will cover a set of points distributed according to the probability $P(x)$. The distribution used to draw the new position from the least one (the step) does not influence the final result and can be chosen by convenience. It is common to use a gaussian or a flat distribution centered in the old position. However, the steps have to be statistically uncorrelated and wide enough to cover the whole space without sampling positions whose contribution to the integral is small. A good empirical method is to ensure that the total number of rejection and acceptance of new positions are almost the same. One of the most interesting features of this procedure is the possibility to optimize the algorithm, parallelizing the process moving independent walkers contemporaneously on different processors and accumulating statistics together. Estimators of local observables can be accumulated as

$$E_N = \sum_{x \in |\Psi|^2}^{N} \frac{H\Psi}{\Psi}. \tag{4.6}$$

MC statistical errors can be evaluated as follow:

$$\delta E = \left\langle f^2 \right\rangle - \left\langle f \right\rangle^2. \tag{4.7}$$

This equation assumes that each sample is independent of the previous one. In order to avoid the correlation of consecutive positions extracted one from each other, observables can be accumulated once in many steps.

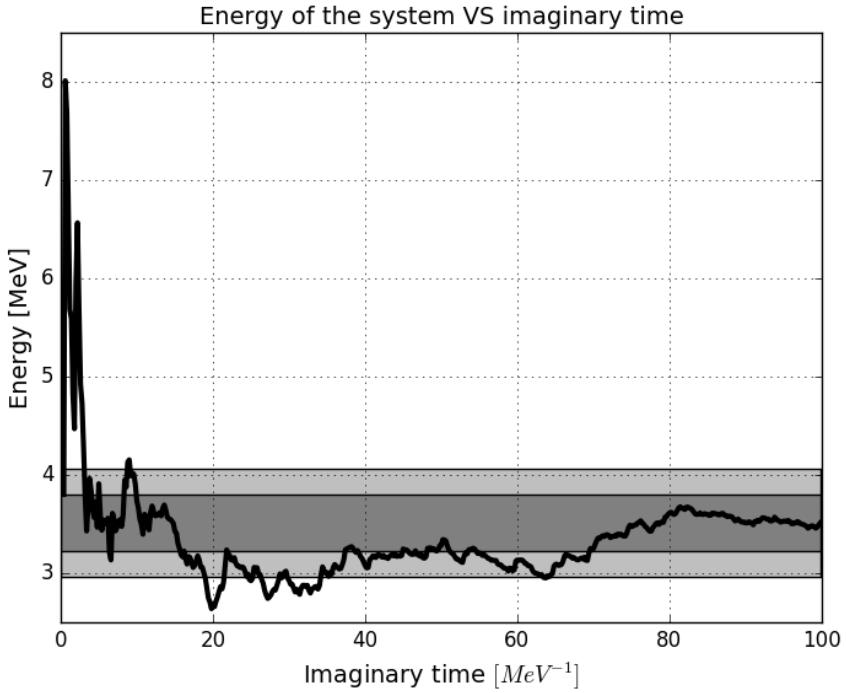

Figure 4.1: Average of the energy at each step of a ^{4}He Variational calculation using EFT($\not\pi$) potential and cut-off 14fm^{-1}. The dark gray band represents the total standard deviation of the calculation averaging all the points of the calculation. The light gray band is the standard deviation after data reblocking.

Wave function

The precision of VMC is limited only by the knowledge of the wave function. Nonetheless, the local energy

$$\frac{\hat{H}\Psi}{\Psi} = -\frac{\hbar^2}{2m}\frac{\nabla^2\Psi}{\Psi} + V(R) \tag{4.8}$$

has to be evaluated for each Walker and step using the wave function, making it the most time-consuming part of the code. Hence it is of great interest to optimize it. It can be seen from Eq.(4.8) that if the wavefunction is already an eigenstate of the system the local energy $\frac{\hat{H}\Psi}{\Psi}$ is a constant, each point in the space contribute equally to the integral and the VMC error is always zero. As a general empiric rule, as close is the used wave function to the real ground state, as small is the calculation standard deviation.

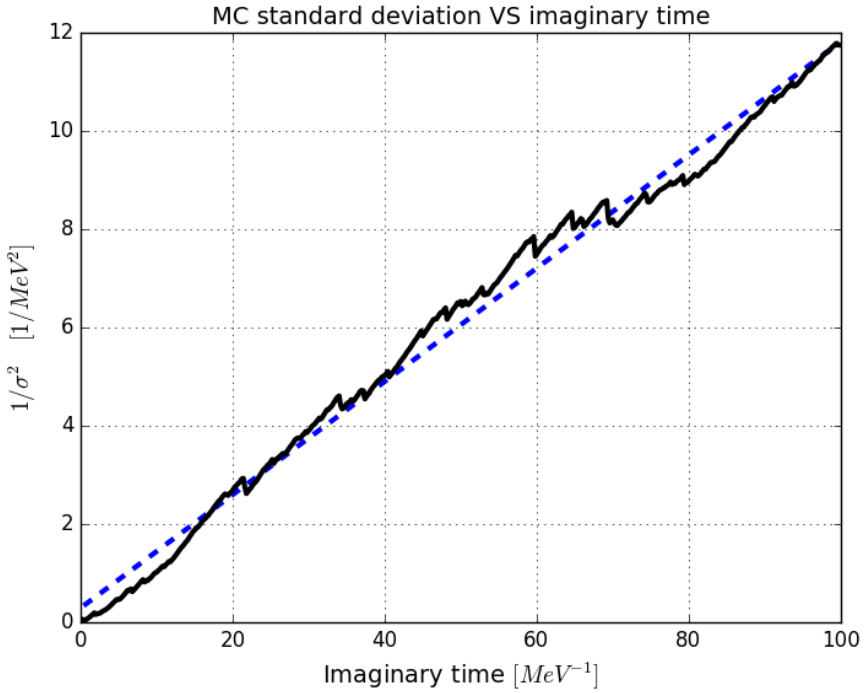

Figure 4.2: Error as function of the imaginary time of a ^{4}He Variational calculation using EFT($\not\pi$) potential and cut-off ∼2800 MeV. The dotted blue line is a linear fit of the data. It can be noticed that the error very well describe the expected behaviour: $\sigma \propto \frac{1}{\sqrt{\tau}}$.

The standard form of the wave function used in QMC calculations of light nuclei reads

$$\langle X|\Psi_T\rangle = \langle X|\Big(\prod_{i<j<k} U_{ijk}\Big)\Big(\prod_{i<j} F_{ij}\Big)|\Phi\rangle\,, \tag{4.9}$$

where $X = \{x_1 \dots x_A\}$ and the generalized coordinate $x_i = \{r_i, \sigma_i, \tau_i\}$ represents the position, spin, and isospin variables of the i-th nucleon.

The **long-range** behavior of the wave function is described by the Slater determinant

$$\langle X|\Phi\rangle = \mathcal{A}\{\phi_{\alpha_1}(x_1), \dots, \phi_{\alpha_A}(x_A)\}\,. \tag{4.10}$$

The symbol $\mathcal{A}$ denotes the antisymmetrization operator and α denotes the quantum numbers of the single-particle orbitals, given by

$$\phi_\alpha(x) = R_{nl}(r)\, Y_{\ell\ell_z}(\hat{r})\; \chi_{ss_z}(\sigma)\, \chi_{\tau\tau_z}(\tau)\,, \tag{4.11}$$

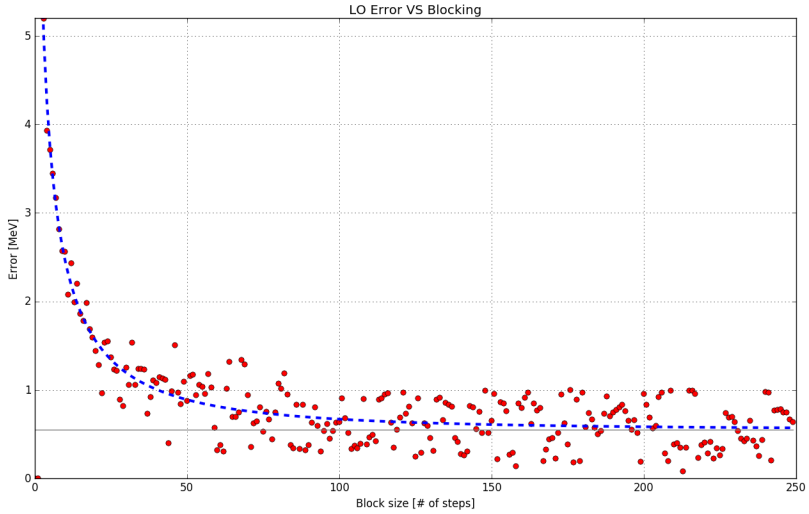

Figure 4.3: Error of the calculation with the blocking size. The correlation between walkers decays esponentially as can be deduced by the exponential fit (dotted line)

where $R_{nl}(r)$ is the radial function, $Y_{\ell\ell_z}(\hat{r})$ is the spherical harmonic, and $\chi_{ss_z}(\sigma)$ and $\chi_{\tau\tau_z}(\tau)$ are the complex spinors describing the spin and isospin of the single-particle state.

In both the GFMC and the latest AFDMC calculations spin-isospin dependent correlations J_{ij} and U_{ijk} are usually adopted. However, these are not necessary for this work. In fact, the two-body LO EFT($\not\pi$) nuclear potential considered in this work does not contain tensor or spin-orbit operators. Moreover, the spinorial contribution of the potential is much smaller than the central one.

J_{ij} represent a **two-particle correlation function** (usually called *Jastrow*) which takes into account the consequences of an interparticle potential to the wave function. A two-body Jastrow can be extracted solving numerically the two-body problem during the calculation using a finite difference method. With the introduction of the automatic optimization algorithm, it resulted more convenient to express the two-body correlation function using spline whose nodes are treated as minimization parameters.

Three body correlations are required only if a three-body interaction is included in the propagation, as in the EFT($\not\pi$) case. The calculation of three-body correlation is less trivial than the two-body one, but one can assume

that his shape can be recover from the two-body in one of the follows ways:

$$J_{3B}^{(1)}\left(r_i, r_j, r_k\right) = e^{-\sum_{\text{cyc}}\left[J_{2b}(r_i,r_j)J_{2b}(r_k,r_j)J_{2b}(r_i,r_k)\right]} \tag{4.12}$$

$$J_{3B}^{(2)}\left(r_i, r_j, r_k\right) = \prod_{\text{cyc}}\left[J_{2b}\left(r_i, r_j\right) + J_{2b}\left(r_k, r_j\right) J_{2b} + \left(r_i, r_k\right)\right] \tag{4.13}$$

$$J_{3B}^{(3)}\left(r_i, r_j, r_k\right) = 1 - \sum_{\text{cyc}}\left[J_{2b}\left(r_i, r_j\right) J_{2b}\left(r_k, r_j\right) J_{2b}\left(r_i, r_k\right)\right] \tag{4.14}$$

All the three option are equivalently viable, but empirically the most successful was Eq.(4.14) in order to minimize the variance of the wave function. The already expansive minimization process makes impossible to try all three the formulas for all the systems so the last one has been used for all the calculation here presented.

Should be mentioned that the Eq.(4.12), (4.13) and (4.14) are just three of the possible three-body correlation function form that have been tried during this work. However, they resulted to be the most successful.

Automatic Optimization

In standard nuclear Variational Monte Carlo (VMC) and GFMC calculations the minimization is usually done adopting a "hand-waving" procedure, while in more recent AFDMC calculations the stochastic reconfiguration (SR) method [57] has been adopted. In both cases the number of variational parameters is reduced by first minimizing the two-body cluster contribution to the energy per particle, as described in Refs. [58, 59]. In this work we adopt, for the first time in a nuclear QMC calculation, the more advanced *linear method* (LM) [60], which allows us to deal with a much larger number of variational parameters.

Within the LM, at each optimization step we expand the normalized trial wave function

$$|\bar{\Psi}_T(\mathbf{p})\rangle = \frac{|\Psi_T(\mathbf{p})\rangle}{\sqrt{\langle\Psi_T(\mathbf{p})|\Psi_T(\mathbf{p})\rangle}} \tag{4.15}$$

at first order around the current set of variational parameters $\mathbf{p}^0 = \{p_1^0, \ldots, p_{N_p}^0\}$,

$$|\bar{\Psi}_T^{\rm lin}(\mathbf{p})\rangle = |\bar{\Psi}_T(\mathbf{p}^0)\rangle + \sum_{i=1}^{N_p} \Delta p_i |\bar{\Psi}_T^i(\mathbf{p}^0)\rangle\,. \tag{4.16}$$

By imposing $\langle\Psi_T(\mathbf{p}^0)|\bar{\Psi}_T(\mathbf{p}^0)\rangle = 1$, we ensure that

$$\begin{aligned} |\bar{\Psi}_T^i(\mathbf{p}^0)\rangle &= \frac{\partial|\bar{\Psi}_T(\mathbf{p})\rangle}{\partial p_i}\Big|_{\mathbf{p}=\mathbf{p}^0} \\ &= |\Psi_T^i(\mathbf{p}^0)\rangle - S_{0i}|\Psi_T(\mathbf{p}^0)\rangle, \end{aligned} \tag{4.17}$$

are orthogonal to $|\Psi_T(\mathbf{p}^0)\rangle$. In the last equation we have introduced

$$|\Psi_T^i(\mathbf{p}^0)\rangle = \frac{\partial|\Psi_T(\mathbf{p})\rangle}{\partial p_i}\Big|_{\mathbf{p}=\mathbf{p}^0}, \tag{4.18}$$

for the first derivative with respect to the i-th parameter, and the overlap matrix is defined by $S_{0i} = \langle\Psi_T(\mathbf{p}^0)|\Psi_T^i(\mathbf{p}^0)\rangle$. The expectation value of the energy on the linear wave function is defined as

$$E_{\rm lin}(\mathbf{p}) \equiv \frac{\langle\bar{\Psi}_T^{\rm lin}(\mathbf{p})|H|\bar{\Psi}_T^{\rm lin}(\mathbf{p})\rangle}{\langle\bar{\Psi}_T^{\rm lin}(\mathbf{p})|\bar{\Psi}_T^{\rm lin}(\mathbf{p})\rangle}\,. \tag{4.19}$$

The variation $\Delta\bar{\mathbf{p}}$ of the parameters that minimizes the energy, $\nabla_{\mathbf{p}} E_{\rm lin}(\mathbf{p}) = 0$, corresponds to the lowest eigenvalue solution of the generalized eigenvalue equation

$$\bar{H}\,\Delta\mathbf{p} = \Delta E\,\bar{S}\,\Delta\mathbf{p}\,, \tag{4.20}$$

where $\bar{H}$ and $\bar{S}$ are the Hamiltonian and overlap matrices in the (N_p+1)-dimensional basis defined by $\{|\bar{\Psi}_T(\mathbf{p}^0)\rangle, |\bar{\Psi}_T^1(\mathbf{p}^0)\rangle, \ldots, |\bar{\Psi}_T^{N_p}(\mathbf{p}^0)\rangle\}$. The authors of Ref. [61] have shown that writing the expectation values of these matrix elements in terms of covariances allows us to keep their statistical error under control even when they are estimated over a relatively small Monte Carlo sample. However, since in AFDMC the derivatives of the wave function with respect to the orbital variational parameters are in general complex, we generalized the expressions for the estimators reported in the appendix of Ref. [61].

For a finite sample size the matrix $\bar{H}$ can be ill-conditioned, spoiling therefore the numerical inversion needed to solve the eigenvalue problem. A practical procedure to stabilize the algorithm is to add a small positive constant ϵ to the diagonal matrix elements of $\bar{H}$ except for the first one, $\bar{H}_{ij} \rightarrow \bar{H}_{ij} + \epsilon(1-\delta_{i0})\delta_{ij}$. This procedure reduces the length of $\Delta\bar{\mathbf{p}}$ and rotates it towards the steepest-descent direction.

It has to be noted that if the wave function depends linearly upon the variational parameters, the algorithm converges in just one iteration. However, in our case strong nonlinearities in the variational parameters make, in some instances, $|\bar{\Psi}_T^{\rm lin}(\mathbf{p})\rangle$ significantly different from $|\bar{\Psi}_T(\mathbf{p}^0+\Delta\mathbf{p})\rangle$. Accounting for the quadratic term in the expansion as in the Newton method [61, 62] would alleviate the problem, at the expense of having to estimate also the Hessian of the wave function with respect to the variational parameters. An alternative strategy consists in taking advantage of the arbitrariness of the wave-function normalization to improve on the convergence by a suitable rescaling of the parameter variation [60, 61]. We found that this procedure was not sufficient to guarantee the stability of the minimization procedure. For this reason we have implemented the following heuristic procedure. For a given value of ϵ, Eq. (4.20) is solved. If the linear variation of the wave function for $\mathbf{p}=\mathbf{p}^0+\Delta\mathbf{p}$ is small,

$$\frac{|\bar{\Psi}_T^{\rm lin}(\mathbf{p})|^2}{|\bar{\Psi}_T(\mathbf{p}^0)|^2} = 1 + \sum_{i,j=1}^{N_p} \bar{S}_{ij}\Delta p^i \Delta p^j \leq \delta\,, \tag{4.21}$$

a short correlated run is performed in which the energy expectation value

$$E(\mathbf{p}) \equiv \frac{\langle\bar{\Psi}_T(\mathbf{p})|H|\bar{\Psi}_T(\mathbf{p})\rangle}{\langle\bar{\Psi}_T(\mathbf{p})|\bar{\Psi}_T(\mathbf{p})\rangle} \tag{4.22}$$

is estimated along with the full variation of the wave function for a set of possible values of ϵ (in our case ≈ 100 values are considered). The optimal ϵ

is chosen so as to minimize $E(\bar{\mathbf{p}})$ provided that

$$\frac{|\bar{\Psi}_T(\bar{\mathbf{p}})|^2}{|\bar{\Psi}_T(\mathbf{p}^0)|^2} \leq \delta\,. \tag{4.23}$$

Note that, at variance with the previous expression, here in the numerator we have the full wave function instead of its linearized approximation. In the (rare) cases where no acceptable value of ϵ is found due to possibly large statistical fluctuations in the VMC estimators, we perform an additional run adopting the previous parameter set and a new optimization is attempted. In our experience, this procedure proved extremely robust.

The chief advantage of the additional constraint is that it suppresses the potential instabilities caused by the nonlinear dependence of the wave function on the variational parameters. When using the "standard" version of the LM, there were instances in which, despite the variation of the linear wave function being well below the threshold of Eq.(4.21), the full wave function fluctuated significantly more, preventing the convergence of the minimization algorithm. As for the wave-function variation, we found that choosing $\delta = 0.2$ guarantees a fast and stable convergence.

The LM exhibits a much faster convergence pattern than the SR, previously used in AFDMC. In Fig. (4.4), we show the ^{4}He variational energy obtained for physical pion mass and $\Lambda = 4$ fm $^{-1}$ as a function of the number of optimization steps for both SR and LM. While the LM takes only $\simeq 15$ steps to converge, the SR is much slower; after 50 steps the energy is still much above the asymptotic limit. We have observed analogous behavior for other values of the cutoff and the pion mass. In the ^{16}O case, the improvement of the LM with respect to the SR is even more dramatic due to the clustering of the wave function, which will be discussed in detail in Chapter{6}.

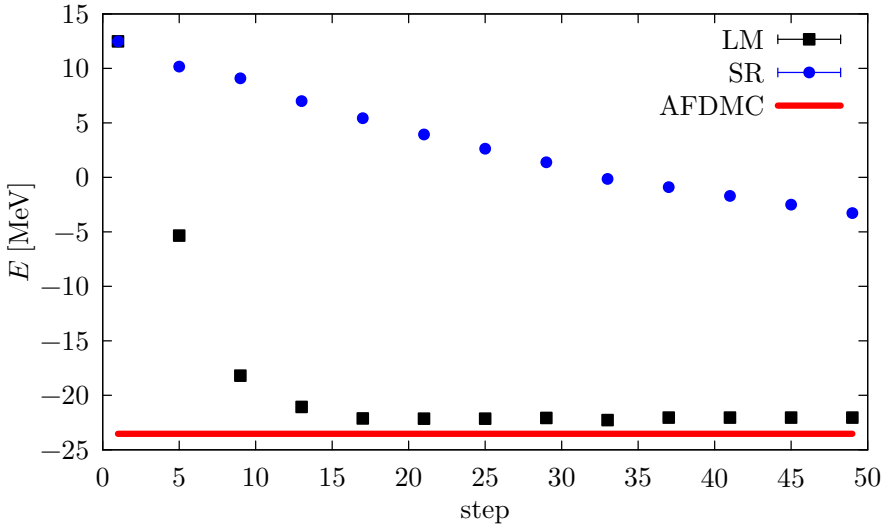

Figure 4.4: Convergence pattern of the ^{4}He variational energy at physical pion mass and Λ =800 MeV as a function of the number of optimization steps for the SR method (black squares) and the LM (blues circles). For comparison, the red line indicates the AFDMC result.

4.2 DMC

DMC is based on the use of the imaginary time propagator to enhance the ground state from any wave function which is not orthogonal to it. Taking the time dependent Schrödinger equation:

$$i\hbar\partial_t\Psi = \hat{H}\Psi = -\frac{\hbar^2}{m}\nabla^2\Psi(\vec{r},t) + (V(\vec{r}) - E_{off})\,(\vec{r},t), \tag{4.24}$$

by making a Wick rotation ($it \to \tau$)

$$-\hbar\partial_\tau\Psi = \hat{H}\Psi = -\frac{\hbar^2}{m}\nabla^2\Psi(\vec{r},\tau) + (V(\vec{r}) - E_{off})\,(\vec{r},\tau) \tag{4.25}$$

we derive a classical diffusion equation. Considering the wave function as the sum of eigenstates of the Hamiltonian

$$\Psi = \sum_{n=0}^{+\infty} C_n\Psi_n, \tag{4.26}$$

such as

$$\hat{H}\Psi_n = \epsilon_n \Psi_n, \tag{4.27}$$

and introducing imaginary time evolution operator

$$\Psi\left(\tau_0+\tau\right) = e^{-\frac{\hat{H}\tau}{\hbar}}\Psi(\tau_0) = \sum_{n=0}^{+\infty} C_n e^{-(\frac{\epsilon_n-\epsilon_0)\tau}{\hbar}}\psi_n, \tag{4.28}$$

the high energy states will quickly disappear, the first excited state will become negligible with respect to the ground state in a time $\Delta\tau \simeq \frac{1}{E_1+E_{gs}}$

$$e^{-\frac{(\hat{H}-E_0)\tau}{\hbar}}\Psi(\tau_0) \overset{\tau\to\infty}{\longrightarrow} c_0\psi_0 \tag{4.29}$$

The procedure is to use this propagation on an ensamble of walkers distributed on the Hilbert space of the many-particle problem. Eq.(4.29) is divided in imaginary time steps $\Delta\tau$. When a sufficiently large number of them has been performed all the high energy components vanish and the algorithm samples the ground state of the system. The path of the walkers can be used as integration points to estimate

$$I_n = \frac{\langle\Psi|H|\Psi_0\rangle}{\langle\Psi|\Psi_0\rangle} \tag{4.30}$$

It is relatively easy to explicit the propagation of a walker from an initial point to the next one according with Eq.(4.28) for a general Hamiltonian,

$$\Psi_{\tau+\Delta\tau}\left(\vec{r}\right) = \int \langle\vec{r}|e^{-H\Delta\tau}|\vec{r'}\rangle\,\langle\vec{r'}|\Psi\rangle\,d\vec{r'} = \int G\left(\vec{r'}\to\vec{r}\right)\Psi_\tau\left(\vec{r'}\right)d\vec{r'}. \tag{4.31}$$

Nonetheless, the green function $G\left(\vec{r'}\to\vec{r}\right)$ might be complicated to be evaluated. The conventional way to approach the propagation is to separate, using a Trotter expansion [63], the exponential in the kinetic and potential contributions:

$$G\left(\vec{r'}\to\vec{r}\right) = \langle\vec{r}|e^{-H\Delta\tau}|\vec{r'}\rangle = \langle\vec{r}|e^{-\Delta\tau\left(\frac{\vec{p}^2}{2m}+V\right)}|\vec{r'}\rangle \simeq \langle\vec{r}|e^{-\Delta\tau\frac{\vec{p}^2}{2m}}e^{-\Delta\tau V)}|\vec{r'}\rangle + O(\Delta\tau) \tag{4.32}$$

that requires $\Delta\tau$ to be small. Using a Fourier Transform and solving the kinetic Green's function one finds

$$\langle \vec{r}|e^{-\Delta\tau\frac{\vec{p}^2}{2m}}|\vec{r'}\rangle \rightarrow e^{\frac{\hbar^2}{2m}\left(\vec{r}-\vec{r'}\right)^2} + O(\Delta\tau) \tag{4.33}$$

which is the probability that a new step at coordinate $\vec{r}$ is sampled from a old one in $\vec{r}'$ and can be easily done sampling a Gaussian distributed random number and shifting the walker position. It is possible to increase the algorithm precision developing further the Trotter expansion in Eq.(4.32) [63]:

$$G\left(\vec{r'} \rightarrow \vec{r}\right) = \langle \vec{r}|e^{-H\Delta\tau}|\vec{r'}\rangle \simeq \langle \vec{r}|e^{-\frac{\Delta\tau V(\vec{r})}{2}} e^{-\Delta\tau\frac{\vec{p}^2}{2m}} e^{-\frac{\Delta\tau V(\vec{r'})}{2}}|\vec{r'}\rangle + O(\Delta\tau^2) \tag{4.34}$$

The potential contribution can be included as a weight w attached to any walker for the purposes of calculating the integral (4.30):

$$w = \left(e^{-\Delta\tau V} e^{-\Delta\tau E_t}\right), \tag{4.35}$$

$$I_N = \frac{\sum_{x\in W}^{N} w_x\, g(x)}{\sum w_x} \tag{4.36}$$

In the above equations, W indicates the population of walkers diffused using the kinetic energy and E_t (trial energy) is a constant needed for renormalization purposes. This procedure leads to the propagation of many walkers whose weights suffer large variations. In fact many of them have small weight and, while consuming computational power, do not contribute to the integration. A common and successful strategy consists to allow the number of walkers to fluctuate using the so called *branching process*: a random number μ uniformly distributed in the interval [0, 1] is added to the weight w

$$\eta_i = \mathrm{INT}(w + \mu), \tag{4.37}$$

where INT(x) represent the integer part of x. Instead of moving each walker, η_i copies of it are instead created at the newly drawn position. In such a way, depending on the potential $V(\vec{r})$ and the trial energy E_t, some configurations will disappear and some other will replicate, resulting in the evolution of walker population.

Trial energy: The trial energy is a parameter needed to stabilize the number of walkers. According to with Eq.(4.35), if the trial energy is too different from the ground state energy, the population of walkers will suffer large fluctuations. Walkers may all be killed if E_t is too high or the population becomes

too large if it is too low. A simple way to stabilize the number of walkers is to adjust E_T step by step along the imaginary time propagation according to

$$\tilde{E}_T = E_T + \frac{1}{\delta\tau} ln \left(\frac{N_w}{N_0} \right) \tag{4.38}$$

where N_w is the current number of walkers and N_0 is the optimal number of walkers. After a sufficient number of steps, E_T will converge at the ground state value, stabilizing the population. This approach is useful when there are no other indications about the energy of the system, but this dynamical adjustments effectively adds an extra piece to the Hamiltonian, which will affect the final result with a systematic error. A convenient method is to adjust E_T till converges, then fix it in the remains of the propagation to find the correct ground state energy without the systematic introduced by Eq.(4.38).

Importance sampling

Diffusing walkers as described in the last section [51, 64] results in a very inefficient method, since the walkers will randomly sample the space just to be killed once they reach an unfavorable area. It is convenient to introduce a *guide function*, $\Psi_g(\vec{r})$, to drive the walkers in more favorable positions for the integration. It is also helpful to introduce a *trial wavefunction* $\Psi_T(\vec{r})$ on which it is easy to calculate numerically the Hamiltonian operator. It is possible to rewrite Eq.(4.30) as

$$E_{\psi_0} = \frac{\langle \psi_0 | H | \Psi_T \rangle}{\langle \psi_0 | \Psi_T \rangle} = \frac{\int \left(\psi_0^* \Psi_g\right) \left(\frac{H\Psi_T}{\Psi_g}\right)}{\int {\psi_0}^* \Psi_T} \tag{4.39}$$

where this relation is exact and Ψ_0 is the ground state of the system. $\Psi_g(\vec{r})$ and $\Psi_T(\vec{r})$ are two distinct functions, but is common to use the same function for both. However, they have different purposes: the first is meant to be the best possible approximation of ϕ and the second has to be easily applied to the Hamiltonian operator.

Importance sampling largely improves the algorithm convergence and usability, but it highlights some problematics of the diffusive process. In general, $({\psi_0}^* \Psi_g)$ might not be always-positive, introducing problems in sampling. This issue, know as Sign Problem will be discussed in more detail in section {4.2}.

It is possible to use the diffusion algorithm to enhance the contribution of $({\psi_0}^* \Psi_g)$ from $(\Psi^* \Psi_g)$ where Ψ is represented by the walkers population. The diffusion green-function with the importance shows some differences with respect to Eq.(4.31), and can be written as

$$\Psi_g\left(\vec{r}\right) \Psi_{\tau+\Delta\tau}\left(\vec{r}\right) = \int G_g\left(\vec{r'} \to \vec{r}\right) \Psi_g(\vec{r'}) \Psi_\tau\left(\vec{r'}\right), \tag{4.40}$$

where

$$G_g\left(\vec{r'} \to \vec{r}\right) G\left(\vec{r'} \to \vec{r}\right) \frac{\Psi_g\left(\vec{r}\right)}{\Psi_g(\vec{r'})}. \tag{4.41}$$

Nonetheless, the kinetic part of the propagator differs from Eq.(4.33) because the inclusion of the piece $\frac{\Psi_g(\vec{r})}{\Psi_g(\vec{r'})}$ which has be included in the propagator. Expanding it around $\vec{r'}$:

$$\langle \vec{r} | e^{-\Delta\tau \frac{\vec{p}^2}{2m}} | \vec{r'} \rangle \to e^{\frac{\hbar^2}{2m}\left(\vec{r} - \vec{r'} + \frac{2m}{\hbar^2}\Delta\tau \frac{\nabla\Psi_g(\vec{r})}{\Psi_g(\vec{r})}\right)^2} + O(\Delta\tau). \tag{4.42}$$

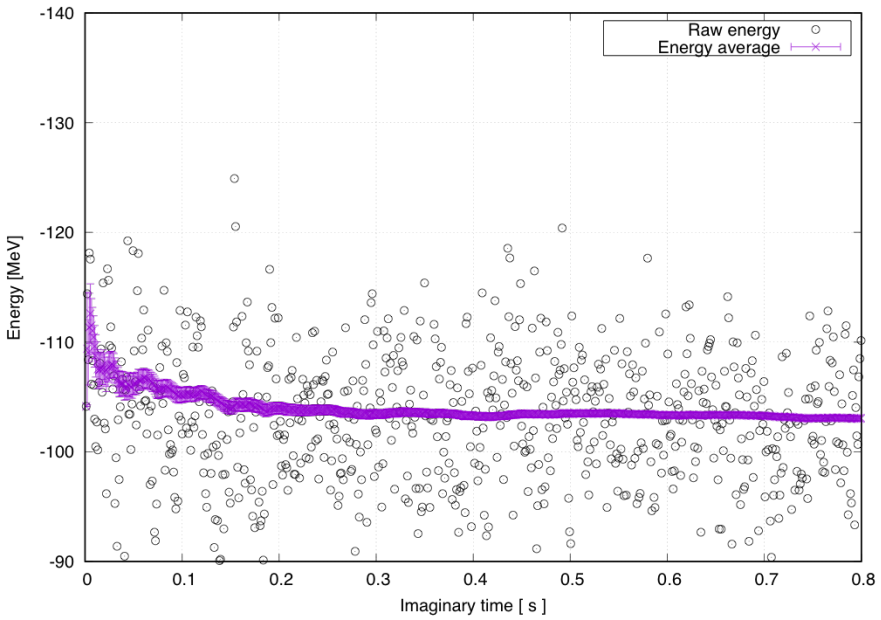

Figure 4.5: In the figure is shown a typical diffusion calculation, the scattered point are the local energies of each walker at a given time. The purple dots are the average energy with the stochastic error of each step. The calculation thermalized after about 0.2 MeV^{-1}.

The term $\frac{2m}{\hbar^2}\Delta\tau\frac{\nabla\Psi_g(\vec{r})}{\Psi_g(\vec{r})}$ is called *drift* and it is a pseudoforce which contributes to push the walkers where the integrand is supposed to be more relevant according with the guide wave function.

QMC in a nutshell

The integral of Eq.(4.40) is transformed in a sum of local energies calculated on points draw from the distribution $(\psi_0{}^*\Psi_g)$.

$$E = \sum_{x\in(\Psi_0{}^*\Psi_g)} \frac{H\Psi_g}{\Psi_g} \tag{4.43}$$

Where the probability $(\psi_0^*\Psi_g)$ is sampled using the relation:

$$\Psi_g\left(\vec{r}\right)\Psi_{\tau+\Delta\tau}\left(\vec{r}\right) = \int \tilde{G}\left(\vec{r'}\rightarrow\vec{r}\right)\frac{\Psi_g\left(\vec{r}\right)}{\Psi_g\left(\vec{r'}\right)}\Psi_g\left(\vec{r'}\right)\phi_\tau\left(\vec{r'}\right) \tag{4.44}$$

$$G\left(\vec{r'}\rightarrow\vec{r}\right) = \langle\vec{r}|e^{-H\Delta\tau}|\vec{r'}\rangle = e^{-\frac{\hbar^2}{2m}\left(\vec{r}-\vec{r'}+2\Delta\tau\frac{\vec{\nabla}\phi_{gs}}{\phi_{gs}}\right)^2} e^{-\Delta\tau(\frac{V(\vec{r})+V(\vec{r'})}{2}-E_T)} \tag{4.45}$$

In the following we report the numerical procedure of the DMC method:

A) Generating configurations

The N initial configurations of the multiparticle Hilbert space are sampled. They can be distributed either in an equispaced grid, random, or according to an arbitrary distribution.

The initial Trial Energy E_T should be chosen to be as close as possible to the ground state energy.

B) Moving

The kinetic energy is used to propose a new position for each walker, the new position is sampled according to:

$$\vec{r} = \vec{r'} + \xi \tag{4.46}$$

where ξ is sampled from the probability

$$\xi = e^{-\frac{\hbar^2}{2m}\left(\vec{r}-\vec{r'}+2\Delta\tau\frac{\vec{\nabla}\Psi_g}{\Psi_g}\right)} \tag{4.47}$$

C) Branching

When the walkers reach the new position, can survive, be killed or even branch according to probability $e^{-\Delta\tau\left(\frac{V(\vec{r})+V(\vec{r'})}{2}-E_T\right)}$. A new random number $\eta \in [0,1]$ should be drawn, the original walker is then replaced with N of copies of himself.

$$N = \mathrm{INT}\left(e^{-\Delta\tau\left(\frac{V(\vec{r})+V(\vec{r'})}{2}-E_T\right)}+\eta\right) \tag{4.48}$$

Where INT is the function which truncate a real number to the lower nearest natural.

D) Operator estimation

The local energy $\frac{H\Phi_g}{\Phi_g}$ is calculated on the new coordinate as described in Eq.(4.43). If a fluctuating trial energy as in Eq.(4.38) is used, it has to be updated using the average local energy among walkers. If the local energy is decreasing with respect to the previous steps, there are still high-energy contribution in the wave function that the algorithm has to suppress.

This means that additional diffusive steps have to be done before accumulating relevant statistic of the ground state (**goto point B** until the energy converges).

If the energy has converged, the walkers are distributed according to $(\psi_0^*\Psi_g)$ and the statistic on the observables can be collected.

E) Accumulating statistics

If the local energy is stable, the energy estimator at each step n reads

$$\langle E\rangle_n = \frac{\sum_{i\leq n}\sum_{w\in Walkers}\left[w_{i,w}\frac{H\phi_g(\vec{r}_{w,i})}{\phi_g(\vec{r}_{w,i})}\right]}{\sum_{i\leq n}\sum_{w\in Walkers}\left[w_{i,w}\right]} \tag{4.49}$$

Where $\vec{r}_{w,i}$ is the generalized coordinate of the walker w at imaginary time step i.

According to the central limit theorem, the energy distribution is gaussian. Therefore, it is possible to estimate the variance of the energy:

$$\sigma_n(E) = \left\langle E^2\right\rangle_n - \langle E\rangle_n^2\,, \tag{4.50}$$

which can be decreased iterating steps **B)**, **C)** and **D)** as many times as needed.

Alternative Green's function implementation

In the case of a problem which is best described within a discrete Hilbert space (like the Harmonic Oscillator or plane waves), might be unfeasible to use the full propagator of Eq.(4.34). However, the problem is greatly reduced if the propagator is expanded as

$$e^{-H\Delta\tau} = \mathbb{1} - \Delta\tau H + \frac{1}{2}(\Delta\tau)^2 H^2 + ... \tag{4.51}$$

and applied linearly. While in the coordinate space it is relatively easy to move a walker with a random step centered on the old positions, in a discrete space is often more convenient to drawn the new position from the ensemble of states connected to the old one with probability

$$\eta_{\chi_{old}\to\chi_{new}} = 1 - \Delta\tau \left\langle \chi_{old}|H|\chi_{new}\right\rangle . \tag{4.52}$$

In the previous equation χ_{old} is the starting configuration and χ_{new} can be any configuration of the space. A detail description of this method and a possible solution for the related Sign Problem can be found extensively in literature: [50, 65–71].

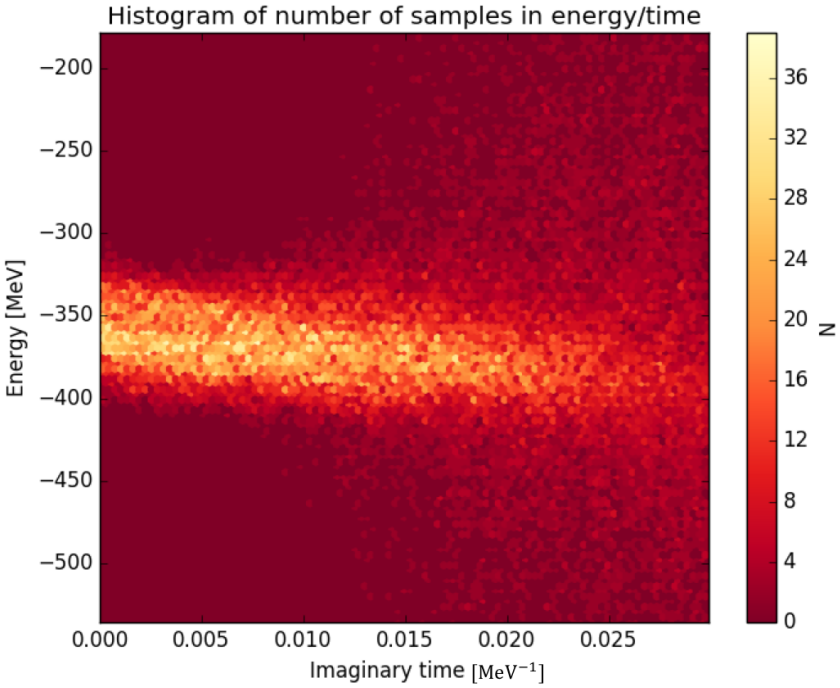

Figure 4.6: The divergence of the error in a Release Node Monte Carlo when the antisymmetric wave function disappear in ^{16}O at $m_\pi = 800$. The histogram represent the number of walkers with a given energy during the imaginary simulation time.

Sign Problem

Above described DMC algorithm can be easily applied to bosonic systems. However, for fermion-like systems or excited states, the diffusion procedure is more critical since nodal surfaces are present in the wave function and $(\psi_0^* \Psi_g)$ is not longer guaranteed to be real and positive. This criticality has a double fold, on the one hand $(\psi_0^* \Psi_g)$ can no longer be interpreted as a probability. On the other one, the error of the calculation will exponentially increase also if $(\psi_0^* \Psi_g) > 0$ because of the disappearance of antisymmetric contributions in the sampled wave function. The two problems are alleviated by the fixed-phase and constrained-path approximations that ensure $(\psi_0^* \Psi_g) > 0$ and the sampled ground state to be antisymmetric.

To understand why the error of the calculation would exponentially increase when simulating fermions, it is sufficient to expand the initial wave function in the base of the Hamiltonian eigenfunctions $\{\varphi\}_n$. This contains

both symmetric and antisymmetric components ($\{\varphi^s\}_n$ and $\{\varphi^a\}_n$),

$$|\Psi\rangle = \sum_{n=0}^{\infty} c_n^s e^{-(E_n^s - E_T)} |\varphi_n^s\rangle + \sum_{n=0}^{\infty} c_n^a e^{-(E_n^a - E_T)} |\varphi_n^a\rangle , \tag{4.53}$$

where c_n are complex coefficients. The energy of the symmetric ground state (E_0^s) is always lower than the antisymmetric one (E_0^a), therefore the only surviving component after the imaginary propagation will be the symmetric one $\{\varphi^s\}_n$. Despite the disappearance of the fermionic contribution the estimator observable

$$\langle O \rangle = \lim_{\tau \to +\infty} \frac{\int \langle \Psi_g | O | \vec{r} \rangle \, \phi(\vec{r}, \tau) d\vec{r}}{\int \Psi_g(\vec{r}) \phi(\vec{r}, \tau) d\vec{r}} \tag{4.54}$$

recovers the correct expectation value if the guide wave function has the same quantum numbers of the ground state. In other words, if the guide wave function of a fermionic ground state is antisymmetric, and has the same quantum number of ϕ, any calculated observables will turn to be correct. However, the projected contribution in Eq.(4.54) will be dominated by exponentially increasing noise, since the antisymmetric contribution in Eq.(4.53) progressively disappears, as can be seen in Fig.(4.6).

A definitive solution of this problem has still to be found. However, it can be controlled introducing some approximations in the algorithm. In this work, we used prevalently coordinate-defined codes, where it is possible to distinguish the ground state from excited states by the phase and nodal surface of the wavefunction and one can apply two methods: *the constrained-path approximation* and *the fixed-phase approximation* to extract results for fermions.

The idea of the **constrained-path approximation** [72] is to constrain the path of walkers to be in space regions where the real part of the wavefunction always has the same sign. It reflects in a modification of Eq.(4.42) in which a real Drift is imposed. A suitable choice for it is:

$$v_d(\vec{r}) = 2 \frac{\nabla Re\left[\Psi_g\right]}{Re\left(\Psi_g\right)}, \tag{4.55}$$

and

$$\frac{Re\left[\Psi_g(\vec{r})\right]}{Re\left[\Psi_g(\vec{r'})\right]} > 0, \tag{4.56}$$

where $\vec{r}$ and $\vec{r}'$ are the coordinates configurations before and after the propagation. To ensure this each walker in which Eq.(4.56) is violated will have its weight set to zero and killed. The observables can be calculated as:

$$\langle \mathcal{O} \rangle = \frac{\sum_{r\in\Gamma} \mathcal{O} Re\left[\Psi_g(\vec{r})\right]}{\sum_{r\in\Gamma} Re\left[\Psi_g(\vec{r})\right]} \tag{4.57}$$

where the points are sampled from Γ: the propagation $(\Psi_g^* \phi)$ with the nodal surface fixed (Eq.4.56).

The second possibility to work around the sign problem is the **fixed phase** approximation, as proposed by Ref.[73]. A generic complex wave function can be written as:

$$\Psi(\vec{r}) = |\Psi(\vec{r})|\, e^{i\varphi(\vec{r})} \tag{4.58}$$

with $\varphi(\vec{r})$ the phase of $\Psi(\vec{r})$. Eq.(4.42) is rewritten as:

$$\vec{v_d}(\vec{r}) = 2\frac{\vec{\nabla}|\Psi_g(\vec{r})|}{|\Psi_g(\vec{r})|} = 2Re\left[\frac{\vec{\nabla}\Psi_g(\vec{r})}{\Psi_g(\vec{r})}\right] \tag{4.59}$$

To practically implement the constrained-phase approximation it suffice to force the walkers to have the same phase as the Importance function Ψ_g. However, the introduction of an extra term in the green function is needed in order to preserve the normalization of the wave function:

$$e^{\left[-\frac{\hbar^2}{2m}\left(\vec{\nabla}\Psi_g(\vec{r})\right)^2 d\tau\right]} \tag{4.60}$$

Which can be included in the branching weight ξ exploiting the relation

$$Re\left[\frac{\vec{\nabla}^2\Psi_g(\vec{r})}{\Psi_g(\vec{r})}\right] = \frac{\vec{\nabla}^2\Psi_g(\vec{r})}{\Psi_g(\vec{r})} - \left(\vec{\nabla}\Psi_g(\vec{r})\right)^2. \tag{4.61}$$

ξ results modified as:

$$\begin{aligned}\xi = &\frac{|\Psi_g(\vec{r'})|}{|\Psi_g(\vec{r})|}\frac{\Psi_g(\vec{r})}{\Psi_g(\vec{r'})}\times \\ &exp\left\{-\frac{1}{2}\left[-\frac{\hbar}{2m}\frac{\nabla^2|\Psi_g(\vec{r})|}{|\Psi_g(\vec{r})|} - \frac{\hbar}{2m}\frac{\nabla^2|\Psi_g(\vec{r'})|}{|\Psi_g(\vec{r'})|} + \frac{(V\Psi_g)(\vec{r})}{2\Psi_g(\vec{r})} + \frac{(V\Psi_g)(\vec{r'})}{2\Psi_g(\vec{r'})}\right]\right\}\end{aligned} \tag{4.62}$$

Which is only partially similar to Eq.(4.47), with a different drift choice. Eq.(4.58) allows to rewrite the last piece of Eq.(4.62) as

$$\frac{|\Psi_g(\vec{r'})|}{|\Psi_g(\vec{r})|}\frac{\Psi_g(\vec{r})}{\Psi_g(\vec{r'})} = e^{i\left[\phi_g(\vec{r})-\phi_g(\vec{r'})\right]} \tag{4.63}$$

Observables are then calculated as:

$$\langle \mathcal{O} \rangle = \sum_{r\in\Gamma} Re\left[\frac{\mathcal{O}\Psi_g(\vec{r})}{\Psi_g(\vec{r})}\right] \tag{4.64}$$

In which $\Gamma = (\Psi_g^*\phi)$ with the fixed phase in order to be real and operators are calculated using the Real part.

We have to recall that, introducing an importance function with a given set of quantum numbers (for example fixing the total angular momentum) allows to get the smallest energy corresponding to those quantum numbers, but the constrained-path/fixed-phase is essential in order to not have exponentially growing uncertainties. The constrained-path method is not guaranteed anymore to give an upper bound to the energy, as DMC does, because of the extra piece introduced in the Hamiltonian. Thus, the extension of DMC to a fermionic system described by complex wavefunctions is not variational anymore. For further details about constrained-path and fixed-phase approximations can be found in the papers [53, 54, 74–76] and in the book [51].

4.3 AFDMC

Nuclear potentials are characterized by nontrivial spin-isospin operatorial structure which can include angular and spinorial components. Their use in QMC implies an exponential growth of the computational cost with the number of nucleons. In fact the spin-isospin components of the wave function are described by a many body vector of dimension $N_i \cdot N_s$ where

$$N_s = 2^A \tag{4.65}$$

$$N_i = \binom{A}{Z} = \frac{A!}{Z!(A-Z)!} \tag{4.66}$$

Deuterium is composed by one proton and one neutron, for a total of $N_s = 2$ and $N_i = 2$. So a total of 4 possible spin-isospin states. The picture changes when inspecting bigger systems: ^{16}O requires $N_s \approx 65000$ and $N_i \approx 13000$ leads to arrays that are difficultly stored or manipulated in a computer.

If we apply the operator $\sigma_i \cdot \sigma_j$ as in the example,

$$\vec{\sigma}_i \cdot \vec{\sigma}_j = 2\left(\sigma_i^+ \sigma_j^- + \sigma_i^- \sigma_j^+\right) + \sigma_i^z \sigma_j^z = 2\mathcal{P}_i j^\sigma - \mathbb{1} \tag{4.67}$$

applied to the 3-body spinor (no isospin nor antisymmetrization included)

$$|\Phi_{3b}\rangle = \begin{pmatrix} \varphi_{\uparrow\uparrow\uparrow} \\ \varphi_{\uparrow\uparrow\downarrow} \\ \varphi_{\uparrow\downarrow\uparrow} \\ \varphi_{\uparrow\downarrow\downarrow} \\ \varphi_{\downarrow\uparrow\uparrow} \\ \varphi_{\downarrow\uparrow\downarrow} \\ \varphi_{\downarrow\downarrow\uparrow} \\ \varphi_{\downarrow\downarrow\downarrow} \end{pmatrix} \tag{4.68}$$

We obtain

$$\vec{\sigma}_2 \cdot \vec{\sigma}_3 \left|\Phi_{3b}\right\rangle = \begin{pmatrix} \varphi_{\uparrow\uparrow\uparrow} \\ 2\varphi_{\uparrow\downarrow\uparrow} - \varphi_{\uparrow\uparrow\downarrow} \\ 2\varphi_{\uparrow\uparrow\downarrow} - \varphi_{\uparrow\downarrow\uparrow} \\ \varphi_{\uparrow\downarrow\downarrow} \\ \varphi_{\downarrow\uparrow\uparrow} \\ 2\varphi_{\downarrow\downarrow\uparrow} - \varphi_{\downarrow\uparrow\downarrow} \\ 2\varphi_{\downarrow\uparrow\downarrow} - \varphi_{\downarrow\downarrow\uparrow} \\ \varphi_{\downarrow\downarrow\downarrow} \end{pmatrix} \tag{4.69}$$

The propagation of this kind of spinor does require the application of a huge non-symmetrical sparse matrix which is extremely computationally expensive. It can be realized that the components written as in Eq.(4.69) are not close with respect to the spin-isospin operators. This is caused by the quadratic spin and isospin operators dependence in the potential. The presence of those parts is why GFDMC can handle up to a dozen of interacting nucleons.

AFDMC method

AFDMC [77–86] method is based to the idea of rewriting the quadratic spin and isospin operators of the potential using the Hubbard–Stratonovich transformation. Since the single particle spin-isospin space is closed with respect to linear operators, it is possible to use single-particle spin-states, instead of the many body-ones. This reduces the spinorial part from $N_s N_i = A^2 \binom{A}{Z}$ to $N_i = 4A$.

Dividing the potential in spin-dependent V_{SD} and spin-independent V_{SI} parts:

$$V = V_{SD} + V_{SI} \tag{4.70}$$

it is possible to apply the Hubbard–Stratonovich transformation to the spin-dependent piece.

In the following, we describe how to express the quadratic part of some of the most common spin/isospin-dependent potentials in order to directly apply

the Hubbard–Stratonovich transformation.

Consider $\sigma_i \cdot \sigma_j$ term, it can be rewritten as

$$\begin{aligned} V_{SD}^{\sigma\sigma} &= \sum_{i<j} v^{\sigma\sigma}\left(\vec{r}_{ij}\right) \vec{\sigma}_i \cdot \vec{\sigma}_j \\ &= \sum_{i<j} \left[\sigma_{ix}\sigma_{jx} + \sigma_{iy}\sigma_{jy} + \sigma_{iz}\sigma_{jz}\right] = \sum_{i<j} \left[\vec{\sigma}_i A_{ij}^{\sigma\sigma} \vec{\sigma}_j\right]. \end{aligned} \tag{4.71}$$

The same can be applied applied to any other spin/isospin operator:

$$\begin{aligned} V_{SD}^{\tau\tau} &= \sum_{i<j} v^{\tau\tau}\left(\vec{r}_{ij}\right) \vec{\tau}_i \cdot \vec{\tau}_j \\ &= \sum_{i<j} \left[\vec{\tau}_i A_{ij}^{\tau\tau} \vec{\tau}_j\right] \end{aligned} \tag{4.72}$$

and

$$\begin{aligned} V_{SD}^{\tau\tau\sigma\sigma} &= \sum_{i<j} v^{\tau\tau\sigma\sigma}\left(\vec{r}_{ij}\right) \left(\vec{\tau}_i \otimes \vec{\sigma}_i\right) \cdot \left(\vec{\tau}_j \otimes \vec{\sigma}_j\right) \\ &= \sum_{i<j} \left[\vec{\tau}_i \vec{\sigma}_i A_{ij}^{\tau\tau\sigma\sigma} \vec{\tau}_j \vec{\sigma}_j\right] \end{aligned} \tag{4.73}$$

The $3A \times 3A$ matrices $A^{\sigma\sigma}$ and $A^{\tau\tau\sigma\sigma}$ as well as the $A \times A$ matrix $A^{\tau\tau}$ represent the two-body interaction. They depend on the relative coordinate $(\vec{r_i} - \vec{r_j})$ and their diagonal is zero (they do not contain self-interaction).

$$\begin{aligned} A_{ij}^{\tau\tau} &= v^{\tau\tau}(\vec{r}_{ij}) \\ A_{i\alpha,\,j\beta}^{\sigma\sigma} &= v^{\sigma\sigma}(\vec{r}_{ij})\delta_{\alpha\beta} + v^{tt}(\vec{r}_{ij}) \left(3\hat{r}_{ij}^{\alpha} \cdot \hat{r}_{ij}^{\beta} - \delta_{\alpha\beta}\right) \\ A_{i\alpha,\,j\beta}^{\sigma\sigma\tau\tau} &= v^{\sigma\sigma\tau\tau}(\vec{r}_{ij})\delta_{\alpha\beta} + v^{tt\sigma\sigma}(\vec{r}_{ij}) \left(3\hat{r}_{ij}^{\alpha} \cdot \hat{r}_{ij}^{\beta} - \delta_{\alpha\beta}\right) \end{aligned} \tag{4.74}$$

They are real and symmetric under cartesian components. Hence they have real eigenvalues and orthogonal eigenstates, given by

$$\begin{aligned} \sum_{j} A_{i,\,j}^{\tau\tau}\ \Xi_{n,\,i}^{\tau\tau} &= \xi_n^{\tau\tau} \Xi_{n,\,i}^{\tau\tau} \\ \sum_{j,\,\beta} A_{i\alpha,\,j\beta}^{\sigma\sigma}\ \Xi_{n,\,i\alpha}^{\sigma\sigma} &= \xi_n^{\sigma\sigma} \Xi_{n,\,i\alpha}^{\sigma\sigma} \\ \sum_{j,\,\beta} A_{i\alpha,\,j\beta}^{\sigma\sigma\tau\tau}\ \Xi_{n,\,i\alpha}^{\sigma\sigma\tau\tau} &= \xi_n^{\tau\tau\sigma\sigma} \Xi_{n,\,i\alpha}^{\sigma\sigma\tau\tau} \end{aligned} \tag{4.75}$$

It is convenient to normalize the eigenstates as follows

$$\sum_{i\alpha} \Xi_{n,\,i\alpha}^{c} \Xi_{m,\,i\alpha}^{c} = \delta_{mn} \tag{4.76}$$

with $c = \tau\tau, \sigma\sigma, \sigma\sigma\tau\tau$. The last equation can be used to write:

$$\sigma_{i\alpha} = \sum_n \left(\sum_{j,\beta} \Xi^{\sigma\sigma}_{n,\,i\beta} \sigma_{j\beta} \right) \Xi^{\sigma\sigma}_{n,\,i\alpha} \tag{4.77}$$

and

$$\sigma_{i\alpha}\vec{\tau_i} = \sum_n \left(\sum_{j,\beta} \Xi^{\tau\tau}_{n,\,i\beta} \sigma_{j\beta} \right) \Xi^{\tau\tau}_{n,\,i\alpha} \tag{4.78}$$

Introducing the new operators

$$\begin{aligned} \mathcal{O}^{\sigma\sigma}_n &= \sum_j \vec{\sigma_j} \vec{\Xi}^{\sigma\sigma}_{n,j} \\ \vec{\mathcal{O}}^{\tau\tau\sigma\sigma}_n &= \sum_j (\vec{\tau_j} \otimes \vec{\sigma_j}) \vec{\Xi}^{\tau\tau\sigma\sigma}_{n,j} \\ \vec{\mathcal{O}}^{\tau\tau}_n &= \sum_j \vec{\tau_j} \Xi^{\tau\tau}_{n,j} \end{aligned} \tag{4.79}$$

Eq.(4.73) can be finally rewritten in therms of A^c_{ij} eigenvectors and eigenvalues:

$$\begin{aligned} V^{\sigma\sigma}_{ij} &= \frac{1}{2} \sum_{n=1}^{A} \vec{\xi}^{\sigma\sigma}_n \cdot (\mathcal{O}^{\sigma\sigma}_n)^2 \\ V^{\tau\tau\sigma\sigma}_{ij} &= \frac{1}{2} \sum_{n=1}^{A} \sum_{\alpha=\{x,y,z\}} \vec{\xi}^{\tau\tau\sigma\sigma}_n \cdot \left(\vec{\mathcal{O}}^{\tau\tau\sigma\sigma}_{n\alpha} \right)^2 \\ V^{\tau\tau}_{ij} &= \frac{1}{2} \sum_{n=1}^{A} \sum_{\alpha=\{x,y,z\}} \vec{\xi}^{\tau\tau}_n \left(\vec{\mathcal{O}}^{\tau\tau}_{n\alpha} \right)^2 \end{aligned} \tag{4.80}$$

In this way the spinorial potential is expressed to make explicit the quadratic form of the operators, making the Hubbard–Stratonovich straightforward applicable. Using the general form of operators in Eq.(4.80) one can write

$$e^{-V^c_{ij}\Delta\tau} = e^{-\frac{\Delta\tau}{2}\sum_{n=1}^{3N} \xi_n \mathcal{O}^2_n} = \prod_n e^{-\frac{\Delta\tau}{2}\xi_n \mathcal{O}^2_n} + O(\Delta\tau^2) \tag{4.81}$$

Quadratic dependencies can be linearized using the Hubbard–Stratonovich introducing a new (auxiliary) field $x(\vec{x})$:

$$e^{-\frac{1}{2}\xi\mathcal{O}^2} = \frac{1}{\sqrt{2\pi}} \int dx e^{-\frac{x^2}{2} + x\sqrt{-\xi}\,\mathcal{O}}, \tag{4.82}$$

In the energy integral there are $3N$ operators, and an auxiliary field should be introduced for each space coordinate of every particle:

$$e^{-V_{ij}^c \Delta\tau} = e^{-\frac{\Delta\tau}{2}\sum_{n=1}^{3N}\xi_n \mathcal{O}_n^2} = \prod_{n=1}^{3N}\left[\frac{1}{\sqrt{2\pi}}\int dx_n e^{-\frac{x_n^2}{2}+\sqrt{-\xi_n\delta\tau}x_n\mathcal{O}_n}\right] \tag{4.83}$$

That can be used to propagate a single particle spinor rotating it inside the single particle basis. It is possible to apply Eq.(4.83) analytically only in the case of two-spinors. However, it is always possible to rotate 4-spinors diagonalizing the rotation matrix.

The propagator of Eq.(4.34) has to be generalized to include the spin and isospin degrees of freedom:

$$\begin{aligned}
&\left\langle \vec{r}', \vec{s}' \left| e^{-(H-E_0)\Delta\tau} \right| \vec{r}, \vec{s} \right\rangle = \\
&= \left(\frac{1}{4\pi\delta\tau}\right)^{\frac{3N}{2}} \left\{ e^{\frac{(\vec{r}-\vec{r}')^2}{4\delta\tau}} e^{-(V_{SI}-E_{off})} \prod_{n=1}^{3N}\left[\frac{1}{\sqrt{2\pi}}\int dx_n e^{-\frac{x_n^2}{2}+\sqrt{-\lambda_n\delta\tau}x_n\mathcal{O}_n}\right]\right\} \\
&= \frac{1}{\sqrt{2\pi}}\int \prod_{n=1}^{3N} dx_n e^{-\frac{x_n^2}{2}} \left(\frac{1}{4\pi\delta\tau}\right)^{\frac{3N}{2}} e^{\frac{(\vec{r}-\vec{r}')^2}{4\delta\tau}} e^{-(V_{SI}-E_{off})} e^{\sqrt{-\lambda_n\delta\tau}x_n\mathcal{O}_n}
\end{aligned} \tag{4.84}$$

The process involves the diagonalization of these spin-isospin matrices, which increases the cost of the whole algorithm up to A^3. This is still more advantageous than GFDMC which scales as $2^A\binom{A}{Z}$. On the other hand, AFDMC requires more integrations than GFDMC: one for each auxiliary field x_n.

Those integrals are independent with respect to the coordinate propagation and among themselves, so they can be performed together with the diffusion process in the spirit of the MC methods. Alternatively, the auxiliary filed can be sampled from a Gaussian during the diffusion.

3-body forces EFT($\not\pi$) potentials, as well as other modern phenomenological and effective potentials, includes 3-body terms. Dealing with a central three-body force is not an issue in the MC framework. However, if the interaction does include spin and isospin operators, it can become difficult to be treated because of the spin rotations.

If a potential of contact kind is used, one can always perform a Fierz transformation to find a favorable form of the interaction. Among the four operators allowed only one interaction is independent since three nucleons can be couped in only one channel. We chose a spin and isospin independent three-body force:

$$V_{3b}^{\mathbb{1}}(r_{ijk}) \propto \sum_{i,j,k} \left[e^{-\frac{\left(\vec{r}_{ij}^2+\vec{r}_{ik}^2\right)\Lambda^2}{4}} + e^{-\frac{\left(\vec{r}_{ij}^2+\vec{r}_{ij}^2\right)\Lambda^2}{4}} + e^{-\frac{\left(\vec{r}_{kj}^2+\vec{r}_{ik}^2\right)\Lambda^2}{4}} \right] \tag{4.85}$$

The three body potential enters in the brancing procedure exactly as the standard two-body forces and does not involves a modification to the DMC algorithm. The following operatorial choice can be, and has been, implemented within AFDMC:

$$V_{3b}^{\tau\tau}(r_{ijk}) \propto \sum_{i,j,k} \left[e^{\frac{\vec{r}_{ij}^2\Lambda^2}{4}} (\tau_i \cdot \tau_j) + e^{\frac{\vec{r}_{ik}^2\Lambda^2}{4}} (\tau_i \cdot \tau_k) + e^{\frac{\vec{r}_{kj}^2\Lambda^2}{4}} (\tau_k \cdot \tau_j) \right] \tag{4.86}$$

A three-body interaction which contains cyclic permutations of spinorial many body components, can be expanded in terms of a two-particle spin-isospin operator weighted by three particles radial functions:

$$\begin{aligned} V_{3b}^{\tau\tau}(r_{ijk}) &= \sum_{i<j<k} \sum_{cyc} e^{-\frac{\left(r_{ij}^2+r_{jk}^2\right)\Lambda^2}{4}} (\vec{\tau}_i \cdot \vec{\tau}_j + \vec{\tau}_i \cdot \vec{\tau}_k + \vec{\tau}_j \cdot \vec{\tau}_k) \\ &\downarrow \\ &= \sum_{i<j<k} \sum_{cyc} \left(e^{\frac{-\left(r_{ij}^2+r_{jk}^2\right)\Lambda^2}{4}} + e^{\frac{-\left(r_{ij}^2+r_{ki}^2\right)\Lambda^2}{4}} + e^{\frac{-\left(r_{ik}^2+r_{jk}^2\right)\Lambda^2}{4}} \right) \vec{\tau}_i \cdot \vec{\tau}_j \end{aligned} \tag{4.87}$$

That can be treated with auxiliary fields as in Sec.{4.3}

4.4 Release node Monte Carlo

In Sec.{4.2} the importance of constraint the path of the diffused function, in order to reduce the error of the calculation, has been discussed. However, the systematic error introduced by the procedure is difficult to be estimated. This is especially true in nuclear physics where there are big systems and stiff potentials. It is common for nucleons to be clusterized inside the nuclei in weakling bound sub-systems. In this case a trial wave function built starting from a shell model will not be an accurate description of the system. In this situations, the constrained-path does not allow the wave function to recover the correct clusterized structure. This results in a wrong ground-state-energy estimation.

However, one can release the path and let the high energy components of the wave function to vanish. This procedure is called RPDMC [87]. It is more expensive with respect constrained-path, since, to keep the error under control, many independent configurations are needed.

The method consists in following Eq.(4.44) for the diffusive process in the constrained-path approximation of Eq.(4.59) but the walkers that not fulfill $[\Psi_g(\vec{r})\Psi_g(\vec{r}') > 0]$ are not killed. This is achieved redefining the trial wave function as

$$\tilde{\Psi}_g = \sqrt{Re\left[\Psi_g\right]^2 + \epsilon\, Im\left[\Psi_g\right]^2} \tag{4.88}$$

where the parameter ϵ can be changed in order to speed the convergence of the method (we used $\epsilon \sim 0.20$). Using $\tilde{\Psi}_g$ the weights will be defined always positive both during the branching the importance sampling. However, when observables are accumulated, the new term

$$\kappa = \frac{\Psi_g}{\tilde{\Psi}_g} \tag{4.89}$$

should be multiplied to the observables in order to recover the correct estimators.

Once the constraints are released, errors diverge quickly as shown in Fig.(4.6). To reduce them one has to propagate a huge number of statistically independent walkers, starting with a limited amount of walkers and propagate them using the constrained propagator, then save the configuration, and continue

with the unconstrained propagator until the errors are too large to have meaningful observables. The stored configurations are then recovered and, few unconstrained steps are performed to reduce auto-correlations. Finally, they are diffused again using RPDMC and statistic accumulated.

This procedure of RPDMC can be summarized as follows:

1. Diffuse the initial wave function with the constrained propagator.
2. Save the configurations (position, weights, spinors... of walkers).
3. Propagate accumulating statistics with the unconstrained propagator until the signal to noise ratio becomes too small.
4. Retrieve the stored configurations.
5. constrained-propagation until the new configurations are uncorrelated with respect the saved ones.
6. repeat from point **3)** until errors are small as needed.

It might happen that the errors of RPDMC are too high to give a converging result, they give a good estimation of the systematic errors of the constrained-path approximation.

In Fig.(4.7) is shown the walker energy distribution in oxygen, the data have been calculated using EFT($\not\pi$) potential described in Sec.{2.4}, and DMC without constrained-path approximation starting from the unconstrained wave function. The histogram represents the number of walkers with a given energy during the imaginary simulation time. It can be noticed that the error increases exponentially.

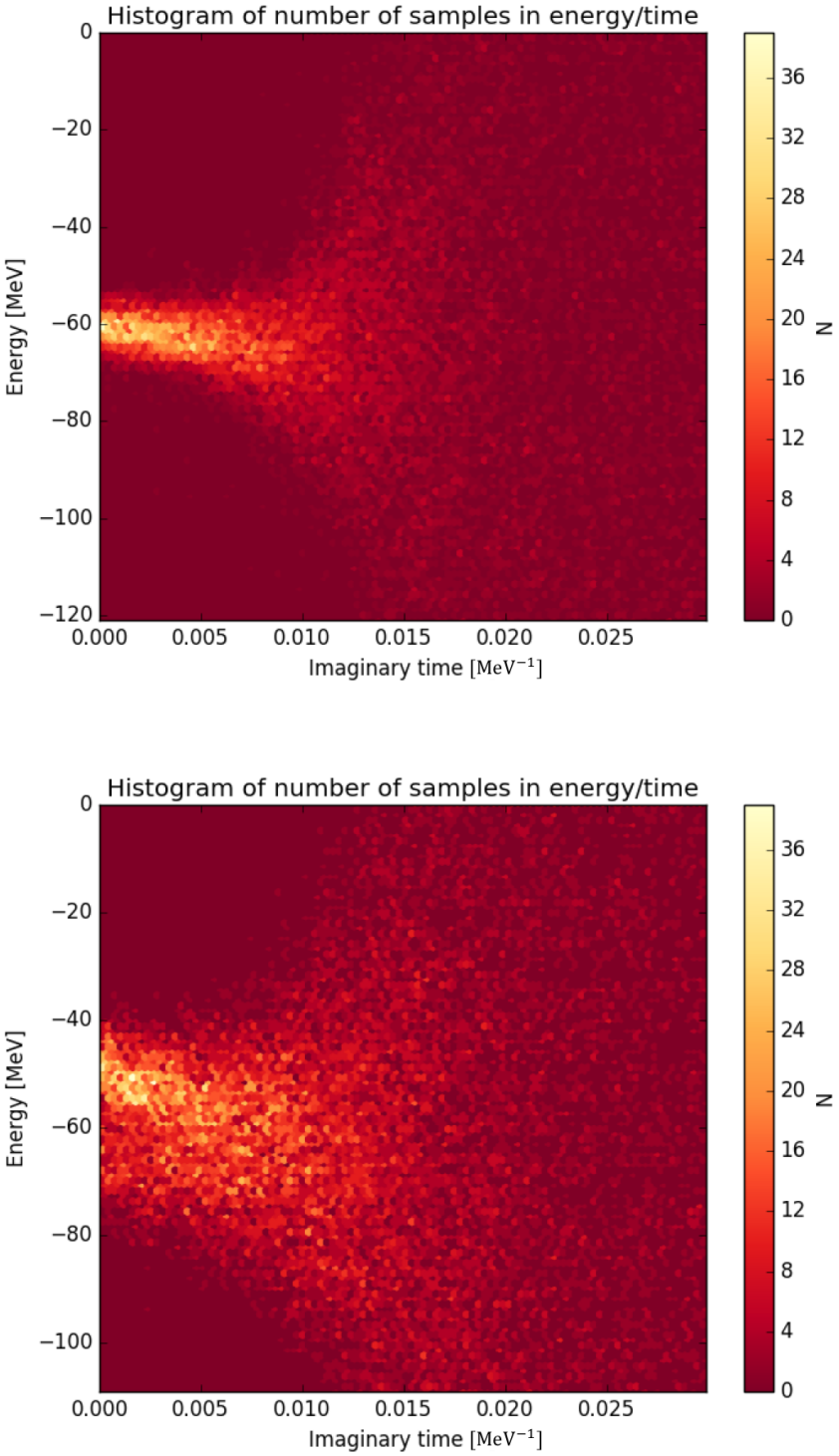

Figure 4.7: Walker energy distribution in oxygen with Physical m_π and cut-off $\Lambda \approx 800$ MeV on the top pannel and $\Lambda \approx 1600$ MeV on the bottom one. See text for full description.

Mixed estimators

Eq.(4.39) shows how to calculate Hamiltonian expectation values. However, the knowledge of the wave function, in principle, gives the possibility of estimating the expectation value of operators that do not commute with the Hamiltonian as nuclear potentials, nuclear densities, and moment distributions. All those operators should not be included in the diffusion algorithm. The mixed estimator of a generic quantum-mechanics operators reads:

$$\langle \mathcal{O} \rangle_{\psi_0} \simeq \frac{\langle \psi_0 | \mathcal{O} | \Psi_g \rangle}{\langle \psi_0 | \Psi_g \rangle} = \frac{\int (\psi_0^* \Psi_g) \left(\frac{\mathcal{O}\Psi_g}{\Psi_g} \right)}{\int \psi_0^* \Psi_g}, \tag{4.90}$$

If $\mathcal{O}$ does not commute with H, the mixed estimator does not coincide with the ground state expectation value. However, since Ψ_g is supposed to be a good approximation of it, two different perturbative expansion can be made. The first one reads:

$$\begin{aligned} \langle \Psi_g | \mathcal{O} | \Psi_g \rangle = \langle \psi_0 + \delta\Psi | \mathcal{O} | \psi_0 + \delta\Psi \rangle = \\ \langle \psi_0 | \mathcal{O} | \Psi_g \rangle + \langle \Psi_g | \mathcal{O} | \psi_0 \rangle + \langle \psi_0 | \mathcal{O} | \psi_0 \rangle + \langle \delta\Psi | \mathcal{O} | \delta\Psi \rangle \end{aligned} \tag{4.91}$$

which, in the case of Hermitian $\mathcal{O}$, becomes

$$\langle \psi_0 | \mathcal{O} | \psi_0 \rangle = 2 \langle \Psi_g | \mathcal{O} | \psi_0 \rangle - \langle \Psi_g | \mathcal{O} | \Psi_g \rangle + O(\delta\Psi) \tag{4.92}$$

The term $\langle \Psi_g | \mathcal{O} | \Psi_g \rangle$ can be calculated using VMC, while $\langle \Psi_g | \mathcal{O} | \psi_0 \rangle$ can be estimated using Eq.(4.90). Hence, the first method to evaluate mixed estimators can be schematically written as:

$$\langle \mathcal{O} \rangle = 2 \langle \mathcal{O} \rangle_{DMC} - \langle \mathcal{O} \rangle_{VMC} \tag{4.93}$$

The second possible expansion can be express in terms of the quotient of the mixed and the "Variational" expectation values.

$$\begin{aligned} \frac{\langle \Psi_g | \mathcal{O} | \psi_0 \rangle^2}{\langle \Psi_g | \mathcal{O} | \Psi_g \rangle} = \frac{\langle \psi_0 | \mathcal{O} | \psi_0 \rangle^2 + 2 \langle \psi_0 | \mathcal{O} | \psi_0 \rangle \langle \psi_0 | \mathcal{O} | \delta\Psi \rangle + \langle \delta\Psi | \mathcal{O} | \delta\Psi \rangle^2}{\langle \psi_0 | \mathcal{O} | \psi_0 \rangle + 2 \langle \psi_0 | \mathcal{O} | \delta\Psi \rangle + O(\delta\Psi)} \\ \approx \langle \psi_0 | \mathcal{O} | \psi_0 \rangle . \end{aligned} \tag{4.94}$$

It can be schematically written as

$$\langle \mathcal{O} \rangle = \frac{\langle \mathcal{O} \rangle_{DMC}^2}{\langle \mathcal{O} \rangle_{VMC}}. \tag{4.95}$$

Both the perturbative corrected estimators, (4.93) and (4.95) give the same result when the trial wave function is accurate. The relevance of having an importance function as close as possible to the ground state is crucial in this kind of calculations. Nonetheless, the discrepancy between the Variational and the Diffusion expectation value, as well as the difference between the result of the two perturbation expansions, is a good check for the convergence of the optimization procedure.

5. Pionless EFT in few-body systems

In this chapter, the results obtained using EFT($\not\pi$) potential in few-body systems will be discussed. We performed calculation for pion mass of ∼140, 500 and 800 MeV [31–35, 37, 38, 40, 41].

The choice of observables to be used in order to fit the LEC is arbitrary. In all the cases except for the physical mass the observables used for the fit are BE(d), BE($n-n$) and BE(^{3}He). In the physical case, where $^1S_0$ channel is not bound, we used the scattering length $a_0(n-n)$. The second fit at physical mass, has been performed using the scattering lengths in both channels in order to test the theory behavior when a different parametrization is used.

The effective range r_0 is not the best choice to fit LO LECs since it represents a correction of higher order (k^2) in pionless theory making it a good candidate for the NLO fit instead. As explained in sec.{2.4}, EFT($\not\pi$) contains three parameters at LO: one for each of the two-body channels and one for the three-body. The parameters have been fitted with the potential written in $^3S_1$ an $^1S_0$ channels, associated to deuterium and dineutron, respectively. However, spin projectors are not directly usable in AFDMC calculations. Then the potential has been rewritten into a more convenient fashion for many-body calculations purposes (we used the operators $\mathbb{1}$ and $\sigma_i \cdot \sigma_j$ in the few- and many-body calculations).

The used potential reads:

$$V_{2B}(\vec{r}_1 \cdots \vec{r}_A) = \sum_{i<j}^{A} e^{-\frac{\left(\vec{r}_{ij\Lambda}\right)^2}{4}} [\underset{\substack{\uparrow \\ \text{d and n-n } BE \text{ or } a}}{C_1 +} \underset{\uparrow}{C_2 \left(\vec{\sigma}_i \cdot \vec{\sigma}_j\right)}] \tag{5.1}$$

$$V_{3B}(\vec{r}_1 \cdots \vec{r}_A) = \begin{array}{l} D_1 \sum_{i,j,k}^{A} \sum_{\{cyc\}} e^{\left(\vec{r}_{kj}^{\,2}\vec{r}_{ik}^{\,2}\right)} \mathcal{O}_{ij} \\ \uparrow \\ BE(^3\mathrm{H}\ ) \end{array} \tag{5.2}$$

where $\mathcal{O}$ is one of the four possible operators of the 3-body interaction that can be arbitrarily chosen according to the Fierz transformation. In this work, we used both $\mathbb{1}$ and $\vec{\tau}_i \cdot \vec{\tau}_j$ as test of consistency for the powercounting and as an estimation of the LO systematics in the EFT($\not\pi$) framework. We use the gaussian regulator $e^{-\frac{r^2\Lambda^2}{4}}$ in accordance with the discussion of sec.{2} and sec.{2.4}. It should be remarked that for each pion mass and a given parametrization a study of the cut-off dependence of the observables is required. All the calculations have been performed for multiple cut-offs ($\Lambda = \{2,\ 4,\ 6,\ 8\}$ fm^{-1}). In the case of physical pion mass, a more extensive study of the cut-off convergence has been done up to $\Lambda = 20$ fm^{-1}. Convergence in the observables when the cut-off is above the breaking scale of the theory (m_π) is expected.

5.1 Deuterium, dineutron and tritium

As for the S-waves, two nucleons are bound only in the ${}^3S_1$ channel. On the other hand, in lattice calculations for large pion masses, ${}^1S_0$ is also bound. Besides those used to fit the LECs, all the others observables are predicted by the theory and should converge for large cut-off within LO uncertainties. These two-body system calculations dysplayed in Fig.(5.2).

Tab.(5.1) summarizes all the fits done during this thesis. In order to fit the two LO LECs, the potential has been conveniently Fierz rotated. The relation between LECs associated to the ${}^1S_0$ and ${}^3S_1$ channels, denoted as C_{01}^{Λ} and C_{10}^{Λ} and ($\mathbb{1}$ and $\vec{\sigma}_i \cdot \vec{\sigma}_j$) channels is:

$$\begin{aligned} C_{01}^{\Lambda} &= C_1^{\Lambda} - 3C_2^{\Lambda} \quad \rightarrow \left({}^1S_0\right) \\ C_{10}^{\Lambda} &= C_1^{\Lambda} + C_2^{\Lambda} \quad \rightarrow \left({}^3S_1\right) \end{aligned} \tag{5.3}$$

The two constants can be fitted independently, then reverting Eq.(5.3) they are transformed back in ($\mathbb{1}$ and $\vec{\sigma}_i \cdot \vec{\sigma}_j$) in order to be used in MC calculations. The LEC are cut-off dependent, as they have to renormalize the potential after regularization. We expect them to have a $C \approx \mathcal{C}\frac{\Lambda^2}{m_N}$ behavior if a sharp cut in the maximum momentum is applied, with $\mathcal{C}$ of natural size according to the EFT($\not\pi$) theory.

The same behavior is found in the case of Gaussian regularization, as shown in Fig.(5.1), where the LECs have been rescaled as $\mathcal{C} = C\frac{m_\pi}{\Lambda^2}$. The plot also highlights the natural size of the scaled LECs. Comparing the pink double dotted and the red dashed lines in the ${}^3S_1$ channel for $m_\pi \sim 140$ MeV, it can be noticed that the LEC converges at the same value (within the accepted uncertainty at LO, $Q/m_\pi \sim 25\%$) even when it is fitted on two different observables. This behavior confirms the robustness of the theory, at least in the two body sector. It is interesting to note that the same LEC converges at the same value for all the values of the pion masses we considered. This common behavior is surprising and deserves more investigations, but it might indicate a class of universality shared by all the two-nucleon systems at different pion masses.

The fact that the LECs of the two channels are very similar reflects the closure of the T-matrix poles. However, this implies that C_2 of $\sigma_i \cdot \sigma_j$ is much smaller than C_1 (Eq.(5.3)), revealing an almost perfect SU(4) symmetry. In

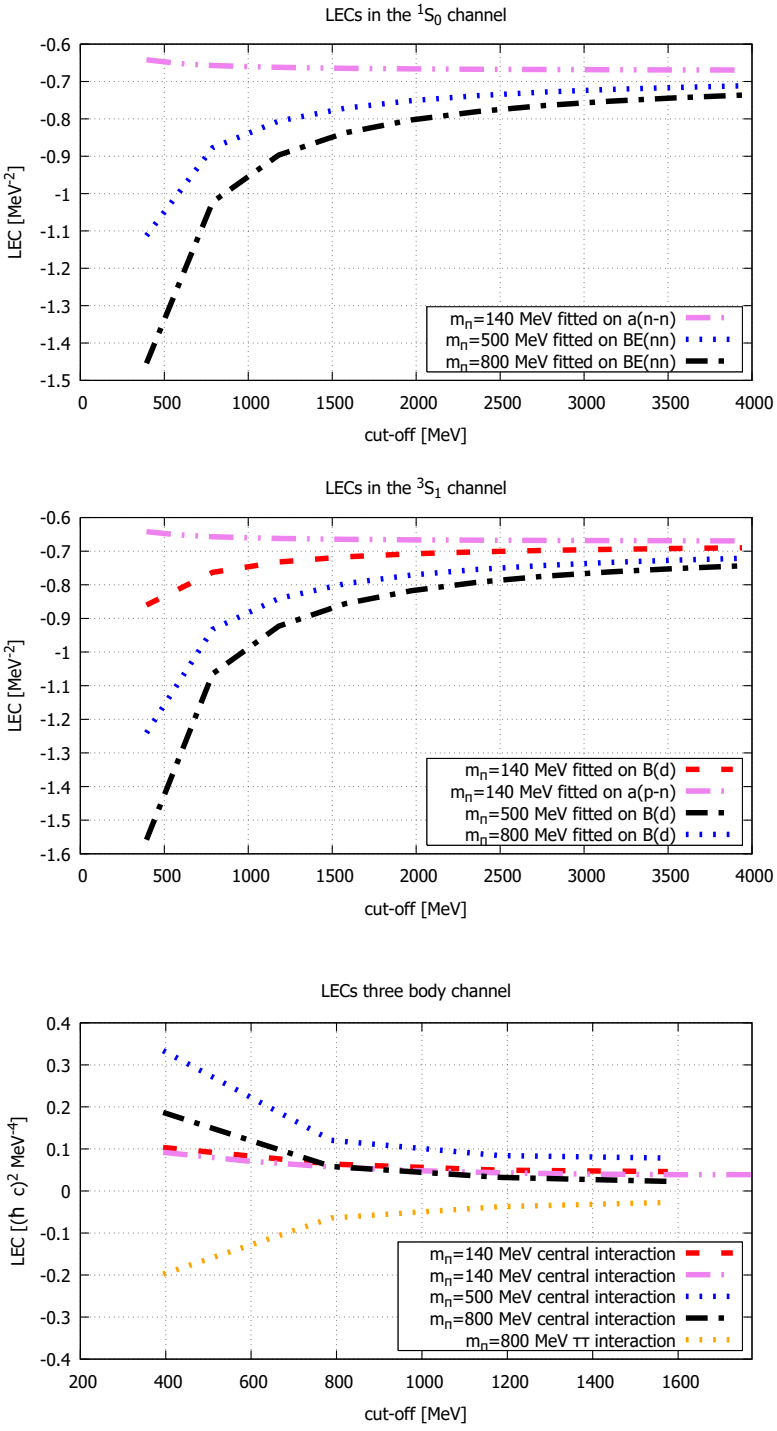

Figure 5.1: Normalized LECs of the two- and three-body EFT($\not\pi$) interaction for the considered m_πs. Different data for the same m_π and channel are obtained fitting different observables. More details on text.

the case of physical m_π the $^1S_0$ channel is unbound and one expects the LECs to be greater than the ones corresponding to large m_π. This is only partially true, hence we can conclude that the position of the T-matrix poles is very sensible to the magnitude of the rescaled constants $\mathcal{C}$. The convergence of LECs is different when they are fitted on the the binding energy with respect to when the scattering length is used. This is expected when the renormalization scheme changes.

We used two different operator structures for the NNN potential: a central interaction, described in Eq.(4.85), and the isospin-dependent force of Eq.(4.87), which we denoted as "$\tau\tau$". In order to fit the binding energy of the ^{3}He, the diagonalization and redundant Gaussians methods have been used. The three body coefficient, plotted as $D = \mathcal{D}\frac{m_\pi}{\Lambda^4}$ is relatively small compared with $\mathcal{C}_{(^1S_0)}$ and $\mathcal{C}_{(^3S_1)}$. This is due to the sub-leading position of the three-body force in the naive powercounting. However, the correlation of the system enhances the three-body force contribution to observables, making it comparable with the one of the two-body potential. Convergence to the same value is shown in the LECs at the m_π considered as in the two body system. Note that the coefficients of the central and $\tau\tau$ three-body forces have different sign.

In Fig.(5.2) some of the observables on which the LECs have not been fitted are shown. In all the cases we observe a convergent behavior. In the physical case, we find that the deuterium binding energy is underestimated with respect to the experimental value of 2.22 MeV. We find a convergent scattering length in the $^3S_1$ channel (to $a_0 \sim 4.4$ fm) to be compared to the experimental value $a \sim 3.8$ fm. A comparison with LQCD calculation results is difficult since the big statistical errors of the latter (see chapter{3}).

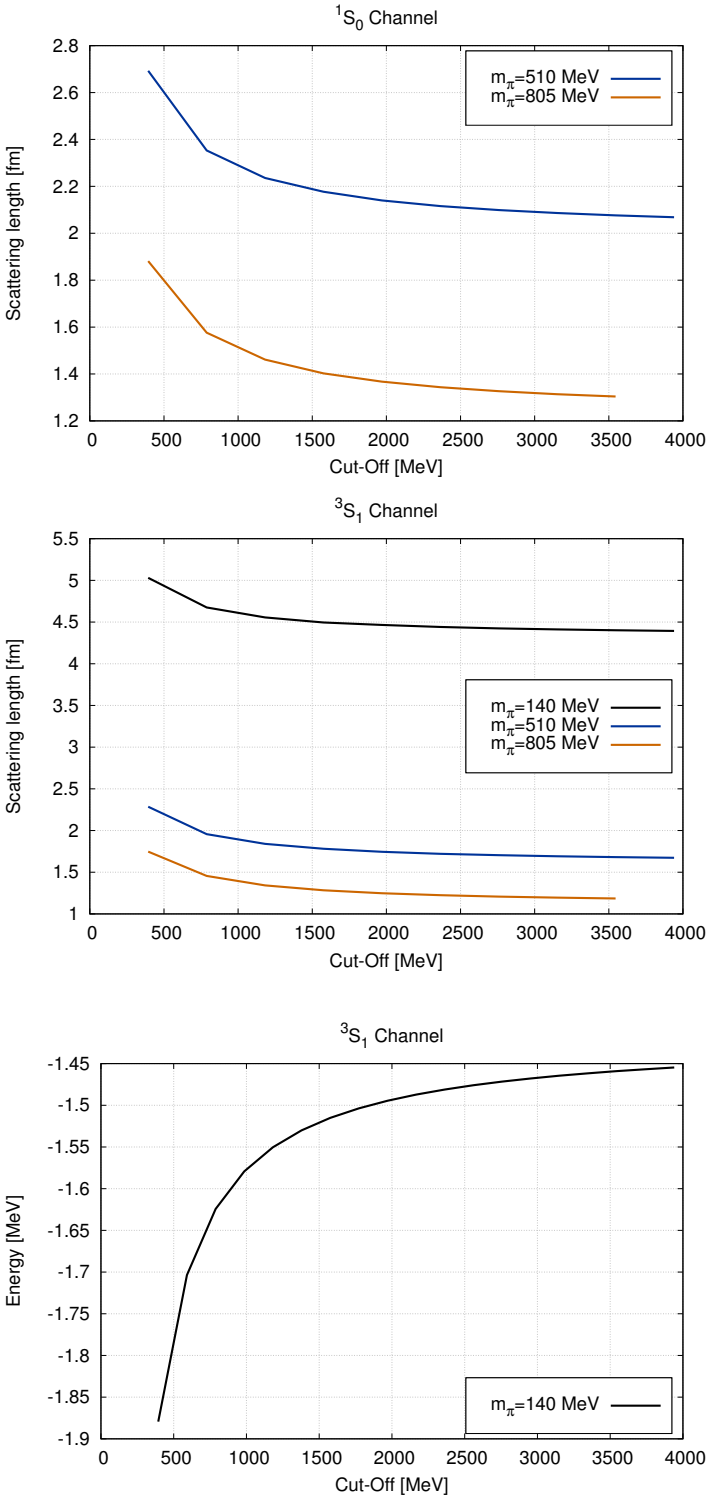

Figure 5.2: Two body observables not fixed by the fitting procedure calculated with EFT($\not\pi$) at LO. It can be seen that the data converge in the limit of large cut-off.

Name	m_π [MeV]	C_{10} $\left({}^1S_0\right)$	C_{01} $\left({}^3S_1\right)$	D_1 (three body)	$D_1(\tau\cdot\tau)$ (three body)
α	140	a_0(n-n)	a_0(p-n)	BE(^{3}He)	-
β	140	a_0(n-n)	BE(d)	BE(^{3}He)	-
γ	500	BE(n-n)	BE(d)	BE(^{3}He)	-
δ	800	BE(n-n)	BE(d)	BE(^{3}He)	-
ϵ	800	BE(n-n)	BE(d)	-	BE(^{3}He)

Table 5.1: Table of different fits.

5.2 Helium

The α particle binding energy has been calculated using AFDMC method and EFT($\not\pi$) potentials. We used different parametrizations and different kind of three-body potentials. The observable used for fitting the two-body LECs are both scattering length (a_0) and binding energies (BE) of the ${}^1S_0$ and ${}^3S_1$ channels. The three body LEC is fitted using the ^{3}He binding energy and both a central and an isospin dependent three-body force. In Tab.(5.1) we summarize the observables that have been used to fit any parametrization used in this thesis; we refer to them with Greek letters from α to ϵ. In Tab.(5.2) are shown the energies of the alpha particle for every parametrization, m_π and cut-offs considered with the relative extrapolation.

In order to remove the cut-off dependency from observables we used the expansion described in Eq.(2.45). We found that an expansion up to $1/\Lambda^2$ suffices to extrapolate the ^{4}He energies for $m_\pi = 140$ MeV since the addition of a cubic term does not change substantially neither the extrapolated value nor the best-fit coefficients. On the other hand, the extrapolations for $m_\pi = 510$ MeV and $m_\pi = 805$ MeV are less clean because of the $\Lambda \sim 400$ MeV cut-off that is smaller or comparable to the expected breaking scale of the theory. Hence, in Tab.(5.2) we report both the extrapolation-fit using Eq.(2.45) done with and without the point at smaller cut-off. The errors reported on the extrapolations are two: the bottom one refers to the error of the fit parameters, while the top one is the difference of the result with the one found using a fit function up to $(1/\Lambda)^3$. It has to be remarked that this cut-off sensitivity study does not account for the EFT truncation error that has to be gauged by means of other techniques, like those reported in Ref. [88].

Param.	α	β	γ	δ	ϵ
Λ	$m_\pi \sim 140$ MeV		$m_\pi \sim 510$ MeV	$m_\pi \sim 805$ MeV	
2 fm^{-1}	$-24.5(1.2)$	$-23.17(2)$	$-31.15(2)$	$-88.09(1)$	$-89.2(1)$
4 fm^{-1}	$-24.3(6)$	$-23.63(3)$	$-34.88(3)$	$-91.40(3)$	$-93.6(1)$
6 fm^{-1}	$-25.08(27)$	$-25.06(2)$	$-36.89(2)$	$-96.97(1)$	$-99.7(3)$
8 fm^{-1}	$-25.9(8)$	$-26.04(5)$	$-37.65(3)$	$-101.72(3)$	$-105.0(1.2)$
$\to \infty$	$-31.0^{(4)}_{(1.8)}$	$-29.87^{(10)}_{(5)}$	$-41.2^{(2.0)}_{(8)}$	$-117^{(7)}_{(3)}$	$-119^{(10)}_{(1)}$
w/o 2 fm^{-1}	$-31.2^{(1)}_{(2.7)}$	$-28.12^{(2.00)}_{(3)}$	$-40.5^{(1.0)}_{(3)}$	$-110^{(13)}_{(3)}$	$-112.5^{(18.0)}_{(1.5)}$
Exp.	-28.30		-	-	
LQCD	-		$-43.0(14.4)$	$-107.0(24.2)$	

Table 5.2: Binding energies of ^{4}He for different values of the pion mass and the cutoff.

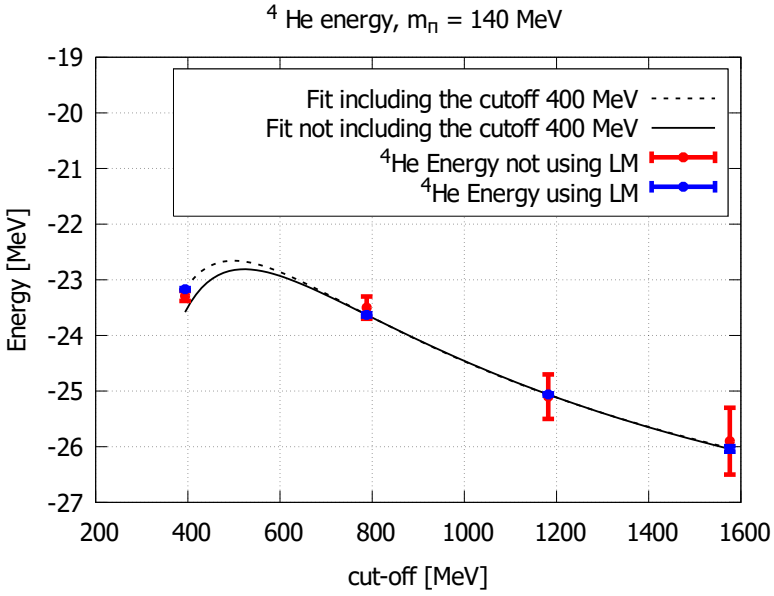

Figure 5.3: Energy of ^{4}He of the physical pion mass.

Fig.(5.3) shows the ^{4}He binding energy at physical m_π using the parametrization "β" of Tab.(5.1). The difference between the *red* and *blue* points lay in the approach used to optimize VMC method. The *blue* dots have been obtained using the Linear optimization procedure as described in sec.{4.1}. The *red* points have been calculated without it, and using the wave-function parametrization and three body correlations described in Sec.{4.2} and Sec.{4.3}.

Despite the somewhat primitive importance function used in the first case, the ground-state energy agrees within statistical errors. This is not unexpected as the Helium ground state does not contain nodes, and, DMC is able to project into the ground state with that wave functions. However, the more advanced wave function found with the LM significantly reduces the statistical errors for the same computational cost. The solid line represents the fit obtained not including the point at $\Lambda = 400$ MeV. The curve does not change significantly once the point is included, as can be seen comparing the solid and the dashed lines. The extrapolation defined including $\Lambda = 400$ MeV point overbinds ^{4}He with respect to experiments value. However, analyzing the errors that we expect from the theory at LO

$$\delta E_{LO} = \frac{\mathcal{Q}}{m_\pi} \approx \frac{\sqrt{2m_N \frac{BE(^4He)}{4}}}{m_\pi} \simeq 50\% = 15\text{MeV} \tag{5.4}$$

it is evident that the results obtained are in agreement with the experimental value.

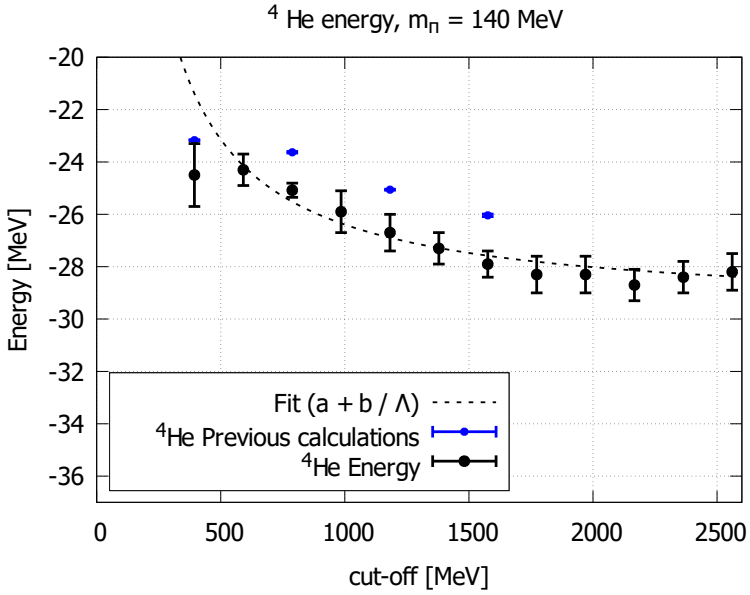

Figure 5.4: (LECs for large Λ courtesy by Betzalel Bazak) Energy of ^{4}He in the case of $m_\pi = 140$ MeV and different parametrization.

Fig.(5.4) displays the binding energy of ^{4}He obtained from the parametrization "α" of Tab.(5.1) as of Fig.(5.3) (*blue* dots are the same data as comparison). To prove the convergence of the LO in the four body system the black points extend to very large Λs.

We used the LM to optimize the variational wave function. Data show that the four body system converges at LO even for large cut-offs. The dashed line represents a fit done on the black points using Eq.(2.45) excluding $\Lambda \sim 400$ MeV. The asymptotic binding-energy can be found in Tab.(5.2). Comparing the parametrization "α" and "β" one can notice that the LO results are in agreement within the LO uncertainty of Eq.(5.4). The results are also in agreement with Ref.[89], which predicts the EFT four body system to be more bound if the two-body energy instead of the scattering length is used to fit LECs.

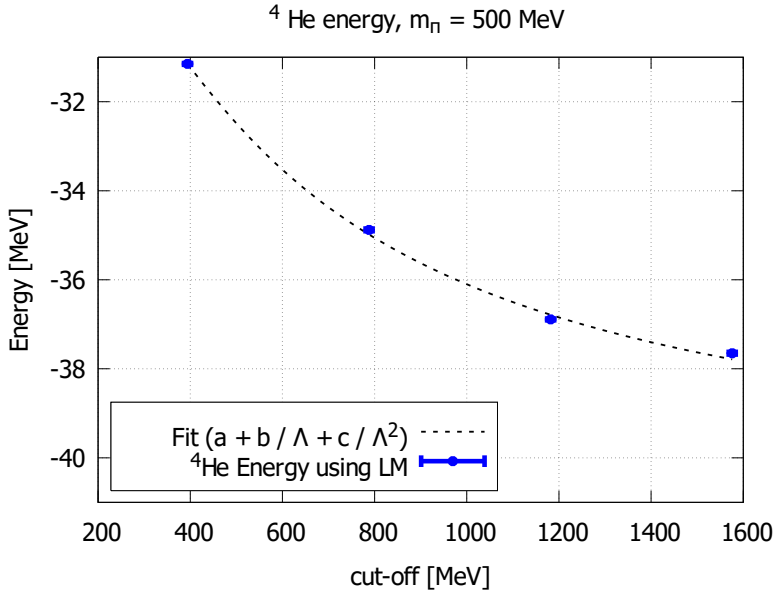

Figure 5.5: Energy of ^{4}He for the $m_\pi = 500$ MeV.

Fig.(5.5) shows the energy of ^{4}He obtained with the parametrization "γ" at $m_\pi \sim 500$ MeV. The extrapolation of the curve is consistent with the LQCD prediction of 43.0 ± 14.4 MeV, while according to Eq.(5.4), $\delta E_{LO} \simeq 35\% = 14$ MeV. Including additional powers of $\left(\frac{1}{\Lambda}\right)$ in the expansion does not change the extrapolation results within the fitting errors. The energy shows a small shift when the point at $\Lambda \sim 400$ MeV is included.

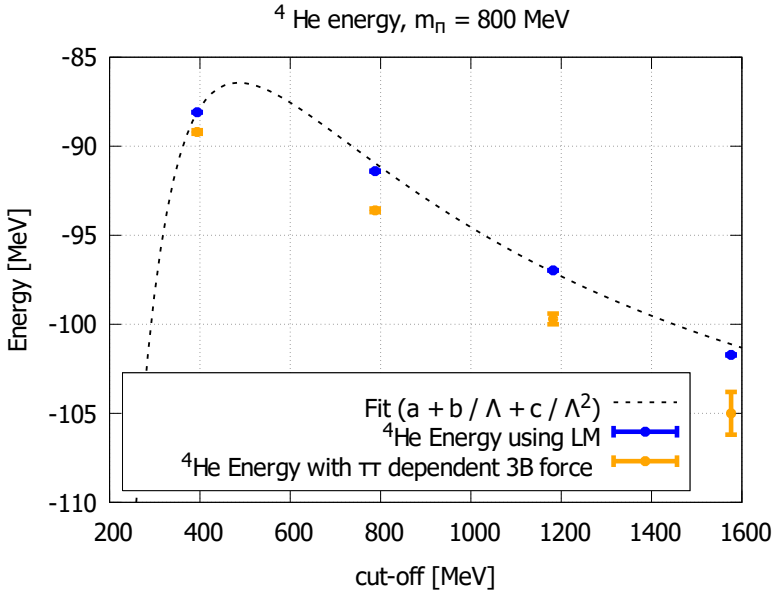

Figure 5.6: Energy of ^{4}He for the $m_\pi = 800$ MeV.

Last, we considered $m_\pi \sim 800$ MeV, whose ^{4}He energy is displayed in Fig.(5.6). *Blue* dots have been calculated with parametrization "δ". The *Orange* points are obtained from parametrization "ϵ". Details can be found in Ref.[30]. Even if we do not expect the same behavior for small cut-offs the results are not far from each other. Nonetheless, the two parameterizations should agree for large cut-off, where we found that the extrapolation values are consistent as expected (see Tab.(5.2)). However, the result including $\Lambda \sim 400$ MeV is not in agreement with respect to the one in which we do not include it. This shows that $\Lambda \sim 400$ is too small and should not be included in the extrapolation. In this case LO error is estimated to be of order $\delta E_{LO} \simeq 30\% = 35$ MeV. The data have a larger error than in the other pion mass considered. This is due to the fact that fewer points are used in the fits, but also because we expect convergence to occur at higher cut-off value compared to smaller m_πs (and breaking-momentum of the theory). Nonetheless, the results are very well in agreement with LQCD calculation results. Yet, the magnitude of the errors is still too large to draw any definitive conclusion, making a study at NLO and more refined LQCD calculations necessary.

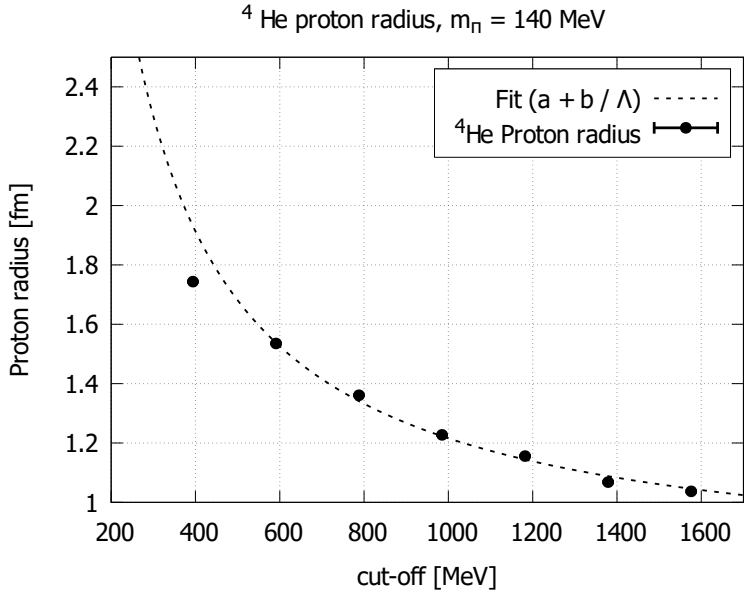

Figure 5.7: (LECs for large Λ courtesy by Betzalel Bazak)Radius of ^{4}He for $m_\pi = 140$ MeV.

It is interesting to study the cutoff dependence of the root-mean-square (rms) point-nucleon radius $\sqrt{\langle r_{\rm pt}^2 \rangle}$ and the single-nucleon point density $\rho_{\rm pt}(r)$. These quantities are related to the charge density, which can be extracted from electron-nucleus scattering data, but are not observable themselves: few-body currents and single-nucleon electromagnetic form factors have to be accounted for. Still, one can gain some insight into the features of the ground-state wave function by comparing results at different pion masses and cutoffs. Since neither $\sqrt{\langle r_{\rm pt}^2 \rangle}$ nor $\rho_{\rm pt}(r)$ commute with the Hamiltonian, the desired expectation values on the ground-state wave function are computed by means of "mixed" matrix elements as described in Sec.{4.4}

The results for the point-proton radius of ^{4}He are reported in Tab.(8.1) and Tab.(8.2). (Since Coulomb is absent in our calculation, the point-nucleon and point-proton radii are the same.) In the physical case, the calculated radius is much smaller than the empirical value — that is, the value extracted from the experimental data of Ref. [90] accounting for the nucleon size, but neglecting meson-exchange currents. A similar result, $\sqrt{\langle r_{\rm pt}^2 \rangle} \approx 1$ fm was obtained by the authors of Ref. [91] using a local form of a chiral interaction. NLO and N^{2}LO potentials in a chiral expansion based on naive dimensional analysis [92–94]

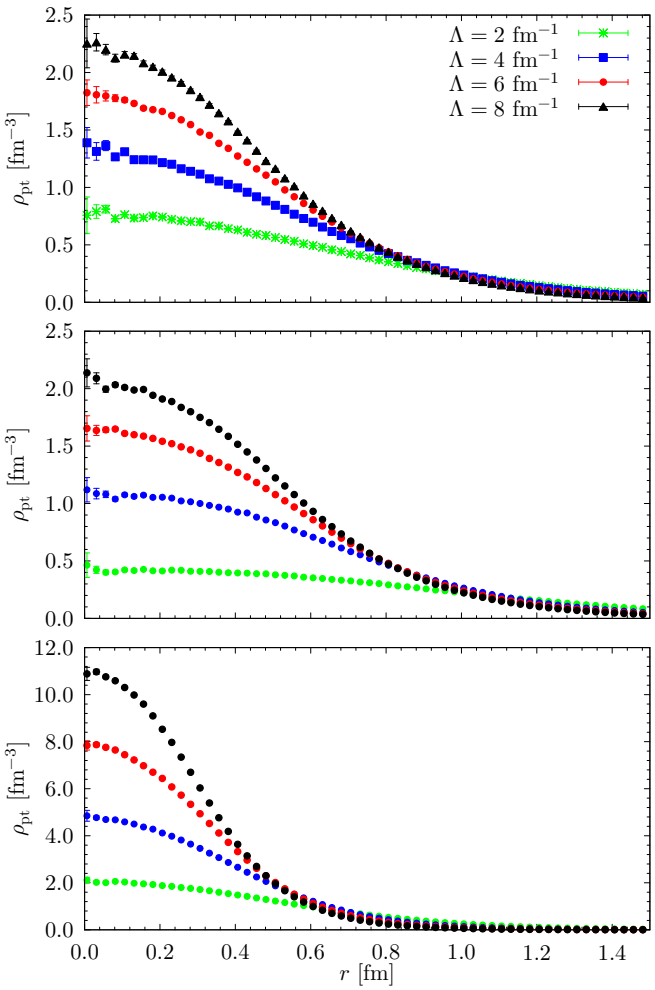

Figure 5.8: ^{4}He single-nucleon point density for $m_\pi = 140$ MeV (upper panel), $m_\pi = 510$ MeV (middle panel), and $m_\pi = 805$ MeV (lower panel), at different values of the cutoff Λ.

bring theory into much closer agreement with the empirical value. Hence, subleading terms in the EFT($\not\pi$) expansion could play a relevant role, at least for physical values of the pion mass.

For unphysically large pion masses, where EFT($\not\pi$) is supposed to exhibit a faster convergence, the point-proton radius is smaller than at $m_\pi = 140$ MeV. The value obtained for $m_\pi = 510$ MeV indicates a spatial extent similar to the physical one, while ^{4}He at $m_\pi = 805$ MeV, in comparison, seems to

be a much more compact object. This is consistent with the behavior of the single-nucleon point density, $\rho_{\rm pt}$, displayed in Fig.(5.8). For all cutoff values, the density corresponding to $m_\pi = 805$ MeV is appreciably narrower than that computed for $m_\pi = 510$ MeV or $m_\pi = 140$ MeV. Focusing on $\Lambda = 1600$ MeV, $\rho_{\rm pt}$ has a maximum value of 11.0 fm^{-3} for $m_\pi = 805$ MeV, while in the $m_\pi = 510$ MeV and $m_\pi = 140$ MeV cases the maximum values are 2.1 fm^{-3} and 2.2 fm^{-3}, respectively.

6. Pionless EFT in many body systems

6.1 Oxygen and Release Phase Monte Carlo

We chose ^{16}O for mainly two reasons: First, because it is a doubly magic nucleus, thereby reducing the technical difficulties related to the construction of wave functions with the correct quantum numbers and symmetries. Second, its central density is sufficiently high to probe saturation properties and thereby serve as a model for even heavier nuclei. The stiffness of the interaction at large cut-off, as well as the non-trivial correlations between particles, makes the calculations particularly challenging. To successfully carry out the study of ^{16}O AFDMC ha been refined to significantly improve the upon the quality of the variational wave function.

The calculations of ^{16}O have been performed using the parametrizations "β", "γ" and "δ" of Tab.(5.1). The ground state energies of ^{16}O and ^{4}He have been calculated using different kinds of correlations and wave functions and are reported in chapter{8}.

The correlation used are:

- *(No J_{3b})*: Two-body Jastrow and Gaussian single-particle orbitals minimized "by hands".

- *(Av.J_{3b})*: Two-body Jastrow and Gaussian wave functions, three body implicit correlations calculated as the average contribution of three body interaction to the two-body Jastrow.

- *(w/ $J_{3b}^{(4.12)}$*)*: Two-body correlation and Gaussian single particle orbitals, but three body defined according to Eq.(4.12).

- *(w/ $J_{3b}^{(4.12-4.14)}$)*: Two-body Jastrow calculated solving the two-body Shrödinger equation and Gaussian single particle orbitals. Three body Jastrow implemented according to Eq.(4.12-4.14).

- *(LM)*: Using the LM minimization and spline lines for correlations and single particle wave functions.

The calculations of ground states performed without the LM are less bound than four alpha particles. These results can not be correct since the diffusion process in imaginary time should project out all the excited-state components of the wave function. The fact that there is a lower state (four separate αs) with lower energy is sufficient to state that the results are somewhat biased and need to be improved. During this thesis, many of the possible systematic errors of the method, as time-step correction and statistic correlations, have been investigated. Our conclusion is that the importance function ψ_g was not a good approximation of the ground state wave function leading results affected by severe sign problem.

Initially, ψ_g was built as a Slater Determinant with only two-body Jastrow whose parameters where found using an "by hand" procedure. Single particle orbitals were calculated using a Skyrme potential [95], fitted on physical experiments, and read by the AFDMC as an input. A variational rescale parameter was added to orbitals to better fit the observed system. The parametrization of Skyrme orbitals is necessary because, in the case of unphysically high m_π, the orbitals and the energy levels are unknown, while in the physical case the wave functions changes with the RG flow.

Since the relative strength of the three-body force is as large as the two-body potential, three-body correlations have been implemented in the code. This has been done in two different ways. The first consists in adding of an average of the three-body to the two-body Jastrow. This has been done estimating the perturbation to the two-body correlations of a couple of particles when a third particle it is approached to it. The second approach consists in solving the two-body problem of the given potential and calculating the three-body correlation as described in sec.{4.1}. Comparing the DMC results obtained with the two methods it is possible to conclude that they do not change much the results. In Fig.(6.1) the ^{16}O energy obtained using only

two-body correlations *(No J_{3b})* and including explicit three-body correlations *(w/ $J_{3b}^{(4.12)}$ *)*.

From the similar results obtained using different correlation emerges that the ground state wave function structure is very different from any parametrization of Ψ_g, i.e. it requires nucleon clusterization. Although, all the parametrizations showed a common convergence to the same results. This might imply the presence of a resonance or an excited state of the system, in which VMC finds a local energy minimum from which DMC is not able to project to the ground state because of orthogonality conditions.

In order to find the ground state of ^{16}O both in the case in which it is bound or it consists in four weakly interacting or even free alpha particle, the RPDMC has been used. In Fig.(6.2-6.9) the energies as function of the imaginary time during RPDMC calculations are shown. The calculations have been performed extracting few hundred independent propagations starting from different thermalized walker configurations. It should be remarked that those calculations have been done using the parametrizations "β", "γ" and "δ". *Blue* points represent DMC calculations with the relative stochastic error. While the error of the calculation increases exponentially, the average energy should still be correct. In all the figures the 4-α threshold is displayed *orange*. This corresponds to the energy of four, non-interacting alpha particles calculated with the same parametrization of the potential. RPDMC is a more computationally expensive method with respect to DMC. This is why we choose to perform calculations only for few m_π and cut-offs values. We chose m_π ∼140 and 800 MeV because they correspond to the cases in which the EFT($\not\pi$) is supposed to work worst and best respectively. In the case $m_\pi \sim 140$ MeV, $\Lambda \sim 400$ MeV we proceed with three kinds of analysis. One starts from DMC thermalized configuration (*Blue* points); one using thermalized configuration without any optimization in the wave function (not showed because on the top of the *Blue* one); and one using random initial configuration (*Red* points). This has been done in order to better understand the behavior of the energy when the phase constraint is released. The energy behavior is a clear indication of the tendency of the calculation to converge to the $4-\alpha$ threshold.

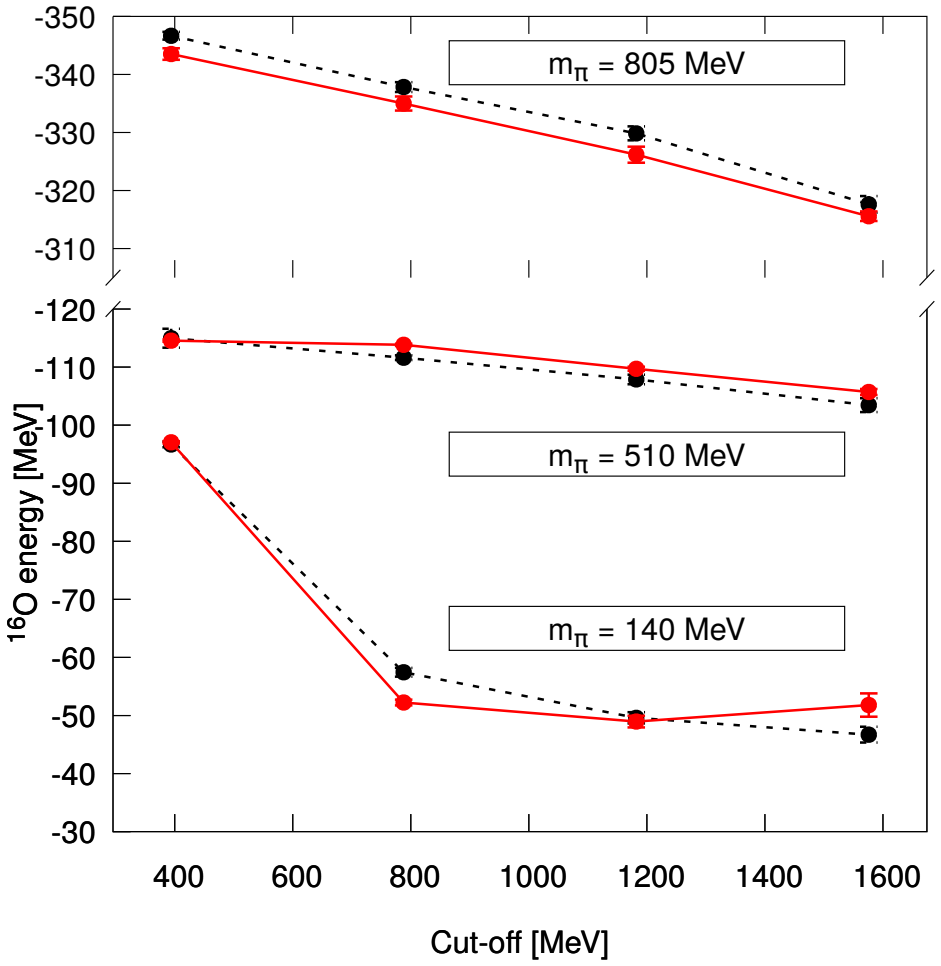

Figure 6.1: ^{16}O energy for different m_π and cut-offs. *Black* points represent the results of AFDMC using only two-body correlations in the importance wave function. *Red* points represent the results after including the three-body correlations too. It can be noticed that the inclusion of new correlations do not substantially change the results.

It can be noticed how RPDMC calculations reveal two very different behaviors. For m_π ∼800 MeV and Λ ∼400 and 800 MeV the releasing phase pushes the energy below the four alpha threshold. For all the other cases the final energy stays above the 4-alpha threshold but it is compatible with it. At first sight, the analysis of m_π ∼140 MeV and α ∼1600 MeV shows a gap in the energy after $\tau = 0.02$ MeV^{-1}. However, a statistical analysis

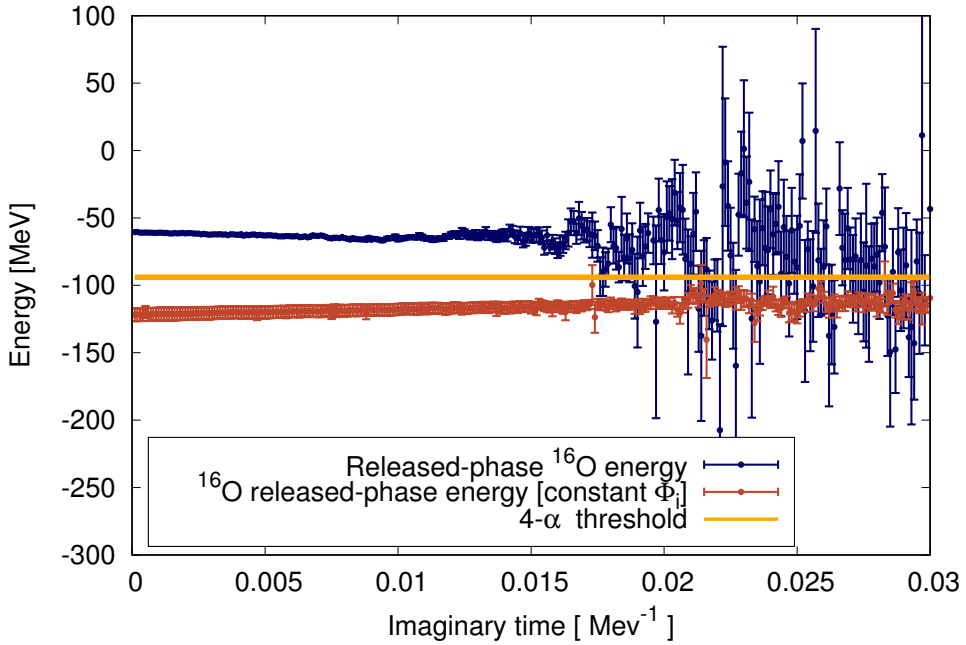

Figure 6.2: ^{16}O with $m_\pi \sim 140$ MeV, $\Lambda \sim 800$ MeV. *Red* data refers to a calculations made using wide single particle orbitals in which the radial contribution of $\Psi_g(|r|)$ is almost constant in all the space. The calculation has been done without termalizing the configurations using the constaint method. However, the curve approaches the 4-α energy.

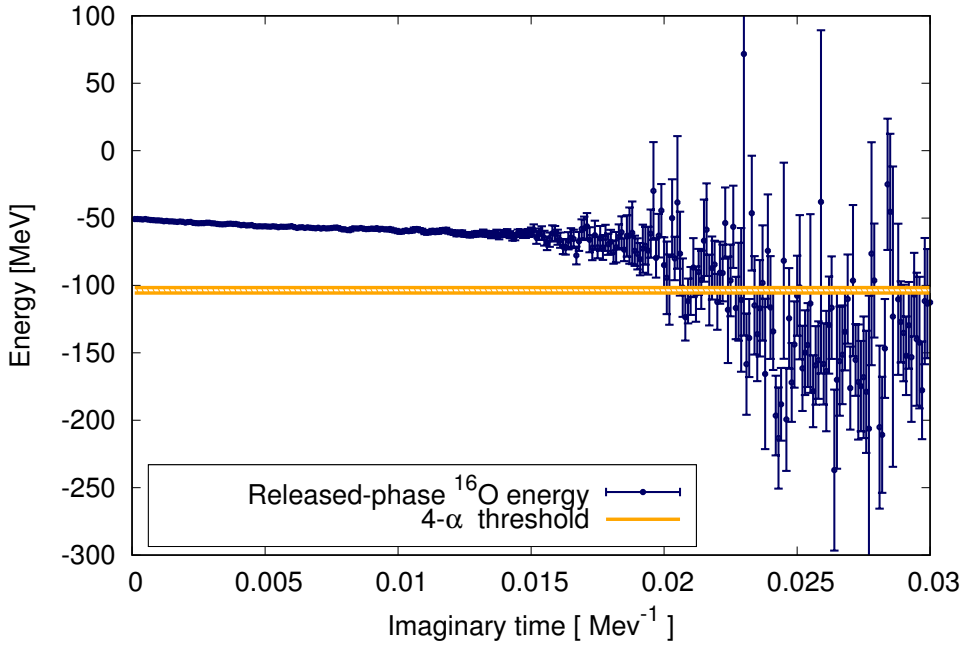

Figure 6.3: ^{16}O with $m_\pi \sim 140$ MeV, $\Lambda \sim 1600$ MeV

Figure 6.4: Oxygen energy behavior with respect the imaginary time calculated using unconstaight RPDMC for $m_\pi \sim 140$ MeV.

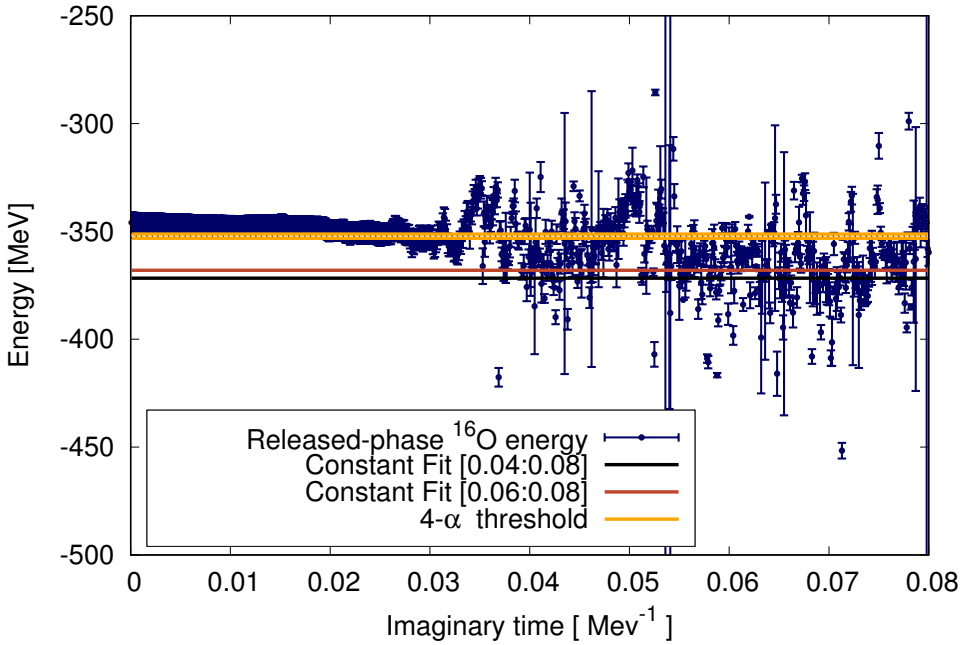

Figure 6.5: ^{16}O with $m_\pi \sim 800$ MeV, $\Lambda \sim 400$ MeV

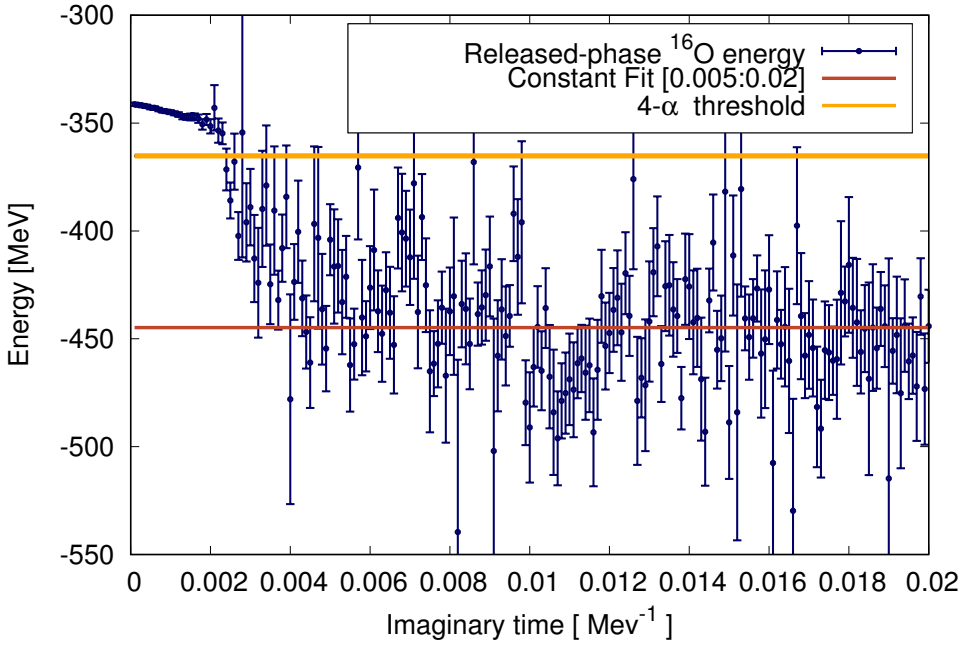

Figure 6.6: ^{16}O with $m_\pi \sim 800$ MeV, $\Lambda \sim 800$ MeV

Figure 6.7: Same as Fig.(6.4) for $m_\pi \sim 800$ MeV.

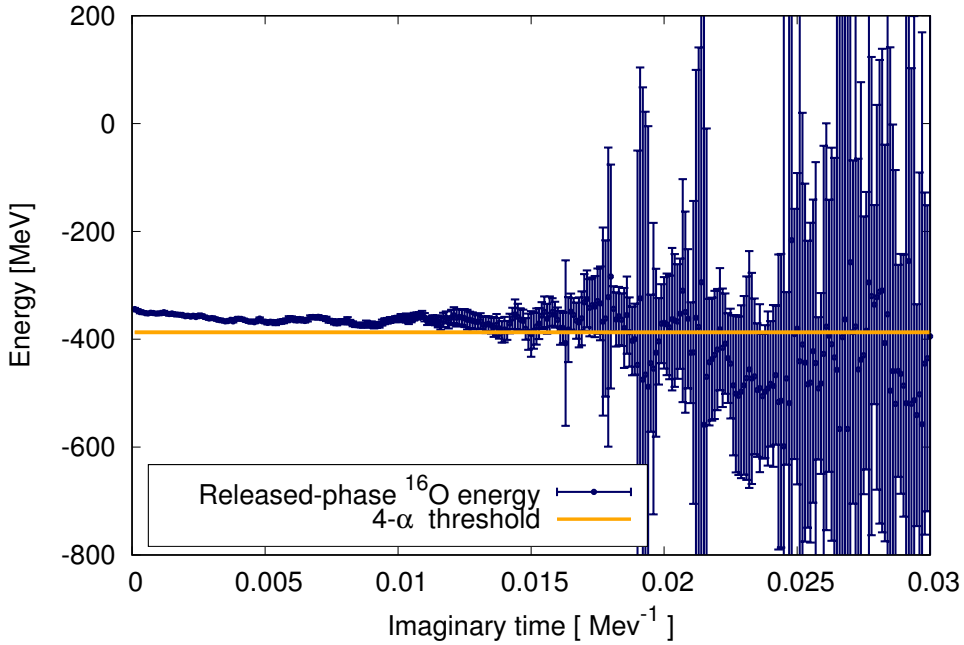

Figure 6.8: ^{16}O with $m_\pi \sim 800$ MeV, $\Lambda \sim 1200$ MeV

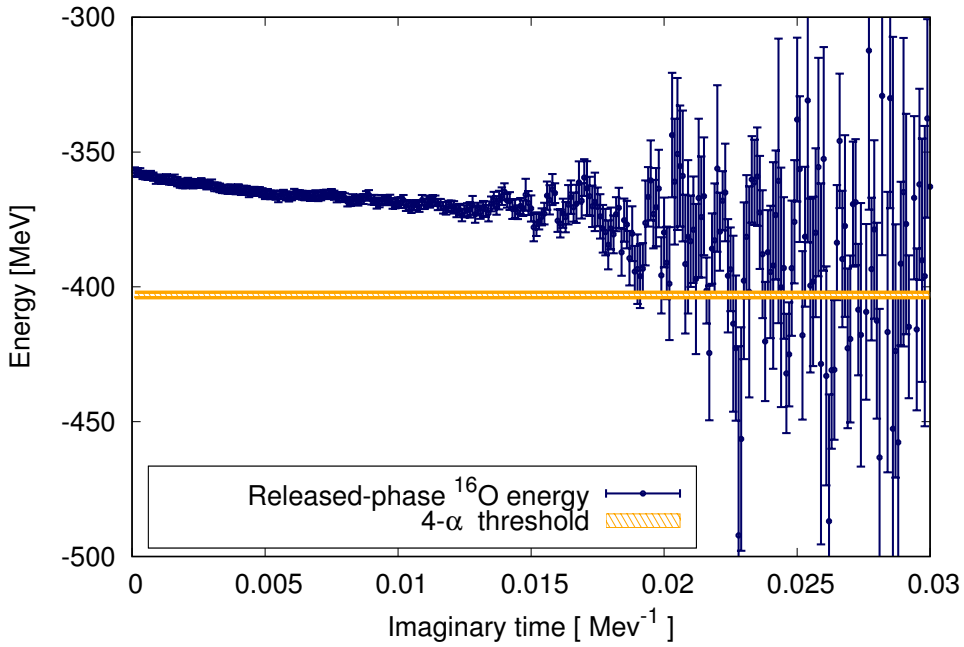

Figure 6.9: ^{16}O with $m_\pi \sim 800$ MeV, $\Lambda \sim 1600$ MeV

Figure 6.10: Same as Fig.(6.4) for $m_\pi \sim 800$ MeV.

reveals the data to be compatible with the threshold within the errors. The data imply that the theory tends to break into free or weakling-interacting $4-\alpha$'s. In most of those cases, the data do not reach the threshold before the exponential growth of the errors. This can be explained by the fact that the "clustered" wave function is very different from the initial trial wave function. In the example of $m_\pi = 800$ MeV and $\Lambda \sim 400$ and 800 MeV, we have signs of the presence of a bound state but the statistical errors are still too large to claim any evidence. Nonetheless, this bound state appears only for the smallest cut-off in which we expect large regularization errors of order $\left(\frac{1}{\Lambda}\right)$ so we claim that the state would be a regularization artifact that disappears when $\Lambda \to +\infty$.

The large statistical errors which plague RPDMC results make difficult to draw any definitive conclusion. However, calculations indicate that the structure of the ^{16}O is much different than the one suggested by the shell-model. To better understand its nature, and to obtain more reliable evidence about the presence/absence of boundstates, we implemented the LM (see sec. {4.1}).

Λ	$m_\pi = 140$ MeV	$m_\pi = 510$ MeV	$m_\pi = 805$ MeV
400 MeV	$-97.19(6)$	$-116.59(8)$	$-350.69(5)$
800 MeV	$-92.23(14)$	$-137.15(15)$	$-362.92(7)$
1200 MeV	$-97.51(14)$	$-143.84(17)$	$-382.17(25)$
1600 MeV	$-100.97(20)$	$-146.37(27)$	$-402.24(39)$
$\to \infty$	$-117.5^{(3.0)}_{(8)}$	$-156^{(5)}_{(1)}$	$-440^{(40)}_{(20)}$
$4-\alpha$	$-119.5^{(4)}_{(2)}$	$-165^{(8)}_{(3)}$	$-440^{(52)}_{(12)}$
Exp.	-127.62	–	–

Table 6.1: ^{16}O energy for different values of the pion mass m_π and the cutoff Λ, compared with experiment (No LQCD results exist for this nucleus.) and the extrapolated four-alpha threshold. See main text for details.

6.2 Oxygen and Linear Method

The ^{16}O ground-state energies calculated using the "β", "γ" and "δ" parametrizations of EFT($\not\pi$) are reported in Tab.(6.1). Those results have been obtained using the LM and the AFDMC within the constrained-path approximation. As we expected by RPDMC calculations, ^{16}O appears to be unstable against breakup into four ^{4}He clusters in almost all the cases, even using the optimized wave function. The only exception occurs for $m_\pi = 140$ MeV and $\Lambda \sim$400 MeV, where ^{16}O is 4.5 MeV more bound than four ^{4}He nuclei. In the other cases, we miss the four-^{4}He threshold by about 5 MeV, which is beyond our statistical errors and reveals a lower bound on the systematic error of our QMC method.

Even considering only statistical and extrapolation errors, the asymptotic values of the ^{16}O energy cannot be separated from the four-^{4}He threshold. The proximity of the threshold suggests that the structure of our ^{16}O should be clustered. Indeed, despite no explicit clustering being enforced in the trial wave function, the linear optimization procedure arranges the two- and three-body Jastrow correlations, as well as the orbital radial functions, in such a way as to favor configurations characterized by four independent ^{4}He clusters.

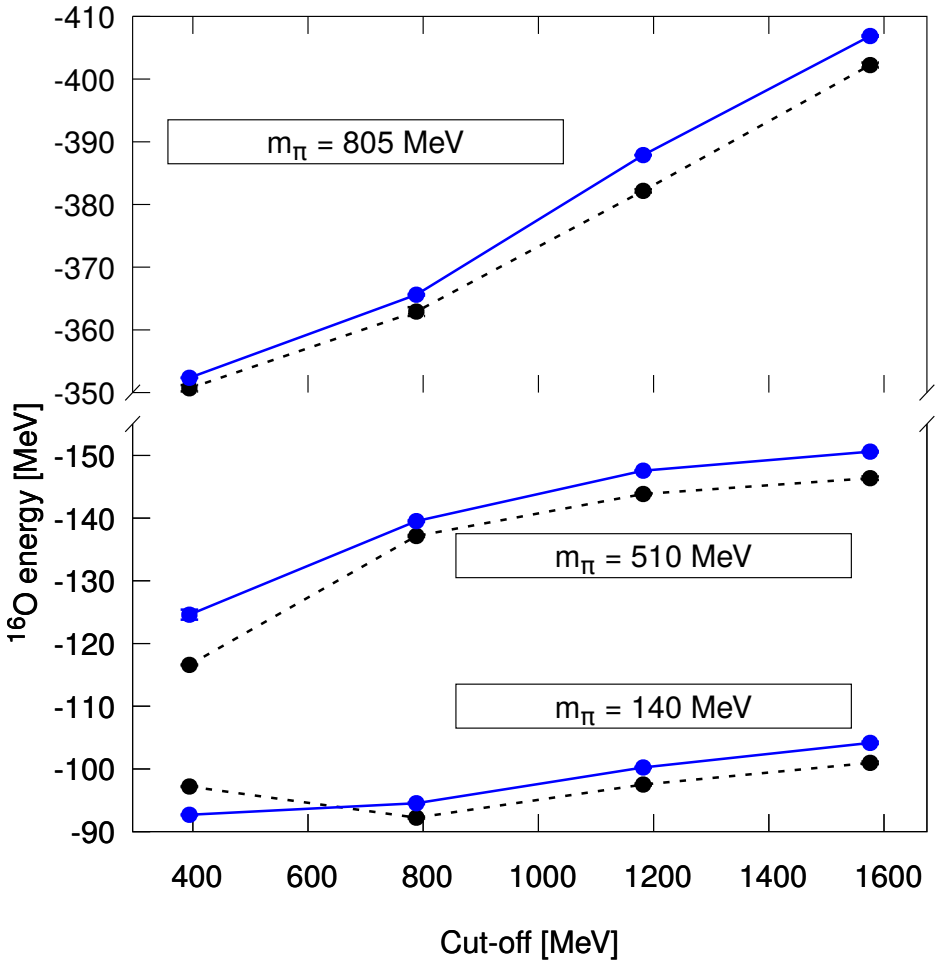

Figure 6.11: ^{16}O energy for different m_π and cut-offs. *Black* points represent the $4-\alpha$ threshold. *Blue* points represent ^{16}O energy calculated with LM.

The single-proton density profiles displayed in Fig.(6.12) indicate that only for the smallest Λs the nucleons are distributed according to the classic picture of a bound wave function. In the other cases, nucleons are pushed away from the center of the nucleus, which is basically empty. The erratic behavior of the peak position of the density profiles as a function of the cutoff has to be ascribed to the fact that the relative position of the four ^{4}He clusters is practically unaffected by the cutoff value. In fact, once the clusters are sufficiently apart, a landscape of degenerate minima in the variational energy emerges. Hence, the single-proton densities correspond to wave functions that,

despite potentially significantly different, lead to almost identical variational energies. In contrast, the width of the peaks decreases with increasing cutoff according to with the shrinking of the individual ^{4}He clusters reported in Tab.(8.1).

In support of the arguments about the proton density, which does not suffice to claim the clustering, the comparison between potential expectation values of ^{16}O and ^{4}He can be performed. For instance, in the $m_\pi = 140$ MeV and $\Lambda \sim$1600 MeV case it turns out that the expectation values of the ^{16}O two- and three-body potentials are $\simeq 4.05$ and $\simeq 4.16$ times larger than the corresponding values for ^{4}He.

The same pattern is observed for all the combinations of pion mass and cutoff where the system's energy is compatible with the threshold. In the other cases, for example, for $\Lambda \sim 400$ MeV and $m_\pi = 140$ MeV, the expectation values of the two- and three-body potentials in ^{16}O have a different value with respect ^{4}He ($\simeq 4.65$ and $\simeq 6.14$ times larger). This difference is a consequence of the fact that the number of interacting pairs and triplets is larger when clusterization does not take place.

To better visualize the clusterization of the wave function, in Fig.(6.13) we display the position of the nucleons following the propagation of a single walker for 5000 imaginary-timesteps, corresponding to $\Delta\tau = 0.125$ MeV^{-1}, printed every 10 steps. In the upper panel, concerning $m_\pi = 140$ MeV and $\Lambda = 400$ MeV, nucleons are not organized in clusters. In fact, during the imaginary time propagation, they diffuse in the region in which the corresponding single-nucleon density of Fig.(6.12) does not vanish. A completely different scenario takes place at the same pion mass when $\Lambda \sim$1600 MeV: the nucleons forming the four ^{4}He clusters remains close to the corresponding centers of mass during the entire imaginary time propagation. This is clear evidence of clustering. It has to be noted that the relative position of the four clusters is not a tetrahedron. To prove this, for each configuration we computed the moment-of-inertia matrix as in Ref.[96]. If the ^{4}He clusters were positioned at the vertices of a tetrahedron, diagonalization would yield only two independent eigenvalues. Instead, we found three distinct eigenvalues, corresponding to an ellipsoid, another indication of the absence of interactions among nucleons belonging to different ^{4}He clusters.

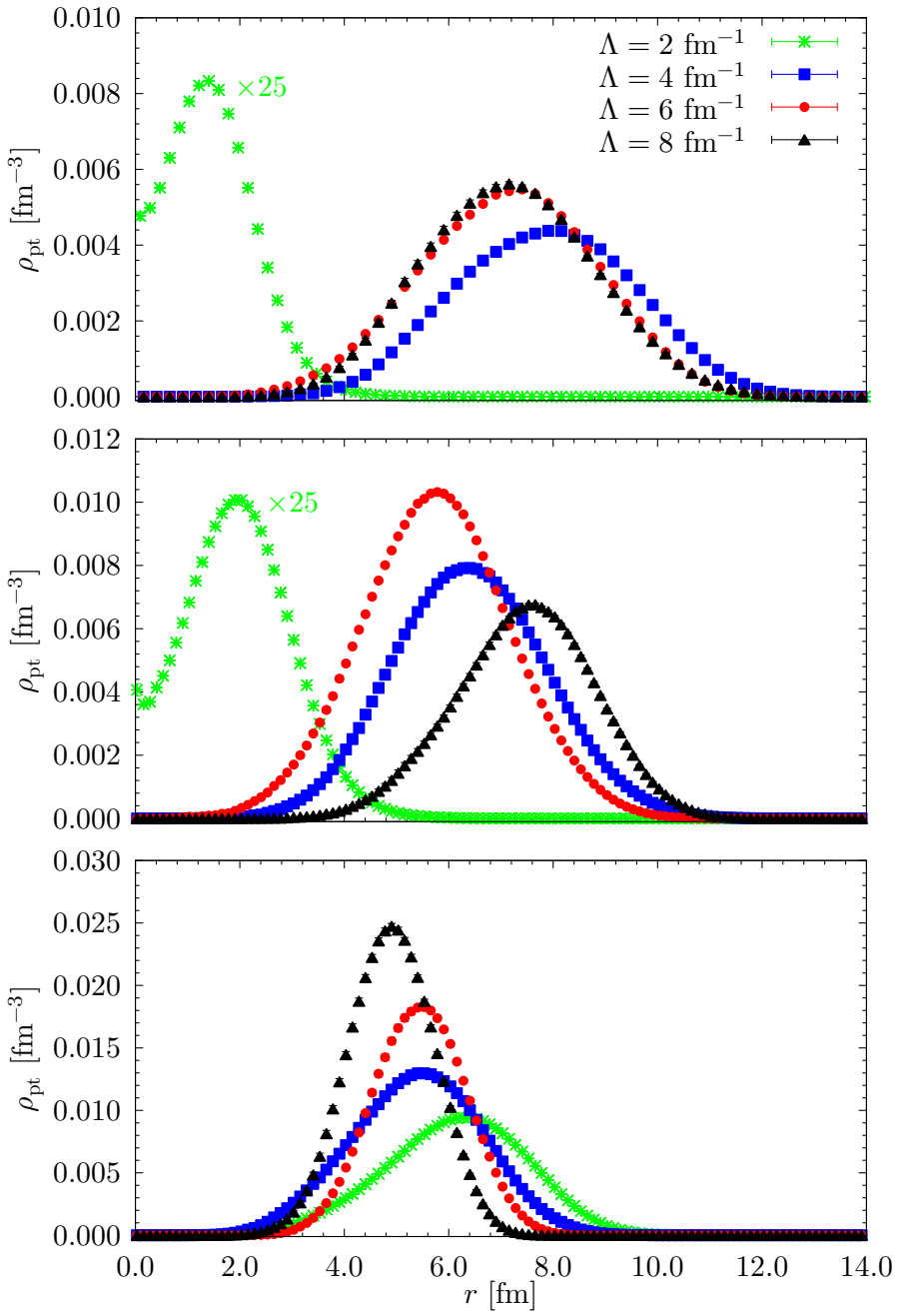

Figure 6.12: ^{16}O single-nucleon point density for $m_\pi = 140$ MeV (upper panel), $m_\pi = 510$ MeV (middle panel), and $m_\pi = 805$ MeV (lower panel), at different values of the cutoff Λ.

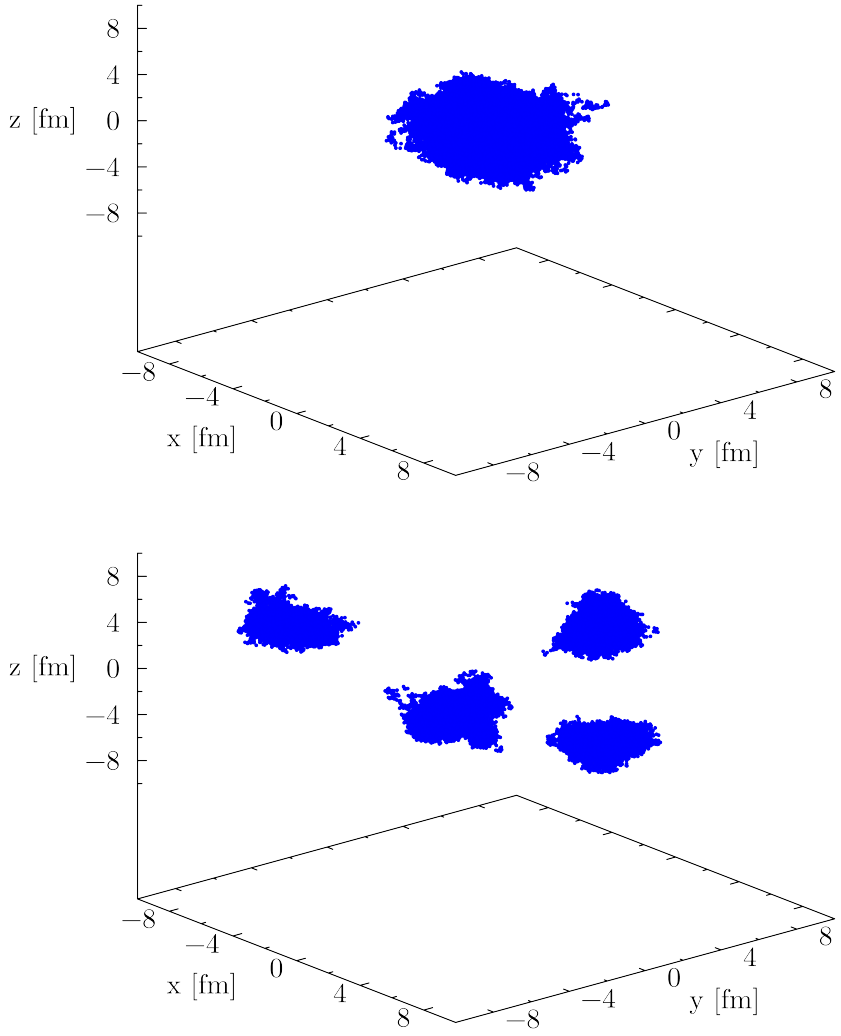

Figure 6.13: Imaginary-time diffusion with time step $\Delta\tau = 0.125$ MeV^{-1} of a single walker for $m_\pi = 140$ MeV, at $\Lambda \sim$400 MeV (upper panel) and $\Lambda \sim$1600 MeV (lower panel).

The smaller relative size of the model space leads to more modest signs of cutoff convergence for ^{16}O than ^{4}He, which are reflected in larger extrapolation errors, especially at $m_\pi = 805$ MeV. At physical pion mass, the central value of the extrapolated total energy is only 10% off from the experiment, which can be bridged by statistical and extrapolation errors. This difference

is small compared to the expected truncation error, $\sim 30\%$. If there is a low-lying resonant or virtual state of ^{4}He nuclei at LO in EFT($\not\pi$) , note that our analysis does neither preclude nor identify such a state, it is possible that the (perturbative) inclusion of higher-order terms up to N^{2}LO will move the ^{16}O energy sufficiently for stability with respect to four ^{4}He clusters.

For unphysical pion mass, our results can be seen as an extension of LQCD to medium-mass nuclei, with no further assumptions about the QCD dynamics. In this case, a determination of the relative position of the four-α threshold would further require much-increased accuracy in the $A = 2, 3$ LQCD results that we use as input.

7. Conclusions

One of the main challenges of current research in nuclear physics is to provide a unified look at the nuclear regime, from QCD to heavy nuclei.

In this thesis, the nuclear QMC algorithm has been optimized to predict observables using EFT potentials with relatively large cut-offs. Different kind of wave function correlations have been implemented and several numerical improvements to the used QMC method have been tested. The technique has been exploited performing calculations at LO in nuclear systems ranging from the deuteron to ^{16}O.

Within this framework, we derived a contact interaction which represents the LO of a systematic expansion of QCD. This enabled us to analyze physical nucleons as well as simulated scenarios with increased quark masses. To overcome the challenges associated to the solution of the Schrödinger equation, the used MC method has been improved, first releasing the walker's paths, then by using a new optimization protocol of the many-body wave function to be employed in the variational stage of the calculation.

In the first case, we manually optimized using VMC method the wave function experimenting different correlations and single-particle wave functions. The wave function obtained in this way was then diffused with and without the constrained path approximation. The groundstate energy behavior of oxygen suggested a break-up in four alpha particles. However, the uncertainties of RPDMC emerged to be too large to be conclusive, implying that a more refined trial wave function was required.

To achieve that, an extension of the linear method has been used. The tests performed with this method showed a much faster convergence in parameter space compared to the manual minimization but also compared with the stochastic reconfiguration, previously adopted in nuclear QMC calculations. We used the trial wave function found with the LM as starting point of the imaginary-time projection in AFDMC, which filters out the "exact"

ground state of the Hamiltonian. This algorithm was used to predict not only ground-state energies, but also radii, densities, and particle distributions.

Using results from LQCD simulations of few-nucleon systems we demonstrate the consistency of EFT($\not\pi$) and LQCD for $m_\pi \sim (800, 500)$ MeV. The agreement between the alpha binding energies calculated with two different methodologies and choice of degrees of freedom is not, a priori, guaranteed and shows how EFTs can be used as coherency benchmark for LQCD calculations. We also showed the consistency of the theory at LO with experimental data for natural m_π. Therefore, we conclude that the EFT($\not\pi$) LO is complete for those systems and the presence of a leading four-body force is not required in EFT($\not\pi$) .

With this successful benchmark, we extended the calculations to ^{16}O. The extrapolated values for the ^{16}O binding energy at all pion masses are indistinguishable from the respective four-^{4}He threshold, even considering only the smaller statistical and extrapolation errors. In fact, for almost all cutoffs and pion masses we considered, both using RPDMC and DMC and LM, ^{16}O is unstable with respect to break-up into four ^{4}He nuclei. Our calculation of the ^{16}O energy is the first time LQCD calculations are extended to the medium-mass region in a model-independent way.

The calculations done using LM revealed to be able to find four α structure also when the clusterization was not included a priori. Interestingly, $m_\pi =$ 140 MeV and Λ ∼400 MeV is the only parametrization yielding a stable ^{16}O. This suggests that the long-range structure of the interaction is deficient at larger cutoff values and might have to be corrected, e.g. via one-pion exchange, to guarantee the binding of heavier nuclei at LO. Alternatively, within a pionless framework, higher-order terms could act as perturbations to move ^{16}O with respect to the four-^{4}He threshold. At physical pion mass, the central value of the total energy is just about 10% off experiment. This is only slightly larger than the statistical and extrapolation errors, and well within the $\sim$ 30% truncation of the effective theory. We cannot exclude the possibility that agreement with data will improve with order. A comprehensive study of the various subsystems of ^{16}O (for example, ^{12}C, ^{8}Be, and ^{4}He-^{4}He scattering) could determine whether a resonant or virtual shallow state at LO is transformed into a bound state by subleading interactions, thus elucidating the relation between clusterization and QCD.

In order to better appreciate the cluster nature of our solution for ^{16}O, we

have studied the radial nucleon density and the sampled probability density for the nucleons. In both cases the occurrence of clusterization is evident. From our results it is not possible to infer any significant correlation between the clusters, which once more confirms the extremely weak interaction among them within EFT($\not\pi$) . We would like to point out that localization was not imposed in the wave function used to project out the ground state; rather, it spontaneously arises from the optimization procedure (despite the correlations being fully translationally invariant) and it is preserved by the subsequent imaginary-time projection.

Current QMC (AFDMC) results have now reached an accuracy level that allows for discussing the few-MeV energies involved in this class of phenomena, which are relevant for a deeper understanding of how the systematics in nuclear physics arises from QCD. Starting from the results of LQCD calculations obtained for values of m_π smaller than the ones employed in this work, and yet larger than the physical one, would allow us to establish the threshold for which nuclei as large as ^{16}O are stable against the breakup into four ^{4}He clusters, if such a threshold exists. To perform this analysis, it is essential to include higher-order terms in the EFT($\not\pi$) interaction, possibly up to N^{2}LO, where tensor contributions appear. This also requires a substantial improvement of the existing LQCD calculations on light nuclei, which, even for large m_π, are currently affected by statistical errors that do not allow for an effective constraint of the interaction parameters.

8. Tables of data

m_π= 140 MeV					
Λ [MeV]:		400	800	1200	1600
^{3}H [MeV]	DMC	-5.54(5)	-8.40(5)	-8.02(9)	-7.92(29)
	Other	Experimental: -8.482 MeV			
^{4}He [MeV]	RRGM ($\pm$1 MeV)	-23.2	-23.1	-23.9	-24.2
	DMC (No J_{3b})	-23.20(3)	-23.68(8)	-24.9(1)	-26.1(1)
	DMC (LM)	-23.17(2)	-23.63(3)	-25.06(2)	-26.04(5)
	Other	Experimental: -28.296 MeV			
^{16}O [MeV]	DMC (No J_{3b})	-96.7(5)	-57.4(8)	-49.6(1.1)	-47(1)
	DMC (Av. J_{3b})	-97.0(2)	-52.2(5)	-49(1)	-52(2)
	DMC (w/ $J_{3b}^{(4.12)*}$)	-97.2(1)	-57.9(3)	-50.1(6)	-46.5(9)
	DMC (w/ $J_{3b}^{(4.12)}$)		-59(1)		-50(1)
	DMC (w/ $J_{3b}^{(4.13)}$)		-58(1)		-50(1)
	DMC (w/ $J_{3b}^{(4.14)}$)		-58.6(1.0)		-52(1)
	DMC (LM)	-97.19(6)	-92.23(14)	-97.51(14)	-100.97(20)
	4α (LM)	-93.2	-94.0(8)	-100(1)	-104(2)
	Other	Experimental: -127.619 MeV			
^{40}Ca [MeV]	AFDMC	-273.3(6)	-130(1)	-84.0(1.3)	-61.3(2.4)
	Other	Experimental: -342.052 MeV			

m_π= 510 MeV					
Λ [MeV]:		400	800	1200	1600
^{3}H [MeV]	DMC	-20.20(5)	-20.35(6)	-20.52(12)	-25.52(12)
	Other	Lattice: 20.3 ± 4.5 MeV			
^{4}He [MeV]	RRGM ($\pm$1 MeV)	-30.8	-33.3	-34.4	-34.6
	DMC (No J_{3b})	-31.21(2)	-34.96(6)	-36.8(1)	-38.2(2)
	DMC (LM)	-31.15(2)	-34.88(3)	-36.89(2)	-37.65(3)
	Other	Lattice: -43 ± 14 MeV			
^{16}O [MeV]	DMC (No J_{3b})	-115(2)	-111.6(4)	-107.9(8)	-103(1)
	DMC (Av. J_{3b})	-114.6(2)	-113.8(2)	-109.71(4)	-105.7(5)
	DMC (LM)	-116.59(8)	-137.15(15)	-143.84(17)	-146.37(27)
	4α (LM)	-124.84(8)	-139.8(2)	-147.2(4)	-152.8(8)
^{40}Ca [MeV]	AFDMC	-270.2(1.5)	-268(2)	-241(2)	-186(4)

m_π= 805 MeV					
Λ [MeV]:		400	800	1200	1600
^{3}H [MeV]	DMC	-53.89(2)	-53.44(17)	-52.99(24)	-53.2(33)
	Other	Lattice: -53.9 ± 10.7			
^{4}He [MeV]	RRGM ($\pm$1 MeV)	-88	-90.9	-95.6	-99.3
	DMC (No J_{3b})	-88.05(8)	-91.3(1)	-96.8(1)	-100.8(3)
	DMC (LM)	-88.09(1)	-91.40(3)	-96.97(1)	-101.72(3)
	Other	Experimental: -28.296 MeV			
^{16}O [MeV]	DMC (No J_{3b})	-346.6(6)	-337.8(8)	-330(1)	-318(1)
	DMC (Av. J_{3b})	-346.7(7)	-335(1)	-326(1)	-315.6(8)
	DMC (w/ $J_{3b}^{(4.12)}$)	-355(2)	-340(2)	-335(2)	-375(1)
	DMC (LM)	-350.69(5)	-362.92(7)	-382.17(25)	-402.24(39)
	4α (LM)	-352.2(3)	-365.2(4)	-387.2(4)	-403(1)
	Other	Experimental: -127.619 MeV			

^{4}He proton radii					
Par.	α	β	γ	δ	ϵ
Λ	$m_\pi = 140$ MeV		$m_\pi = 510$ MeV	$m_\pi = 805$ MeV	
400 MeV	1.7438(23)	1.374(4)	1.482(3)	0.898(1)	0.95
800 MeV	1.5353(19)	1.203(4)	1.133(3)	0.699(1)	0.74
1200 MeV	1.3608(18)	1.109(3)	1.035(2)	0.609(1)	0.65
1600 MeV	1.2273(21)	1.054(3)	0.976(1)	0.542(1)	0.57
1600 MeV	1.1558(26)	-	-	-	0.51
$\to \infty$	0.76(8)	0.86(19)	0.76(13)	0.253(55)	
Exp.	1.45		–	-	

Table 8.1: Point proton radii of ^{4}He for different values of the pion mass and the cutoff. The extrapolations are performed without the point at 400 MeV.

Λ [MeV]	Be(^{4}He) [MeV]	r [fm]
400	$-24.5(1.2)$	1.7438(23)
600	$-24.3(6)$	1.5353(19)
800	$-25.08(27)$	1.3608(18)
1000	$-25.9(8)$	1.2273(21)
1200	$-26.7(7)$	1.1558(26)
1400	$-27.3(6)$	1.0682(3)
1600	$-27.9(5)$	1.0369(26)
1800	$-28.3(7)$	1.0098(15)
2000	$-28.3(7)$	0.9039(12)
2200	$-28.7(6)$	0.9834(13)
2400	$-28.4(6)$	0.9238(12)
2600	$-28.2(7)$	0.969(1)
$\to \infty$	0.72(5)	$31.0^{(4)}_{(1.8)}$
w/o 400 MeV	0.76(8)	$31.2^{(1)}_{(2.7)}$

Table 8.2: Point proton radii of ^{4}He for different values of the pion mass and the cutoff. The extrapolations are performed without the point at 400 MeV.

Bibliography

[1]H. Yukawa, "On the Interaction of Elementary Particles I", Proc. Phys. Math. Soc. Jap. **17**, [Prog. Theor. Phys. Suppl.1,1(1935)], 48–57 (1935) 10.1143/PTPS.1.1.

[2]A. R. Erwin, R. March, W. D. Walker, and E. West, "Evidence for a pi pi Resonance in the I = 1, J=1 State", Phys. Rev. Lett. **6**, 628–630 (1961) 10.1103/PhysRevLett.6.628.

[3]R. Bryan and B. L. Scott, "Nucleon-nucleon scattering from one-boson-exchange potentials. iii. s waves included", Phys. Rev. **177**, 1435–1442 (1969) 10.1103/PhysRev.177.1435.

[4]M. Lacombe, B. Loiseau, J. M. Richard, R. V. Mau, J. Côté, P. Pirès, and R. de Tourreil, "Parametrization of the paris n-n potential", Phys. Rev. C **21**, 861–873 (1980) 10.1103/PhysRevC.21.861.

[5]R. Machleidt, K. Holinde, and C. Elster, "The bonn meson-exchange model for the nucleon—nucleon interaction", Physics Reports **149**, 1–89 (1987) http://dx.doi.org/10.1016/S0370-1573(87)80002-9.

[6]S. Weinberg, "Phenomenological lagrangians", Physica A: Statistical Mechanics and its Applications **96**, 327–340 (1979) http://dx.doi.org/10.1016/0378-4371(79)90223-1.

[7]D. B. Kaplan, M. J. Savage, and M. B. Wise, "A New expansion for nucleon-nucleon interactions", Phys. Lett. **B424**, 390–396 (1998) 10.1016/S0370-2693(98)00210-X.

[8]S. Fleming, T. Mehen, and I. W. Stewart, "NNLO corrections to nucleon-nucleon scattering and perturbative pions", Nucl. Phys. **A677**, 313–366 (2000) 10.1016/S0375-9474(00)00221-9.

[9]U. van Kolck, "Effective field theory of short range forces", Nucl. Phys. **A645**, 273–302 (1999) 10.1016/S0375-9474(98)00612-5.

[10]S. König, H. W. Grießhammer, H. W. Hammer, and U. van Kolck, "Effective theory of 3H and 3He", J. Phys. **G43**, 055106 (2016) 10.1088/0954-3899/43/5/055106.

[11]G. P. Lepage, "How to renormalize the Schrodinger equation", in Nuclear physics. Proceedings, 8th Jorge Andre Swieca Summer School, Sao Jose dos Campos, Campos do Jordao, Brazil, January 26-February 7, 1997 (1997), pp. 135–180.

[12]J.-W. Chen, G. Rupak, and M. J. Savage, "Nucleon-nucleon effective field theory without pions", Nucl. Phys. **A653**, 386–412 (1999) 10.1016/S0375-9474(99)00298-5.

[13]J. Vanasse, "Fully perturbative calculation of nd scattering to next-to-next-to-leading-order", Phys. Rev. **C88** (2013) 10.1103/PhysRevC.88.044001.

[14]X. Kong and F. Ravndal, "Coulomb effects in low-energy proton proton scattering", Nucl. Phys. **A665**, 137–163 (2000) 10.1016/S0375-9474(99)00406-6.

[15]M. Lüscher, "Two-particle states on a torus and their relation to the scattering matrix", Nuclear Physics B **354**, 531–578 (1991) http://dx.doi.org/10.1016/0550-3213(91)90366-6.

[16]K. G. Wilson, "The renormalization group and critical phenomena", Rev. Mod. Phys. **55**, 583–600 (1983) 10.1103/RevModPhys.55.583.

[17]J. Polchinski, "Renormalization and Effective Lagrangians", Nucl. Phys. **B231**, 269–295 (1984) 10.1016/0550-3213(84)90287-6.

[18]C. Wetterich, "Effective average action in statistical physics and quantum field theory", Int. J. Mod. Phys. **A16**, [,315(2001)], 1951–1982 (2001) 10.1142/S0217751X01004591.

[19]B. A. Lippmann and J. Schwinger, "Variational Principles for Scattering Processes. I", Phys. Rev. **79**, 469–480 (1950) 10.1103/PhysRev.79.469.

[20]I. Mitra, A. DasGupta, and B. Dutta-Roy, "Regularization and renormalization in scattering from Dirac delta potentials", Am. J. Phys. **66**, 1101–1109 (1998) 10.1119/1.19051.

[21]S. König, H. W. Grießhammer, H. W. Hammer, and U. van Kolck, "Effective theory of 3H and 3He", J. Phys. **G43**, 055106 (2016) 10.1088/0954-3899/43/5/055106.

[22]J.-W. Chen, G. Rupak, and M. J. Savage, "Nucleon-nucleon effective field theory without pions", Nucl. Phys. **A653**, 386–412 (1999) 10.1016/S0375-9474(99)00298-5.

[23]H. A. Bethe and C. Longmire, "The effective range of nuclear forces 2. photodisintegration of the deuteron", Phys. Rev. **77**, 647–654 (1950) 10.1103/PhysRev.77.647.

[24]L. Platter, H. W. Hammer, and U.-G. Meissner, "The Four boson system with short range interactions", Phys. Rev. **A70**, 052101 (2004) 10.1103/PhysRevA.70.052101.

[25]L. H. Thomas, ""the interaction between a neutron and a proton and the structure of 3h"", Phys. Rev. **47**, 903–909 (1935) 10.1103/PhysRev.47.903.

[26]V. Efimov, "Energy levels arising form the resonant two-body forces in a three-body system", Phys. Lett. **B33**, 563–564 (1970) 10.1016/0370-2693(70)90349-7.

[27]P. F. Bedaque, H. W. Hammer, and U. van Kolck, "Effective theory for neutron deuteron scattering: Energy dependence", Phys. Rev. **C58**, R641–R644 (1998) 10.1103/PhysRevC.58.R641.

[28]P. F. Bedaque, H. W. Hammer, and U. van Kolck, "Effective theory of the triton", Nucl. Phys. **A676**, 357–370 (2000) 10.1016/S0375-9474(00)00205-0.

[29]P. F. Bedaque, H. W. Hammer, and U. van Kolck, "Renormalization of the three-body system with short range interactions", Phys. Rev. Lett. **82**, 463–467 (1999) 10.1103/PhysRevLett.82.463.

[30]N. Barnea, L. Contessi, D. Gazit, F. Pederiva, and U. van Kolck, "Effective Field Theory for Lattice Nuclei", Phys. Rev. Lett. **114**, 052501 (2015) 10.1103/PhysRevLett.114.052501.

[31]S. R. Beane et al., "Nucleon-Nucleon Scattering Parameters in the Limit of SU(3) Flavor Symmetry", Phys. Rev. **C88**, 024003 (2013) 10.1103/PhysRevC.88.024003.

[32]S. R. Beane, E. Chang, S. D. Cohen, W. Detmold, H. W. Lin, T. C. Luu, K. Orginos, A. Parreno, M. J. Savage, and A. Walker-Loud, "Light Nuclei and Hypernuclei from Quantum Chromodynamics in the Limit of SU(3) Flavor Symmetry", Phys. Rev. **D87**, 034506 (2013) 10.1103/PhysRevD.87.034506.

[33]T. Yamazaki, "Bound state of two-nucleon systems in quenched lattice-QCD", PoS **LATTICE2011**, 147 (2011).

[34]E. Berkowitz, T. Kurth, A. Nicholson, B. Joo, E. Rinaldi, M. Strother, P. M. Vranas, and A. Walker-Loud, "Two-Nucleon Higher Partial-Wave Scattering from Lattice QCD", (2015).

[35]T. Yamazaki, K.-i. Ishikawa, Y. Kuramashi, and A. Ukawa, "Helium nuclei, deuteron and dineutron in 2+1 flavor lattice QCD", Phys. Rev. **D86**, 074514 (2012) 10.1103/PhysRevD.86.074514.

[36]S. Aoki, T. Doi, T. Hatsuda, Y. Ikeda, T. Inoue, N. Ishii, K. Murano, H. Nemura, and K. Sasaki, "Lattice QCD approach to Nuclear Physics", PTEP **2012**, 01A105 (2012) 10.1093/ptep/pts010.

[37]K. Orginos, A. Parreno, M. J. Savage, S. R. Beane, E. Chang, and W. Detmold, "Two nucleon systems at mpi 450 MeV from lattice QCD", Phys. Rev. **D92**, 114512 (2015) 10.1103/PhysRevD.92.114512.

[38]T. Yamazaki, K.-i. Ishikawa, Y. Kuramashi, and A. Ukawa, "Study of quark mass dependence of binding energy for light nuclei in 2+1 flavor lattice QCD", Phys. Rev. **D92**, 014501 (2015) 10.1103/PhysRevD.92.014501.

[39]T. Yamazaki, "Light Nuclei and Nucleon Form Factors in Nf=2+1 Lattice QCD", PoS **LATTICE2015**, 081 (2016).

[40]C. collaboration, "Private comunication".

[41]R. W. Hackenburg, "Neutron-proton effective range parameters and zero-energy shape dependence", Phys. Rev. C **73**, 044002 (2006) 10.1103/PhysRevC.73.044002.

[42]T. Yamazaki, Y. Kuramashi, and A. Ukawa, "Helium Nuclei in Quenched Lattice QCD", Phys. Rev. **D81**, 111504 (2010) 10.1103/PhysRevD.81.111504.

[43]Y. Demkov and G. Drukarev., "Second-order poles of the s matrix and resonance scattering", Sov.Phys.JETP,22,479 (1966).

[44]E. P. Wigner, "Lower Limit for the Energy Derivative of the Scattering Phase Shift", Phys. Rev. **98**, 145–147 (1955) 10.1103/PhysRev.98.145.

[45]P. Terry, "The Asymptotic Form of the Continuum Wave Functions and Redundant Poles in the Heisenberg Condition", J. Math. Phys. **23**, 87 (1982) 10.1063/1.525211.

[46]K. Yamamoto, "Physical meaning of redundant poles of s-matrix", Progress of Theoretical Physics **27**, 219 (1962) 10.1143/PTP.27.219.

[47]S. N. Biswas, T. Pradhan, and E. C. G. Sudarshan, "Completeness of states, shadow states, heisenberg condition, and poles of the S matrix", Nucl. Phys. **B50**, 269–284 (1972) 10.1016/S0550-3213(72)80018-X.

[48]S. Gandolfi, F. Pederiva, S. Fantoni, K. E. Schmidt, F. Pederiva, S. Fantoni, and K. E. Schmidt, "Auxiliary field diffusion Monte Carlo calculation of properties of oxygen isotopes", Phys. Rev. **C73**, 044304 (2006) 10.1103/PhysRevC.73.044304.

[49]D. Ceperley, G. V. Chester, and M. H. Kalos, "Monte Carlo simulation of a many-fermion study", Phys. Rev. **B16**, 3081–3099 (1977) 10.1103/PhysRevB.16.3081.

[50]A. Roggero, A. Mukherjee, and F. Pederiva, "Quantum Monte Carlo with Coupled-Cluster wave functions", Phys. Rev. **B88**, 115138 (2013) 10.1103/PhysRevB.88.115138.

[51]M. Kalos and P. Whitlock, *Monte carlo methods*, A Wiley Interscience publication v. 1 (Wiley, 2008).

[52]E. Y. Loh, J. E. Gubernatis, R. T. Scalettar, S. R. White, D. J. Scalapino, and R. L. Sugar, "Sign problem in the numerical simulation of many-electron systems", Phys. Rev. **B41**, 9301–9307 (1990) 10.1103/PhysRevB.41.9301.

[53]D. Lonardoni, "From Hypernuclei to Hypermatter: a Quantum Monte Carlo Study of Strangeness in Nuclear Structure and Nuclear Astrophysics", PhD thesis (Trento U., 2013).

[54]P. Armani, "Progress of Monte Carlo methods in nuclear physics using EFT-based NN interaction and in hypernuclear systems", PhD thesis (Trento U., 2011).

[55]P. Billingsley, *Probability and measure*, 3rd ed. (Wiley, Apr. 1995).

[56]W. K. Hastings, "Monte carlo sampling methods using markov chains and their applications", Biometrika **57**, 97–109 (1970) 10.1093/biomet/57.1.97.

[57]S. Sorella, "Wave function optimization in the variational monte carlo method", Phys. Rev. B **71**, 241103 (2005) 10.1103/PhysRevB.71.241103.

[58]I. E. Lagaris and V. R. Pandharipande, "Variational Calculations of Realistic Models of Nuclear Matter", Nucl. Phys. **A359**, 349–364 (1981) 10.1016/0375-9474(81)90241-4.

[59]A. Arriaga, V. R. Pandharipande, and R. B. Wiringa, "Three body correlations in few body nuclei", Phys. Rev. **C52**, 2362–2368 (1995) 10.1103/PhysRevC.52.2362.

[60]J. Toulouse and C. J. Umrigar, "Optimization of quantum Monte Carlo wave functions by energy minimization", jcp **126**, 084102–084102 (2007) 10.1063/1.2437215.

[61]C. J. Umrigar and C. Filippi, "Energy and variance optimization of many-body wave functions", Phys. Rev. Lett. **94**, 150201 (2005) 10.1103/PhysRevLett.94.150201.

[62]M. W. Lee, M. Mella, and A. M. Rappe, "Electronic quantum monte carlo calculations of atomic forces, vibrations, and anharmonicities", The Journal of Chemical Physics **122**, 244103 (2005) http://dx.doi.org/10.1063/1.1924690.

[63]N. Hatano and M. Suzuki, "Finding Exponential Product Formulas of Higher Orders", [Lect. Notes Phys.679,37(2005)], 37–68 (2005) 10.1007/11526216_2.

[64]B. Hammond, W. Lester, and P. Reynolds, *Monte carlo methods in ab initio quantum chemistry*, Lecture and Course Notes In Chemistry Series (World Scientific, 1994).

[65]G. H. Lang, C. W. Johnson, S. E. Koonin, and W. E. Ormand, "Monte carlo evaluation of path integrals for the nuclear shell model", Phys. Rev. C **48**, 1518–1545 (1993) 10.1103/PhysRevC.48.1518.

[66]Y. Alhassid, D. J. Dean, S. E. Koonin, G. Lang, and W. E. Ormand, "Practical solution to the monte carlo sign problem: realistic calculations of 54fe", Phys. Rev. Lett. **72**, 613–616 (1994) 10.1103/PhysRevLett.72.613.

[67]Y. ALHASSID, "Quantum monte carlo methods for nuclei at finite temperature", International Journal of Modern Physics B **15**, 1447–1462 (2001) 10.1142/S0217979201005945.

[68]H. J. M. van Bemmel, D. F. B. ten Haaf, W. van Saarloos, J. M. J. van Leeuwen, and G. An, "Fixed-node quantum monte carlo method for lattice fermions", Phys. Rev. Lett. **72**, 2442–2445 (1994) 10.1103/PhysRevLett.72.2442.

[69]S. Sorella and L. Capriotti, "Green function monte carlo with stochastic reconfiguration: an effective remedy for the sign problem", Phys. Rev. B **61**, 2599–2612 (2000) 10.1103/PhysRevB.61.2599.

[70]A. Szabo and N. Ostlund, *Modern quantum chemistry: introduction to advanced electronic structure theory*, Dover Books on Chemistry (Dover Publications, 1989).

[71]A. Roggero, A. Mukherjee, and F. Pederiva, "Quantum Monte Carlo calculations of neutron matter with non-local chiral interactions", Phys. Rev. Lett. **112**, 221103 (2014) 10.1103/PhysRevLett.112.221103.

[72]M. Nightingale and C. Umrigar, *Quantum monte carlo methods in physics and chemistry*, Nato Science Series C: (Springer Netherlands, 1998).

[73]S. Zhang and H. Krakauer, "Quantum Monte Carlo method using phase-free random walks with Slater determinants", Phys. Rev. Lett. **90**, 136401 (2003) 10.1103/PhysRevLett.90.136401.

[74]P. J. Reynolds, D. M. Ceperley, B. J. Alder, and W. A. Lester Jr, "Fixed-node quantum monte carlo for molecules", The Journal of Chemical Physics **77**, 5593–5603 (1982).

[75]E. Y. Loh, J. E. Gubernatis, R. T. Scalettar, S. R. White, D. J. Scalapino, and R. L. Sugar, "Sign problem in the numerical simulation of many-electron systems", Phys. Rev. B **41**, 9301–9307 (1990) 10.1103/PhysRevB.41.9301.

[76]F. Bolton, "Fixed-phase quantum monte carlo method applied to interacting electrons in a quantum dot", Phys. Rev. B **54**, 4780–4793 (1996) 10.1103/PhysRevB.54.4780.

[77]J. Carlson, S. Gandolfi, F. Pederiva, S. C. Pieper, R. Schiavilla, K. E. Schmidt, and R. B. Wiringa, "Quantum Monte Carlo methods for nuclear physics", Rev. Mod. Phys. **87**, 1067 (2015) 10.1103/RevModPhys.87.1067.

[78]S. Gandolfi, F. Pederiva, S. Fantoni, and K. E. Schmidt, "Auxiliary Field Diffusion Monte Carlo calculation of nuclei with A ¡= 40 with tensor interactions", Phys. Rev. Lett. **99**, 022507 (2007) 10.1103/PhysRevLett.99.022507.

[79]F. Pederiva, A. Sarsa, K. E. Schmidt, and S. Fantoni, "Auxiliary field diffusion Monte Carlo calculation of ground state properties of neutron drops", Nucl. Phys. **A742**, 255–268 (2004) 10.1016/j.nuclphysa.2004.06.030.

[80]A. Sarsa, S. Fantoni, K. E. Schmidt, and F. Pederiva, "Neutron matter at zero temperature with auxiliary field diffusion Monte Carlo", Phys. Rev. **C68**, 024308 (2003) 10.1103/PhysRevC.68.024308.

[81]S. Gandolfi, A. Y. Illarionov, S. Fantoni, J. C. Miller, F. Pederiva, and K. E. Schmidt, "Microscopic calculation of the equation of state of nuclear matter and neutron star structure", Mon. Not. Roy. Astron. Soc. **404**, L35–L39 (2010) 10.1111/j.1745-3933.2010.00829.x.

[82]E. Lipparini, "Modern many-particle physics",

[83]S. Gandolfi, "The Auxiliary Field Diffusion Monte Carlo Method for Nuclear Physics and Nuclear Astrophysics", PhD thesis (Trento U., 2007).

[84]A. Lovato, "Ab initio calculations on nuclear matter properties including the effects of three-nucleons interaction", PhD thesis (SISSA, Trieste, 2012).

[85]D. Lonardoni, F. Pederiva, and S. Gandolfi, "From hypernuclei to the Inner Core of Neutron Stars: A Quantum Monte Carlo Study", J. Phys. Conf. Ser. **529**, 012012 (2014) 10.1088/1742-6596/529/1/012012.

[86]I. Tews, S. Gandolfi, A. Gezerlis, and A. Schwenk, "Quantum Monte Carlo calculations of neutron matter with chiral three-body forces", Phys. Rev. **C93**, 024305 (2016) 10.1103/PhysRevC.93.024305.

[87]M. D. Jones, G. Ortiz, and D. M. Ceperley, "Released-phase quantum Monte Carlo method", Phys. Rev. **E55**, 6202–6210 (1997) 10.1103/PhysRevE.55.6202.

[88]S. Binder et al., "Few-nucleon systems with state-of-the-art chiral nucleon-nucleon forces", Phys. Rev. **C93**, 044002 (2016) 10.1103/PhysRevC.93.044002.

[89]L. Platter, H. .-.-W. Hammer, and U.-G. Meissner, "On the correlation between the binding energies of the triton and the alpha-particle", Phys. Lett. **B607**, 254–258 (2005) 10.1016/j.physletb.2004.12.068.

[90]C. R. Ottermann, G. Kobschall, K. Maurer, K. Rohrich, C. Schmitt, and V. H. Walther, "ELASTIC ELECTRON SCATTERING FROM HE-3 AND HE-4", Nucl. Phys. **A436**, 688–698 (1985) 10.1016/0375-9474(85)90554-8.

[91]J. E. Lynn, J. Carlson, E. Epelbaum, S. Gandolfi, A. Gezerlis, and A. Schwenk, "Quantum Monte Carlo Calculations of Light Nuclei Using Chiral Potentials", Phys. Rev. Lett. **113**, 192501 (2014) 10.1103/PhysRevLett.113.192501.

[92]P. F. Bedaque and U. van Kolck, "Effective field theory for few nucleon systems", Ann. Rev. Nucl. Part. Sci. **52**, 339–396 (2002) 10.1146/annurev.nucl.52.050102.090637.

[93]E. Epelbaum, H.-W. Hammer, and U.-G. Meissner, "Modern Theory of Nuclear Forces", Rev. Mod. Phys. **81**, 1773–1825 (2009) 10.1103/RevModPhys.81.1773.

[94]R. Machleidt and D. R. Entem, "Chiral effective field theory and nuclear forces", Phys. Rept. **503**, 1–75 (2011) 10.1016/j.physrep.2011.02.001.

[95]T. Skyrme, "The effective nuclear potential", Nucl. Phys. **9**, 615–634 (1959) 10.1016/0029-5582(58)90345-6.

[96]R. B. Wiringa, S. C. Pieper, J. Carlson, and V. R. Pandharipande, "Quantum Monte Carlo calculations of A = 8 nuclei", Phys. Rev. **C62**, 014001 (2000) 10.1103/PhysRevC.62.014001.

ACKNOWLEDGMENTS

I would like to thank all the people that have been close to me during these years of doctorate. I will also take advantage of this section to acknowledge all those (someone already fled abroad) that contributed to the path that brought me here.

First of all, I have to thank my supervisor, Francesco, that trusted me and gave me always good hints, even if I not always got them. His patience and foresight allowed me to grow as physicist and person (still much work has to be done here). I am honored to have the chance to be one of his students and I am grateful for all the time he spent with me despite the numerous tasks his work requires. I would also thank Alessandro Lovato, who has been a wonderful supervisor, advisor, confidant, friend, and host. I should be grateful to him and his hard work if anything on my Ph.D. was possible. Heartily thanks also to Bira, whose patience in answering my futile questions (and the ability not to show how stupid they appeared) was fundamental. I should be grateful to him for the long discussions about Physics and life, as well as some pleasure and leisure moments. I would also thank all the collaborators and mentors I found during the way, especially Nir, Abhishek, Johannes, and Betzalel, with whom I always could discuss and be treated as an equal, regardless their ability and experience. I am also grateful to the Ph.D. students of the past years. They showed me that one can survive the doctorate. I want to especially thank Ale and Diego. Despite we shared very few moments together in Trento, they were an inspiration to me. I am also grateful to my referees for the careful revision of my work, and for the constructive suggestions. Finally, I would like to thank our secretaries: Micaela, Marina, and Lucia, without whose help everything not would have been possible (or extremely complicated).

On the personal side, some particular thank goes to my family that was close to me and supported me during this years. I will never end to thank my mother, who made everything possible, supporting all my decisions and ideas. My father that always helped me to take the right decision with logic

and criticism. I should give credit to my parents and their explanations to my curiosities if I have chosen to become a physicist (for better or worse). I have to thank also my grandparents for the patience in trying to understand what I was going to do and their wonderful ability to put life in rimes.

A very special thank goes to Sara that stayed close to me in the good and bad moments of this Ph.D.. She had not only the patience to follow me during travels and to hear countless discussions about my work and physics, but she was always there when I had the most need. It is sure that my Ph.D. would have been much harder without Sara, she had a special place in these years and so she does in my heart. A eulogy should be given also to my "mother in law" for the hospitality she gave me, the wonderful dinners and for having embraced me as her own son.

Here I will acknowledge all my friends that in a way or in another walked with me up to this point, I will try to go through all, however, since the acknowledges should not be longer than the thesis, I can not list literally everyone separately. (sorry). I would start with Allo, with whom I shared wonderful moments since when we were very young. Regardless the moments in which we were more or less close he is one of my deepest and long term confidants, which, I can say with honesty, knows a lot about me. Martino, with whom I shared many passions, a room and endless late night discussions (for the sake of Davide happiness). He taught me how important is to read terms and conditions, but also that having a roommate that does it for you is priceless. Michele, Brizio (that celebrate his birthday today) and Simone and the long hours passed together in ludicrous (and not) activities and discussions. How to forget my ex-housemates, Fabio, Zeno and Davide, the long after-dinner, the laughs, but also the day routines and the beers. And, of course, all FISICI_TN that I cannot mention more specifically without the risk to double this thesis length. I am grateful to all of you guys, for the wonderful years spent together. A special thank goes to the "mathematicians" (Ilaria, Elena, Adriano, and Giulia). Not only you are good friends, but I should also be grateful for all we have done together: Juggling, evenings of chatting, skating, Capoeira, Dance... Without you, all these years would have been much emptier (and full of physicians (Sorry again, Davide, you has been accepted as Physician ad honoree)).

I should dedicate some words to my office-mates, maybe because the long time passed together or the common love for physics, it seems I shared with

you much of my recent time. You taught me that everyone has his fobies, problems, and satisfactions, but also that to achieve something one should hold on and do not give-up. Hence, thanks to Giulia and her sometimes too many worries (but some other times justified). Fabrizio and his calm and peace. Sergio for the nice discussions, the music and for the way too many "Bu dat tss"s. Thanks also to Francesco, lately refugee in our office; it has been brief yet intense moments.

Last but not the least I would thank my sword master and assistants (I am looking to you: Andrea, Enrico, and Stefano). Fencing was not only a way to discharge tension with friends, but it was also a discipline that taught me a lot about myself, others and life.